REPORT DOCUMENTATION PAGE

Form Approved OMB NO. 0704-0188

The public reporting burden for this collection of information is estimated to average 1 hour per response, including the time for reviewing instructions, searching existing data sources, gathering and maintaining the data needed, and completing and reviewing the collection of information. Send comments regarding this burden estimate or any other aspect of this collection of information, including suggesstions for reducing this burden, to Washington Headquarters Services, Directorate for Information Operations and Reports, 1215 Jefferson Davis Highway, Suite 1204, Arlington VA, 22202-4302. Respondents should be aware that notwithstanding any other provision of law, no person shall be subject to any oenalty for failing to comply with a collection of information if it does not display a currently valid OMB control number.
PLEASE DO NOT RETURN YOUR FORM TO THE ABOVE ADDRESS.

1. REPORT DATE (DD-MM-YYYY)	2. REPORT TYPE	3. DATES COVERED (From - To)
20-01-2015	Ph.D. Dissertation	-

4. TITLE AND SUBTITLE
Cationic Polymers Developed for Alkaline Fuel Cell Applications

5a. CONTRACT NUMBER
W911NF-10-1-0520

5b. GRANT NUMBER

5c. PROGRAM ELEMENT NUMBER
611103

6. AUTHORS
Yating Yang

5d. PROJECT NUMBER

5e. TASK NUMBER

5f. WORK UNIT NUMBER

7. PERFORMING ORGANIZATION NAMES AND ADDRESSES
Colorado School of Mines
1500 Illinois Street, Guggenheim Hall, Room 130

Golden, CO 80401 -1887

8. PERFORMING ORGANIZATION REPORT NUMBER

9. SPONSORING/MONITORING AGENCY NAME(S) AND ADDRESS (ES)
U.S. Army Research Office
P.O. Box 12211
Research Triangle Park, NC 27709-2211

10. SPONSOR/MONITOR'S ACRONYM(S)
ARO

11. SPONSOR/MONITOR'S REPORT NUMBER(S)
58161-CH-MUR.64

12. DISTRIBUTION AVAILIBILITY STATEMENT
Approved for public release; distribution is unlimited.

13. SUPPLEMENTARY NOTES
The views, opinions and/or findings contained in this report are those of the author(s) and should not contrued as an official Department of the Army position, policy or decision, unless so designated by other documentation.

14. ABSTRACT
Alkaline fuel cells (AFCs) recently have gained renewed interest because of their facile electrode reaction kinetics, reduced fuel crossover and better water management compared to their protonic fuel cell counterpart. The emerging anionic exchange membrane fuel cell (AEMFC) adopts cationic group-functionalized polymers as the solid electrolyte instead of liquid potassium hydroxide or sodium hydroxide used in the traditional AFC, avoiding leakage problems, bicarbonate and carbonate salt induced electrode degradation issues that accompany liquid electrolytes. The polymer electrolyte applied in fuel cells should have good mechanical properties as well as high

15. SUBJECT TERMS
Anion Exchange Membranes, Polymer Synthesis, Cation Stability

16. SECURITY CLASSIFICATION OF:			17. LIMITATION OF ABSTRACT	15. NUMBER OF PAGES	19a. NAME OF RESPONSIBLE PERSON
a. REPORT	b. ABSTRACT	c. THIS PAGE			Andrew Herring
UU	UU	UU	UU		19b. TELEPHONE NUMBER 303-384-2082

Report Title

Cationic Polymers Developed for Alkaline Fuel Cell Applications

ABSTRACT

Alkaline fuel cells (AFCs) recently have gained renewed interest because of their facile electrode reaction kinetics, reduced fuel crossover and better water management compared to their protonic fuel cell counterpart. The emerging anionic exchange membrane fuel cell (AEMFC) adopts cationic group-functionalized polymers as the solid electrolyte instead of liquid potassium hydroxide or sodium hydroxide used in the traditional AFC, avoiding leakage problems, bicarbonate and carbonate salt induced electrode degradation issues that accompany liquid electrolytes. The polymer electrolyte applied in fuel cells should have good mechanical properties as well as high thermal and chemical stabilities, considering the basic, humid and elevated temperature operating conditions and the constant start-ups and shutdowns in fuel cell operation.

The chemical stability of guanidinium ion under an alkaline environment was studied in this research with the aim of using guanidinium ion in alkaline exchange membranes. The high pKa value (~13) of protonated quanidinium suggests a high dissociation of hydroxide ions from a hexa-alkylated guanadinium resulting in a high hydroxide conductivity of a functionalized polymer electrolyte. Model guanidinium compounds were synthesized to study the alkaline stability under different temperatures.

In order to form membranes with ion conducting channels, block copolymers can be designed that contain a hydrophilic cationic functional block separated from a hydrophobic block. This type of material can undergo microphase separation and form continuous ion conductive channels with the mechanical properties determined by the

iii

hydrophobic block material. In the present research, novel diblock copolymers were designed to combine an aromatic polymer block with a functionalized styrenic polymer block, aiming for combined mechanical and chemical merits from the good film forming, thermally and chemically stable poly(2,6-dimethyl-1,4-phenylene oxide) block (PPO) and the hydrophilic conductive poly(vinylbenzyltrimethylammonium) (PVBTMA) block. A poly(vinylbenzyl chloride) (PVBC) block was grown from the end of a PPO block through nitroxide mediated polymerization. The final quaternized PPO-b-PVBTMA film was obtained through hot pressing PPO-b-PVBC powder into films, followed by quaternizing in aqueous trimethylamine solution. Phase separation was indicated for the PPO-b-PVBC polymers based on the evidence of two Tgs from differential scanning calorimetry analysis. The PPO-b-PVBTMA membranes exhibited hydroxide conductivities as high as 166 ± 5 mS/cm at 60 °C under fully hydrated conditions. Comparing to the reported anionic exchange membranes, PPO-b-PVBTMA membranes showed promising conductivity with suppressed water uptake.

In a similar design to the PPO-b-PVBTMA membranes, triblock copolymers were synthesized through NMP with polysulfone as the center block and PVBC as the outer blocks. The PVBC blocks were quaternized by Menshutkin reaction to produce PVBTMA blocks. PPO and polysulfone are both well known engineering polymers that function as the hydrophobic domains in these membranes, providing mechanical support, while the PVBTMA block(s) form hydrophilic domains to transport anions. Diblock copolymers and triblock copolymers with different weight percentage of PVBTMA block were synthesized and characterized by electrochemical impedance spectroscopy to study the effect of temperature, different counter ions, ion exchange capacity (IEC) and water uptake on ionic conductivity.

CATIONIC POLYMERS DEVELOPED FOR ALKALINE FUEL CELL APPLICATIONS

by

Yating Yang

A thesis submitted to the Faculty and the Board of Trustees of the Colorado School of Mines in partial fulfillment of the requirements for the degree of Doctor of Philosophy (Applied Chemistry).

Golden, Colorado

Date_____

Signed:_____

Yating Yang

Signed:_____

Dr. Daniel M. Knauss

Thesis Advisor

Golden, Colorado

Date_____

Signed:_____

Dr. David T. Wu

Professor and Head

Department of Chemistry and Geochemistry

ABSTRACT

Alkaline fuel cells (AFCs) recently have gained renewed interest because of their facile electrode reaction kinetics, reduced fuel crossover and better water management compared to their protonic fuel cell counterpart. The emerging anionic exchange membrane fuel cell (AEMFC) adopts cationic group-functionalized polymers as the solid electrolyte instead of liquid potassium hydroxide or sodium hydroxide used in the traditional AFC, avoiding leakage problems, bicarbonate and carbonate salt induced electrode degradation issues that accompany liquid electrolytes. The polymer electrolyte applied in fuel cells should have good mechanical properties as well as high thermal and chemical stabilities, considering the basic, humid and elevated temperature operating conditions and the constant start-ups and shutdowns in fuel cell operation.

The chemical stability of guanidinium ion under an alkaline environment was studied in this research with the aim of using guanidinium ion in alkaline exchange membranes. The high pK_a value (~13) of protonated quanidinium suggests a high dissociation of hydroxide ions from a hexa-alkylated guanadinium resulting in a high hydroxide conductivity of a functionalized polymer electrolyte. Model guanidinium compounds were synthesized to study the alkaline stability under different temperatures.

In order to form membranes with ion conducting channels, block copolymers can be designed that contain a hydrophilic cationic functional block separated from a hydrophobic block. This type of material can undergo microphase separation and form continuous ion conductive channels with the mechanical properties determined by the

hydrophobic block material. In the present research, novel diblock copolymers were designed to combine an aromatic polymer block with a functionalized styrenic polymer block, aiming for combined mechanical and chemical merits from the good film forming, thermally and chemically stable poly(2,6-dimethyl-1,4-phenylene oxide) block (PPO) and the hydrophilic conductive poly(vinylbenzyltrimethylammonium) (PVBTMA) block. A poly(vinylbenzyl chloride) (PVBC) block was grown from the end of a PPO block through nitroxide mediated polymerization. The final quaternized PPO-*b*-PVBTMA film was obtained through hot pressing PPO-*b*-PVBC powder into films, followed by quaternizing in aqueous trimethylamine solution. Phase separation was indicated for the PPO-*b*-PVBC polymers based on the evidence of two T_gs from differential scanning calorimetry analysis. The PPO-*b*-PVBTMA membranes exhibited hydroxide conductivities as high as 166 ± 5 mS/cm at 60 °C under fully hydrated conditions. Comparing to the reported anionic exchange membranes, PPO-*b*-PVBTMA membranes showed promising conductivity with suppressed water uptake.

In a similar design to the PPO-*b*-PVBTMA membranes, triblock copolymers were synthesized through NMP with polysulfone as the center block and PVBC as the outer blocks. The PVBC blocks were quaternized by Menshutkin reaction to produce PVBTMA blocks. PPO and polysulfone are both well known engineering polymers that function as the hydrophobic domains in these membranes, providing mechanical support, while the PVBTMA block(s) form hydrophilic domains to transport anions. Diblock copolymers and triblock copolymers with different weight percentage of PVBTMA block were synthesized and characterized by electrochemical impedance spectroscopy to study

the effect of temperature, different counter ions, ion exchange capacity (IEC) and water uptake on ionic conductivity.

TABLE OF CONTENTS

LIST OF FIGURES

LIST OF SCHEMES

LIST OF TABLES

ACKNOWLEDGEMENT

I would like to take this opportunity to give my sincere appreciation to my advisor, Dr. Daniel M. Knauss, who has guided my research work through my graduate career. Not only did I learn knowledge from him, I also learned scientific attitude, critical thinking, and the ability to continually be evaluating and solving problems. My PhD study could never be finished if I didn't have his support, guidance, and patience. I would also like to thank Dr. Andrew M. Herring, Dr. Stephen G. Boyes, and Dr. John Dorgan for serving on my committee. I enjoyed learning from Dr. Boyes' courses on fundamental polymer chemistry and advanced polymer synthesis. I had the pleasure of working with Dr. Herring on anion exchange membrane development. I would like to thank him for generously offering conductivity instruments and suggestions on my research. I would also like to thank Dr. Dorgan for his support and valuable suggestions.

I appreciate the help from Dr. Yuan Yang for her constant help on my research and being a good friend. I would also like to thank Dr. Nathanial T. Rebeck for answering my countless questions since I joined the group. Many thanks go to my group fellow members and the members in Dr. Boyes' group as we shared the laboratory and encouraged each other.

I owe sincere gratefulness to my parents and grandparents for their support and caring. My success is based on their unconditional love and understanding.

My beloved husband, Feilong Liu was constantly giving me strength and courage to get this far. I am grateful for his wisdom, positive attitude, and that I have him in my life.

In dedication to my loving grandfather for

his inspiration and encouragement

献给爱我的和我爱的爷爷

感谢我的家人一直以来的理解与支持

CHAPTER 1 INTRODUCTION TO ALKALINE FUEL CELLS

1.1 Fuel cells

A fuel cell is a device that converts the chemical energy from a fuel into electricity and heat through chemical reactions. The electrolyte between the cathode and anode is responsible for transporting protons or hydroxides from one electrode to another. During the course of investigation of new technologies aimed at finding alternative energy sources and alternative energy conversion processes, fuel cells have drawn great attention because they meet energy needs at acceptable cost, with higher efficiency, and less greenhouse gas emission compared to combustion of fossil fuels.[1-3]

Fuel cells now can provide power for many fields, such as military and research submarines, automobiles, stationary, and portable power generation.[4-6] Based on the different types of electrolyte, fuel cells can be divided into five categories: proton exchange membrane fuel cell (PEMFC), alkaline fuel cell (AFC), molten carbonate fuel cell (MCFC), solid oxide fuel cell (SOFC) and phosphoric acid fuel cell (PAFC).[7,8] The different types of electrolyte dictate the operating temperature and application area. MCFC, SOFC and PAFC belong to high temperature fuel cell, which can be applied in stationary power generation. PEMFC and AFC belong to low temperature fuel cell and have the potential to replace combustion engines to be applied in automobiles and also applied in portable devices. The low temperature operation can fulfill the requirements to automobiles of fast start-up and quick dynamic response.[6]

1.2 Polymer electrolyte fuel cells

The main function of the polymer electrolyte is to serve as electrolyte to transport ions between electrodes. PEMFC uses a polymer as electrolyte and works under acidic conditions and the transporting ion is the proton. Up to the present, the state-of-the-art PEMFC are the Nafion membranes.[9-11] Nafion exhibits excellent mechanical properties, chemical and thermal stabilities as well as high proton conductivities. PEMFCs remain limited for widespread use because of the uncertainties regarding the future availability and price of platinum group metals.[12-14]

1.3 Traditional alkaline fuel cells and alkaline exchange membrane fuel cells

Alkaline fuel cell converts chemical fuel into electricity using alkaline electrolyte. Hydrogen reacts with hydroxide ion to produce water and electrons. The hydroxide ions are transported by the electrolyte from cathode to anode and an external circuit is generated from the anode to cathode. At the cathode, oxygen combines with water and electrons to produce hydroxide ions again to transport through the electrolyte. A typical AFC using hydrogen as the fuel has cell reaction below (Figure 1.1):

$$\text{Cathode: } O_2 + 2H_2O + 4e^- \longrightarrow 4OH^-$$

$$\text{Anode: } 2H_2 + 4OH^- \longrightarrow 4H_2O + 4e^-$$

$$\text{Overall reaction: } 2H_2 + O_2 \longrightarrow 2H_2O$$

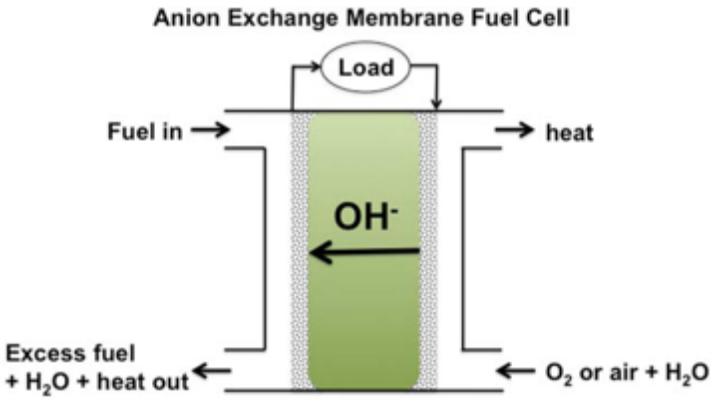

Figure 1.1 A schematic of an alkaline fuel cell fueled with hydrogen.

Traditional alkaline fuel cells operate with KOH as electrolyte and have advantages over PEMFC: (1) enhanced kinetics of oxygen reduction at cathode and less alcohol permeability through the membrane, which could decrease the fuel loss, increase cathode potential and have the potential for use of non-precious metals as catalyst such as Ag or Ni, which could greatly reduce the cost of AEMFCs;[15-18] (2) improved membrane swelling and water management.[15] However, the liquid electrolyte brings problems of potential leakage and also bicarbonate and carbonate salts can be formed that precipitate and block the pores of the catalysts therefore decreasing fuel cell efficiency.[19]

The emerging anionic exchange membrane fuel cell (AEMFC) adopts polymers functionalized with cationic groups as the solid electrolyte instead of liquid potassium hydroxide or sodium hydroxide as found in the traditional AFC, avoiding the existing problems with liquid electrolyte like leaking or catalyst poisoning induced by carbonate and bicarbonate precipitates.[19]

In the solid AFC, the anion exchange membrane can greatly affect the fuel cell performance. The membrane must meet certain requirements in order to display good performance, long durability, and operate at reasonable cost. Considering the humid and basic

environment for a fuel cell at elevated temperatures, the anion exchange membranes need to meet these requirements:

- High hydroxide ion conductivity
- High thermal and mechanical stability while remaining insoluble in water
- Minimal dimensional swelling during operation
- Barrier for electrons and fuels between cathode and anode
- Good chemical stability under alkaline environment
- Low interfacial resistance between the AEMs and the electrodes

The operation of an AFC requires the anion exchange membranes to transport hydroxide ions from the cathode to the anode in order to produce electric current. High ionic conductivity is necessary for anion exchange membranes to lower the cost by requiring fewer combined cells in a fuel cell stack. The fewer cells can enhance the fuel cell performance by the reduced resistance loss.[20]

Elevated conductivity can be achieved by higher ion exchange capacity from more ion conducting groups attached to the polymer.[20] However, the mechanical properties of the membrane tend to be compromised from the excessive water uptake that typically coincides with the increased number of ionic conducting groups. Furthermore, greater swelling occurs with more ion conducting groups while dimensional stability is necessary for the application in fuel cells. Due to the trade-off between water uptake, dimensional swelling and ion exchange capacity for a given polymer system, a balance must be found. Different polymer materials should be studied to find systems that can maintain reasonable mechanical properties with high ion exchange capacity.

Ionic conductivity of the AEMs can be affected greatly by the hydration level such that water management is important in AFCs, where water is produced at the anode and consumed at the cathode. Due to the water concentration difference between the electrodes, water can diffuse from the anode to the cathode. The hydroxide ions are generated in the cathode and the electro-osmotic drag can bring water through the membrane from the cathode to the anode, where the electro-osmosis of the water flux is accompanying the hydroxide flux. It has been shown that the overall water movement direction is from the anode to the cathode in AFCs.[21] Therefore if the water management is not efficient, the cathode can suffer from dehydration due to the fast decrease of relative humidity in the cathode, and the anode can suffer from flooding phenomenon where the contact between the hydrogen and the anode is blocked because water is filled in the pores of the anode.[22]

The membrane is also required to be stable under an alkaline environment because the cationic groups are susceptible to the nucleophilic attack from hydroxide ions.[23] The degradation of the cationic groups can cause the loss of ion conducting groups and therefore decreasing the ionic conductivity of the polymer electrolyte. Chemically stable cations are required to be applied in AFCs so that stability studies of the catonic groups should be conducted before consideration of the cations in AEMs.

The anion exchange membranes should be barriers for the electrons to force the electrons to move through an external circuit and create an electric current. It is also important for anion exchange membranes functioning as barriers for the fuels because the diffusion of the fuels will decrease the efficiency of the fuel cells.

Different processing techniques can affect the performance of the AEMs so that the processing methods should be investigated to achieve balanced ionic conductivity and water uptake for the membranes. Another requirement for useful anion exchange membranes is a simple synthesis method as the membrane should be readily synthesized and scaled up for commercialization.

The interfacial resistance between the electrodes and the AEMs is important in AFCs because the interfacial resistance is associated with the electrode performance. One way to reduce the interfacial resistance is to bind certain amount of polymer electrolyte in the electrode to extend the electrochemical triple-phase boundary formation.[24] Because the polymer electrolytes bound with the electrodes need to be soluble for processing,[25] it is possible that the electrode bound polymer electrolytes and the AEMs are different and the compatibility between the electrolytes is important. The chemical similarity of the polymer electrolyte in the electrodes and in the membrane needs to be considered in the design of the AEMs.

In this dissertation, emphasis was placed on the evaluation of the chemical stability of guanidinium groups under alkaline environment. Efforts were made to increase the alkaline stability of guanidinium group through bulkier substituting group with higher electron-donating ability. The design of AEMs was investigated for high ionic conductivity and low water uptake in this dissertation. Block copolymers were utilized due to their potential to displaying phase separation between the hydrophilic phase and hydrophobic phase. The connected hydrophilic phase can facilitate the formation of ion conducting pathways and increase the ionic conductivity. Different processing techniques were studied for the AEMs in this dissertation including melt pressing and solvent casting. Block copolymers with different ion exchange capacity values were

controlled by the length of the hydrophilic block and quaternized AEMs were studied regarding their water uptake, phase separated structures, and conductivities with different counter ions.

High ionic conductivity can be achieved with more ionic groups and the extreme scenario is attaching ionic groups on every repeat unit of the polymer. However, too many ionic groups can make this polymer soluble in water and unable to maintain properties during fuel cell operation. So anion exchange membranes have been designed with a hydrophobic part and a hydrophilic part. The hydrophobic component functions as the mechanical matrix to keep the membrane from dissolving and sustain the integrity of the membrane under the dynamic temperature and humidity environment in fuel cell operation. The hydrophilic component performs as the ion-conducting carrier to transport the hydroxide ions from the cathode to the anode.

1.4 Different methods to generate hydrophobic and hydrophilic segments in anion exchange membranes

Multiple synthetic methods can be used to generate the both the hydrophobic and hydrophilic parts in an anion exchange membrane. The dispersion of the ionic sites can be spread randomly through the polymer chain or connected to each other in segments or blocks. Much research has been done on post-functionalization of existing polymers to generate randomly distributed ionic groups.[26-28] Other research has been directed to the use of functional monomers for the random distribution of hydrophilic ionic groups,[29,30] while more recent research has investigated the synthesis of block copolymers where only one of the blocks can be functionalized.[31-33] Proper selection of monomers and rationale polymer design can generate hydrophilic and hydrophobic groups in a controlled way along the polymer backbone.

1.4.1 Generation of hydrophobic and hydrophilic parts through random copolymers

1.4.1.1 Random copolymers based on poly(2,6-dimethyl-1,4-phenylene oxide) (PPO)

PPO is an engineering polymer with good film forming ability, high thermal and chemical properties.[34] The substituted methyl groups, aromatic ring, and terminal phenolic groups provide opportunities to modify PPO with functional groups to be applied in alkaline fuel cells. The methyl groups can undergo radical substitution reactions like bromination and chlorination. The aromatic ring can be substituted through electrophilic reactions such as bromination, chlorination, choromethylation or Friedel-Crafts alkylation/acylation. The phenolic groups can be employed for polycondensation reactions.[35-37]

The methyl groups of PPO have been used for modification through radical bromination using either liquid bromine or N-bromosuccinimide. In a specific example, Wu and coworkers developed different series of silica/PPO hybrid anion exchange membranes.[38-40] These hybrid membranes were designed because the predicted combined merits from the ion conducting organic component and the good mechanical strength, chemical and thermal stability from the inorganic component. PPO was brominated and then reacted with 3-aminopropyl-trimethoxylsilane and trimethylamine to give a dipping solution. The hybrid membranes were then prepared by dipping an alumina plate in the dipping solution and then dried at elevated temperature. The resulting membrane showed improved thermal stability and microphase separation.[38]

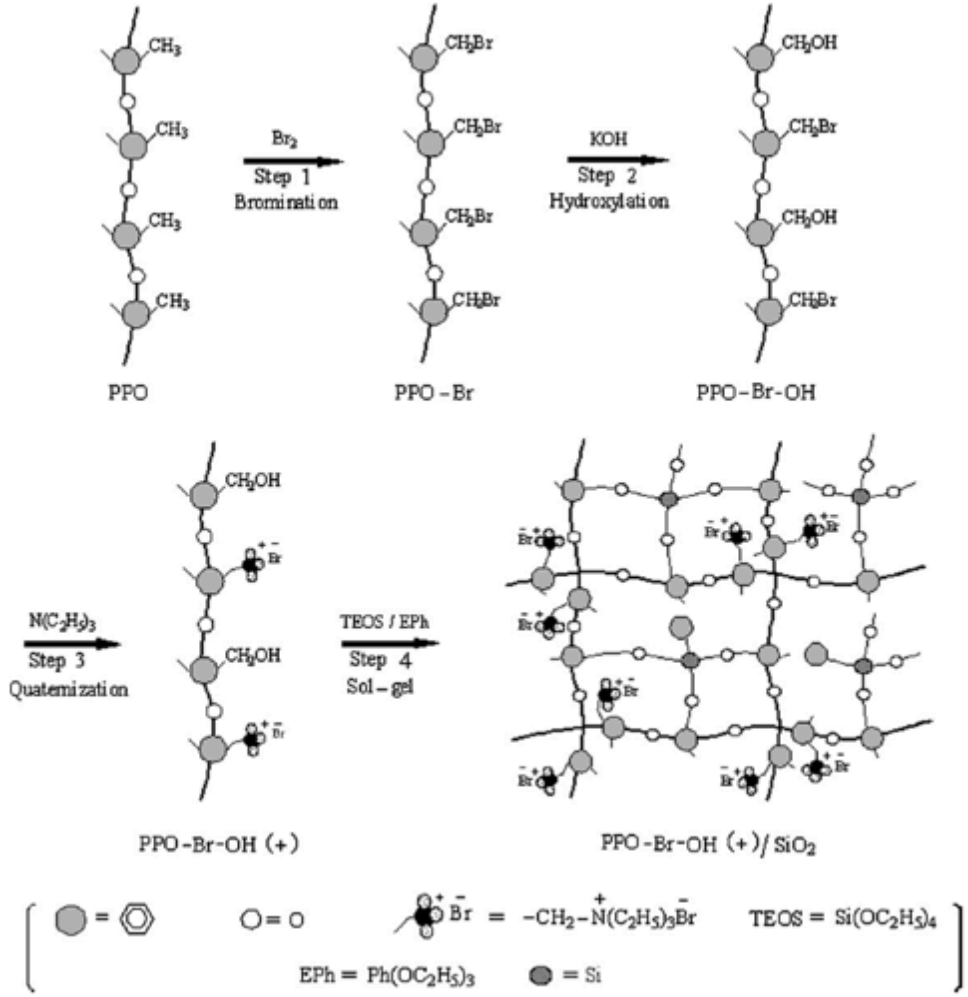

Figure 1.2 Synthetic route for crosslinked hybrid membrane based on PPO.

Wu and coworkers later deepened the hybrid membrane work by crosslinking the quaternized hybrid PPO.[39] They found that the IEC value and water uptake was greatly reduced, alkaline resistance and thermal stability was improved. However, the membranes after thermal treatment showed hydroxide conductivity between 1 to 8.5 mS/cm, which is too low for application. Later Wu and coworkers extended their work to crosslinking between silica and PPO, instead of thermal treatment induced crosslinking.[40] The original PPO underwent bromination, partial hydrolysis, quaternization, and sol-gel process to give the final crosslinked

hybrid membrane (Figure 1.2). Compared with their previous research, the membranes from this study showed improved swelling resistance and higher ion exchange capacities.

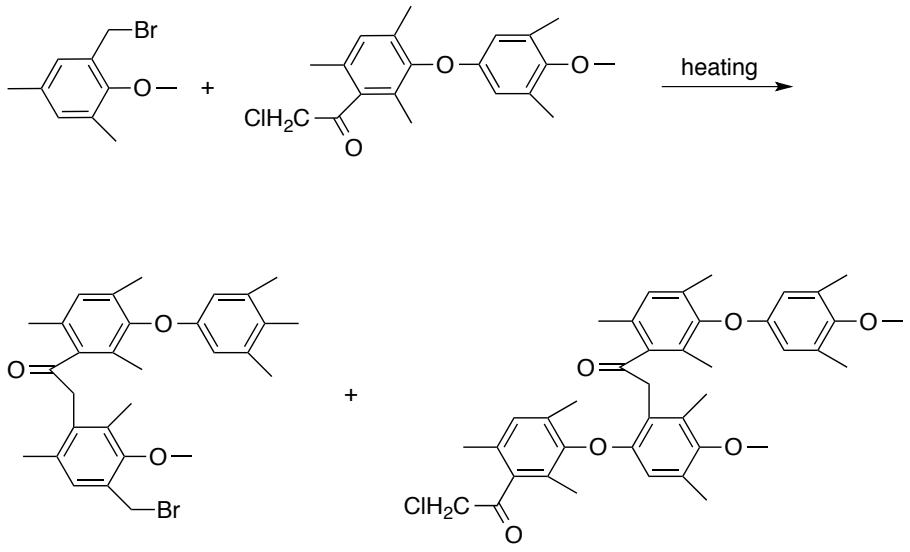

Scheme 1.1 Crosslinking between chloroacetylated PPO and brominated PPO during heat treatment.

PPO can also be chloroacetylated for synthesis of anion exchange membranes. Zhang and coworkers chloroacetylated PPO through a Friedel-Crafts reaction.[41] The chloroacetylated PPO was then blended with brominated PPO then dissolved in chlorobenzene. The solution was then cast on a clean glass slide dried at 30 °C. Crosslinking was carried out during the drying process like Scheme 1.1 shows. Their research showed that the properties of the quaternized membrane, such as ion exchange capacity, water uptake, hydroxide conductivity, and methanol permeability decreases with increased chloroacetylated PPO percentage. A blend percentage of chloroacetylated PPO of 30 ~ 40 % was recommended in this research.

1.4.1.2 Random copolymers based on polysulfone

Polysulfone is known for its high thermal and chemical stabilities, excellent mechanical properties, good film forming ability, and solubility in multiple solvents.[42] Extensive research has been done using modified polysulfone in anion exchange membrane applications. A common method for modification is to functionalize polysulfone with cationic groups through chloromethylation and quaterization. Wang and coworkers studied the optimized conditions for chloromethylation and different quaternization approaches.[43] They found gelation could happen at certain chloromethylation extent. Later research showed that chloromethylation for 75 min at 40 °C gave the highest extent of chloromethylation with the least gelation. Pan and coworkers also modified polysulfone with benzyltrimethylammonium cations.[44] The resulting membranes showed reasonable hydroxide conductivities (22 mS/cm at 25 °C), high mechanical properties, and good alkaline stabilities. The good solubility of the quaternized polymer in organic solvents makes it able to be recast into films. However, the problem for this research is that the substitution can never reach one chloromethyl group per repeat unit. And the resulting quaternized polymer only had ion exchange capacity as high as 1.18 meq/g.

Watanabe and coworkers increased the ion exchange capacity through a polysulfone synthesized using 9,9'-bis(4-hydroxyphenyl)-fluorene instead of bisphenol A.[45] The synthetic route is presented in Scheme 1.2. This polysulfone could carry as high as 1.8 chloromethyl groups per repeat unit without significant side reactions. The resulting quaternized polymer was obtained through quantitative reaction with trimethylamine, which exhibited high ion exchange capacity as high as 2.5 meq/g. The membrane with the highest IEC also showed the highest hydroxide conductivity in this series, 50 mS/cm at 30 °C and 78 mS/cm at 60 °C.

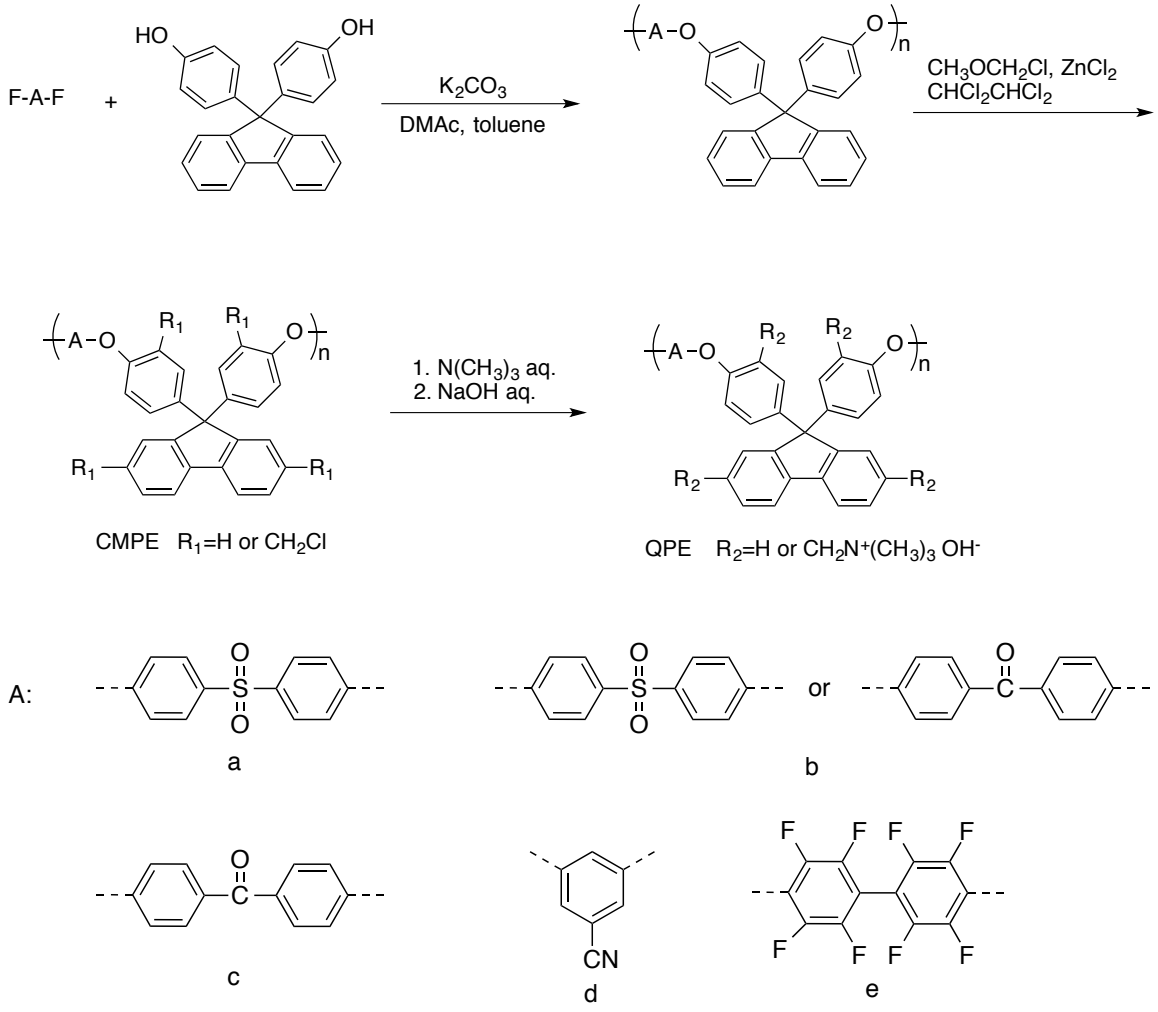

Scheme 1.2 Synthesis of polyethers (PEs), chloromethylated polyethers (CMPEs), and quaternized ammonio-substituted polyethers (QPEs) containing (a) biphenyl sulfone, (b) biphenyl sulfone/biphenyl ketone, (c) biphenyl ketone, (d) benzonitrile, and (e) perfluorobiphenyl moieties.

1.4.1.3 Random copolymers based on poly(phenylene)

Hibbs and coworkers developed anion exchange membranes based on poly(phenylene), which is a wholly aromatic polymer exhibiting excellent chemical stability (Scheme 1.3).[26] High molecular weight poly(phenylene) was synthesized in this research and resulting anion exchange

membrane was robust and creasable. The quaternized membrane showed hydroxide conductivity as high as 50 mS/cm. The anion exchange membrane also showed higher water uptake compared to that based on polysulfone with similar ion exchange capacities. The loose packing of the poly(phenylene) based polymer was speculated to be the reason due to the irregularity of the poly(phenylene) backbone and the bulky pendent groups.

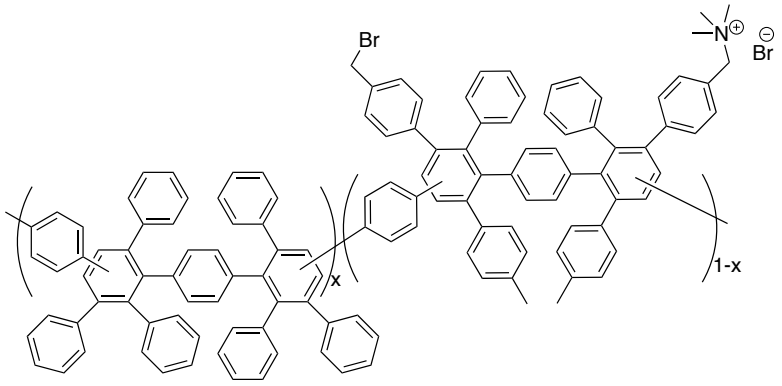

Scheme 1.3 Poly(phenylene) based anion exchange membrane.

1.4.1.4 Random copolymers based on ring opening metathesis polymerization synthesized polyolefins

Coates and coworkers synthesized tetraalkylammonium functionalized polyethylene through ring opening metathesis polymerization for anion exchange membrane.[46] The advantage of using ring opening metathesis polymerization is the high tolerance to various functional groups of using Grubbs 2nd generation catalyst. This polymerization can proceed with the presence of cationic groups on the monomer, providing the synthetic method without the need for post-polymerization modification and thus simplifying the synthetic process.

The synthetic route for the membrane is presented in Scheme 1.4. The membrane exhibited an IEC value of 1.50 meq/g with a water uptake of 132 %. The corresponding

hydroxide conductivity was 48 mS/cm at 20 °C and 65 mS/cm at 50 °C. This quaternized polymer was also found to be soluble in aqueous *n*-propanol (50 vol. % of water), but insoluble in aqueous methanol (50 vol. % of water), demonstrating solvent processability in low boiling point solvent and the ability to be applied in fuel cells because of the insolubility in water and methanol.

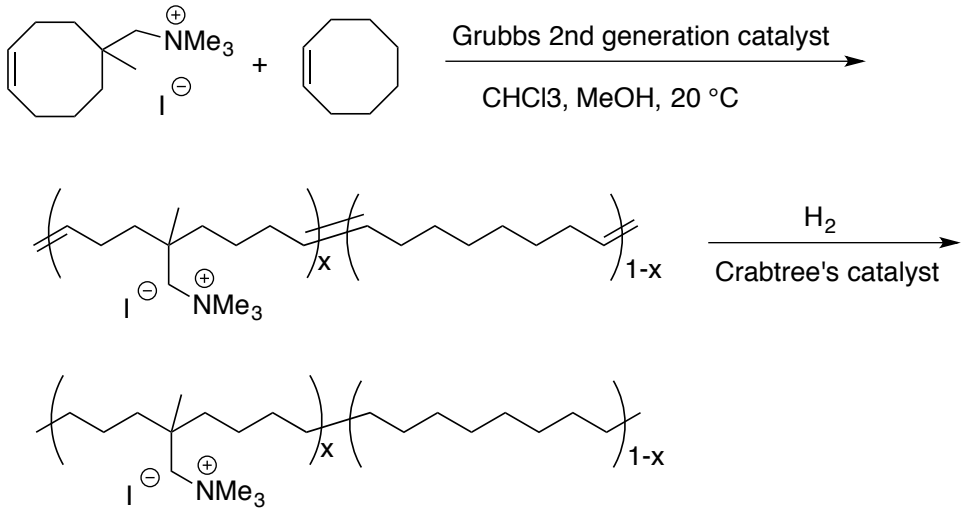

Scheme 1.4 Synthesis of tetraalkylammonium functionalized polyethylene through ring opening metathesis polymerization.

1.4.2 Generate hydrophobic and hydrophilic part through block copolymers

Taking the mobility of hydroxide ion into account, the above research reports demonstrate encouraging conductivities compared to proton exchange membranes because the mobility of proton is faster than hydroxide ion by a factor of 1.77.[47] The above research all revealed the importance of connected hydrophilic phases in the anion exchange membrane to efficiently transport hydroxide ions. A recent study by Balsara and coworkers showed that micro-phase separation could affect the membrane performance in ionic conductivity, water

uptake and mechanical properties.[48] The study shows that random copolymers tend to have isolated ionic clusters due to the random nature of the copolymer. Ion-free domains exist in the anion exchange membrane and the transportation of hydroxide ions is interrupted. Therefore, the hydroxide conductivity is compromised. At the same time, block copolymers could suppress the formation of separated ionic clusters through directed microphase separation, potentially resulting in a homogenous ion-conducting microphase.[48] In this case, the hydrophobic phase behaves as the mechanical support and the hydrophilic phase behaves as the ion transportation carrier through the conducting pathways. The ionic conductivity can be improved with the reduction or absence of spacing between the ion clusters where the ion motion is impeded.

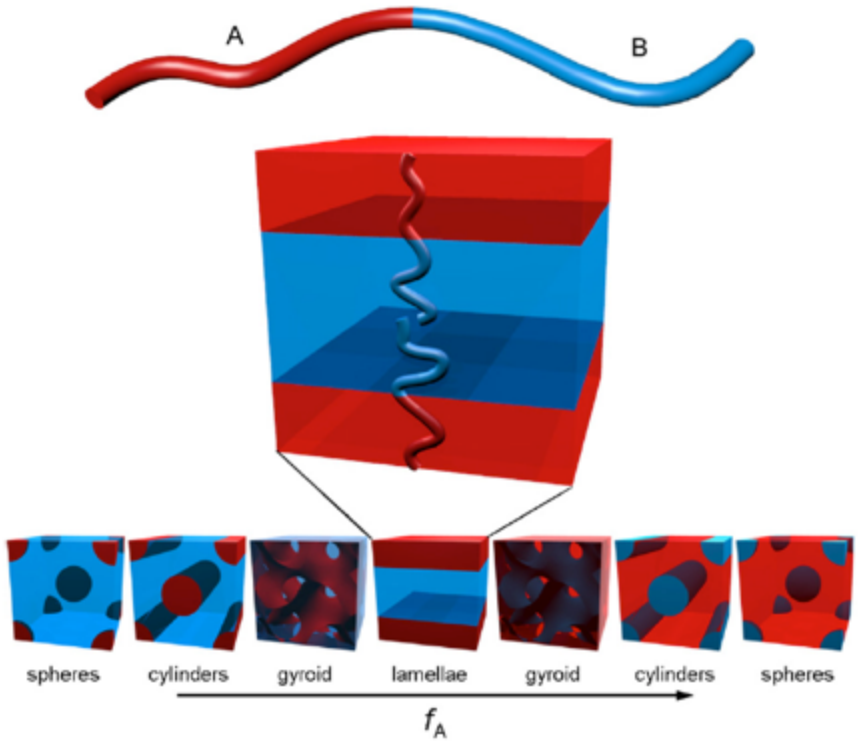

Figure 1.3 Schematics of phase separation of A-B diblock copolymers. The morphology of the micro-phase separation depends on relative weight percentage of the two polymer blocks (f_A).

Multiple groups have studied the phase-separated behavior of block copolymers in the past years.[49-52] Figure 1.3 demonstrates the morphology of A-B diblock copolymer corresponding to different weight percentage of the A block. It is clear to see that as the weight percentage of the A block increases, the morphology of the polymer changes from discontinuous spheres to continuous cylinders, gyroid, and lamellae. Phase inversion occurs as the A block becomes the major phase. For fuel cell applications purpose, the hydrophilic phase is required to be continuous to guarantee high ion conductivity. Therefore, morphologies like cylinder, gyroid, and lamellae are preferred in the fabrication of anion exchange membranes.

1.4.2.1 Generate hydrophobic and hydrophilic part through atom transfer radical polymerization (ATRP)

ATRP is a controlled/living radical polymerization technique that can synthesize block copolymers with uniform polymer chain length.[53] If the blocks from the copolymer are immiscible, phase separation occurs and different morphologies develop depending on the ratio of the blocks ranging from cylinder, lamellar, bicontinuous, gyroid, and so on.[54] Since the benzyl chloride group can readily react with trimethylamine to produce benzyltrimethylammonium groups, vinylbenzyl chloride is often a desirable monomer in the synthesis of anion exchange membranes with amine quaternization performed in a post-polymerization functionalization. However, ATRP is not suitable for polymerizing vinylbenzyl chloride because the dissociation between carbon and chloride bond would lead to a hyperbranched polymer.[55,56]

Coughlin and coworkers synthesized polystyrene-*b*-poly(vinylbenzyl trimethylammonium) copolymers directly through ATRP.[33] Instead of using vinylbenzyl chloride as the starting material, quaternized vinylbenzyltrimethylammonium chloride was used as

monomer (Scheme 1.5). The counterion was found to be important for maintaining solubility of the amphiphilic polymer. From this synthetic route, well-defined block copolymers were synthesized and micro-phase separation of the block copolymers was determined by small-angle X-ray scattering. The morphology of the three samples in this study, PS-*b*-PVBTMA-0.58, PS-*b*-PVBTMA-1.19, PS-*b*-PVBTMA-1.36 (the number at the end of each sample name represents the corresponding ion exchange capacity), were found to be spherical, cylindrical, and lamellae, respectively.Their research also found that the three samples showed that higher ion exchange capacity resulted in higher conductivity above 45 °C under 50 % relative humidity (Figure 1.4 (a)). However, under the same relative humidity when the temperature was under 45 °C, the conductivity had a reverse order with ion exchange capacity (Figure 1.4). This reversed feature was explained by the swelling and shrinkage of the PVBTMA[OH] domain and the presence of grain boundaries in the microstructure. For the samples with the cylinder and lamellar morphology, PS-*b*-PVBTMA-1.19 and PS-*b*-PVBTMA-1.36, SAXS measurements showed that different temperatures at 50 % relative humidity did not induce any morphological transition or *d*-spacing change. Therefore, these two samples kept the same *d*-spacing and the same morphology at 50 % relative humidity at different temperatures. Low temperature at 50 %RH lead to the shrinkage of PVBTMA[OH] domain and the appearance of grain boundaries in the microstructure, accompanied by the reduced efficiency for ion transportation; therefore, the ion conductivity of the sample was reduced. As the temperature increased, the PVBTMA[OH] domain swelled and connected to form effective ion conducting pathways and then resulted in higher conductivity. For the sample with spherical morphology, PS-*b*-PVBTMA-0.58, its smaller *d*-spacing already made the conducting pathways packed with the PVBTMA[OH] spheres at low temperature and relative humidity. The further temperature increase induced swelling could not

have as significant an impact on conductivity as the samples with cylindrical or lamellar morphologies.

Figure 1.4 (b) showed the conductivity of PS-*b*-PVBTMA-0.58, PS-*b*-PVBTMA-1.19, PS-*b*-PVBTMA-1.36 at different temperatures under 70 % relative humidity. A similarly reversed trend was found with a refraction temperature at 35 °C, which was lower than that at 50 % RH (45 °C). This is because lower temperature was required to facilitate ion transportation at relatively higher humidity.

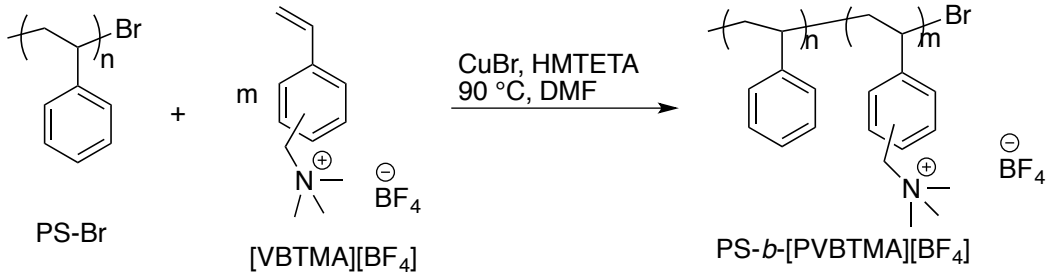

Scheme 1.5 Synthesis of polystyrene-*b*-poly(vinyl benzyl trimethylammonium tetrafluoborate) (PS-*b*-PVBTMA[BF_4] block copolymers.

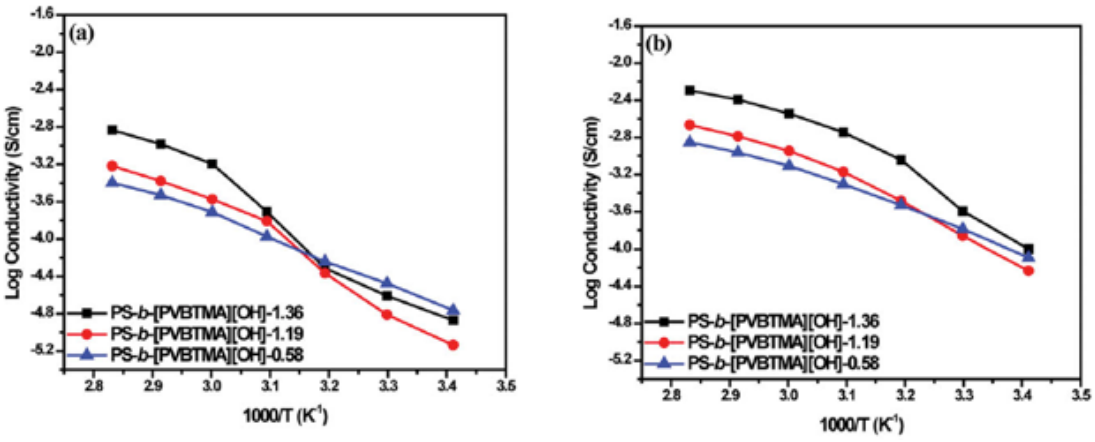

Figure 1.4 Temperature-dependent conductivity of PS-b-PVBTMA[OH] membranes at (a) RH = 50%, (b) RH =70%.

1.4.2.2 Generate hydrophobic and hydrophilic part through nitroxide mediated polymerization (NMP)

Nitroxide mediated polymerization is a controlled/living radical polymerization technique that can be applied in polymerizing vinylbenzyl chloride for anion exchange membrane synthesis. Balsara and coworkers synthesized polystyrene-*b*-poly(vinylbenzyl chloride) through NMP.[57] The polymer was then quaternized with either trimethylamine or *n*-butylimidazole to produce polystyrene-*b*-poly(vinylbenzyltrimethylammonium) and polystyrene-*b*-poly(vinylbenzylbutylimidazolium), which was referred to as SAM and SIM (Scheme 1.6).

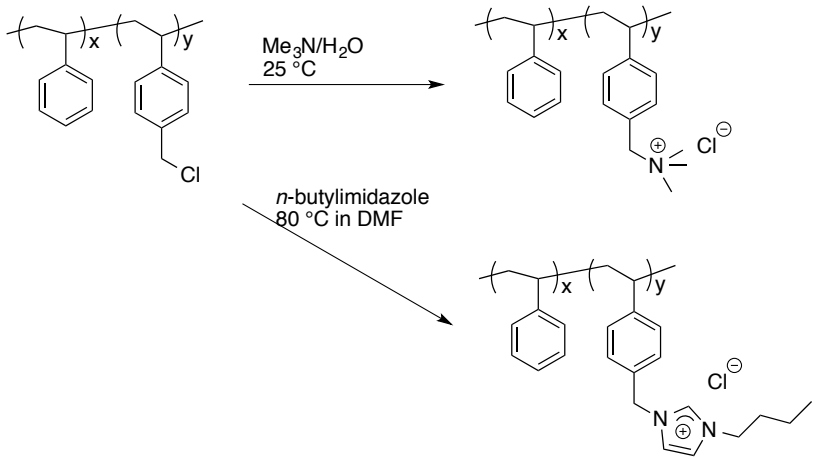

Scheme 1.6 Synthesis of polystyrene-*b*-poly(vinylbenzyl trimethylammonium chloride) and polystyrene-*b*-poly(vinylbenzyl butylimidazolium chloride).

The SAXS measurements to SAM and SIM that derived from the same polystyrene-*b*-poly(vinylbenzyl chloride) precursor showed similar SAXS profiles regardless of the different quaternized groups. They also found the peak width in the SAXS profiles of SIM was smaller

than that for SAM. Another difference between SAM and SIM is that the SIM membranes equilibrated more slowly in liquid water than SAM membranes. They also studied the influence of different counter ions on the ionic conductivity of the SAM and SIM membranes. The conductivity increased by a factor of 10 when the counter ion was switched from chloride to hydroxide.

Mahanthappa and coworkers also synthesized polystyrene-*b*-poly(vinylbenzyl alkylimidazolium) from quaternization of NMP synthesized polystyrene-*b*-poly(vinylbenzyl chloride).[58] A series of samples were synthesized through the synthetic route in Scheme 1.7 in this research and different morphologies from lamellae to cylinder were obtained from SAXS and TEM measurement.

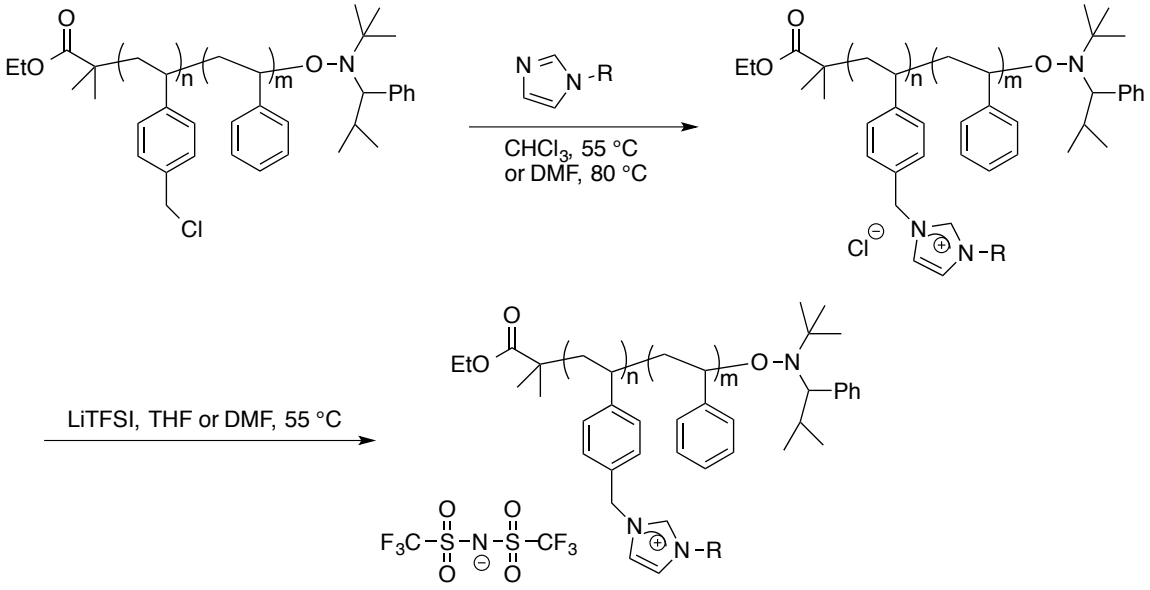

Scheme 1.7 Synthesis of polystyrene-b-poly(vinylbenzyl alkylimidazolium) block copolymers.

The conductivity measurement showed that the lamellae sample (derived from PS-*b*-PVBC having 17.0 % PVBC) exhibited conductivity higher than the lamellae with cylinder

coexistence sample (derived from PS-*b*-PVBC having 8.6 % PVBC) by an order of magnitude. The decrease of conductivity of the latter sample was explained by the defects in cylindrical morphology. The existence of the grain boundaries in cylindrical morphology could damage the ion pathway connectivity and compromise the conductivity. This phenomenon demonstrated the importance of the connected hydrophilic pathways to the efficiency of ion transportation and ion conductivity, which was further supported by the low conductivity for the sample with poorly arranged cylindrical morphologies.

1.4.2.3 Generate hydrophobic and hydrophilic part through reversible addition-fragmentation chain-transfer polymerization (RAFT)

Hickner and Wang synthesized poly(vinylbenzyl chloride)-*b*-poly(butenylstyrene) through RAFT polymerization and the copolymer was then crosslinked through metathesis reaction, followed by quaternization in trimethylamine to produce the anion exchange membrane.[59] The synthetic route is displayed in Scheme 1.8. Bifunctional monomer, 4-(3-butenyl)styrene, was used in this research. This monomer combined the polymerizable styrene group and a butane group, which could form a block copolymer with pendent groups that enable the crosslinking of the polymer through metathesis reaction. Crosslinked and uncrosslinked AEMs were prepared in this research. SAXS measurements showed that the uncrosslinked AEMs had a narrow scattering peak with higher order reflections, indicating long-range morphologies. In contrast, crosslinked AEMs showed only a broad scattering peak, which was explained by the limited time for the organization and restriction of the polymer during solvent casting and crosslinking. This study also showed that the crosslinked AEMs had lower water

uptake and reduced dimensional swelling than the crosslinked ones. The crosslinked feature restrained the arrangement of the morphologies in the film, leading to films without long-range configuration. The morphologies of the AEMs was proven to be important in the efficient ion transport and increasing ion conductivity.[58] However, the advantage of crosslinking was also proven in this study[59] for the reduced water uptake and suppressed dimensional swelling. A balance should be found in the crosslinking extent to have desirable ion conductivity and suppressed dimensional swelling and water uptake.

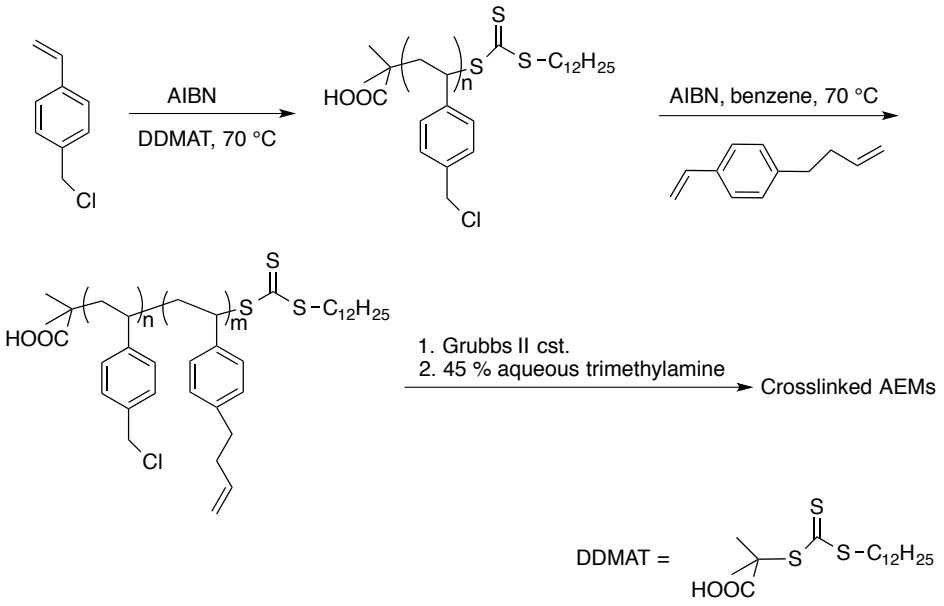

Scheme 1.8 Synthetic route of crosslinked AEM through RAFT synthesized poly(vinylbenzyl chloride)-b-poly(butenyl styrene) and crosslinking by Grubbs II catalyst.

1.4.2.4 Generate hydrophobic and hydrophilic part through multi-block copolymer synthesis

Multiblock copolymers are usually synthesized by polycondensation through step-growth polymerization.[60] Watanabe and coworkers synthesized multiblock copolymers for anion

exchange membrane application based on poly(arylene ether).[31] The synthesis of multiblock copolymer required the synthesis of two complementary sets of oligomers. These two sets of oligomers needed to have different end groups that can subsequently react. The multiblock copolymer was then synthesized by reacting the two sets of oligomer under step growth polymerization conditions. Two kinds of blocks were obtained in the multiblock copolymer originated from the two sets of oligomers. In the research od Watanabe and coworkers, one kind of blocks cannot be chloromethylated while the other kind of the block can be chloromethylated and then quaternized. Therefore, one of the blocks becomes the hydrophobic matrix and the other kind becomes the hydrophilic domain, leading to micro-phase separation and organized arrangement. The generation of the hydrophobic and hydrophilic domains in the multiblock copolymer is presented in Scheme 1.9.

Compared to previous investigation on the similarly composed but random AEM,[45] the multiblock AEM in this study was synthesized by optimizing the chloromethylation conditions and the chloromethylated group reached 2.78 per repeat unit. The membrane with the highest ion exchange capacity in this study, 1.93 meq/g, exhibited hydroxide conductivity as high as 144 mS/cm at 80 °C. STEM images demonstrated that the multiblock copolymer had distinct micro-phase separation between the hydrophobic and hydrophilic domains. Compared to the random fluorenyl AEMs with the same repeat groups, the multiblock AEMs maintained their mechanical properties and chemical stabilities. Their research on the random and multiblock fluorenyl containing poly(arylene ether) again supported the importance of phase separation and connected ion pathways to higher ion conductivity. The multiblock copolymers showed their potential in alkaline fuel cell applications by the increased conductivity compared to the random copolymers

with same ion exchange capacity, and at the same time maintained excellent mechanical properties.

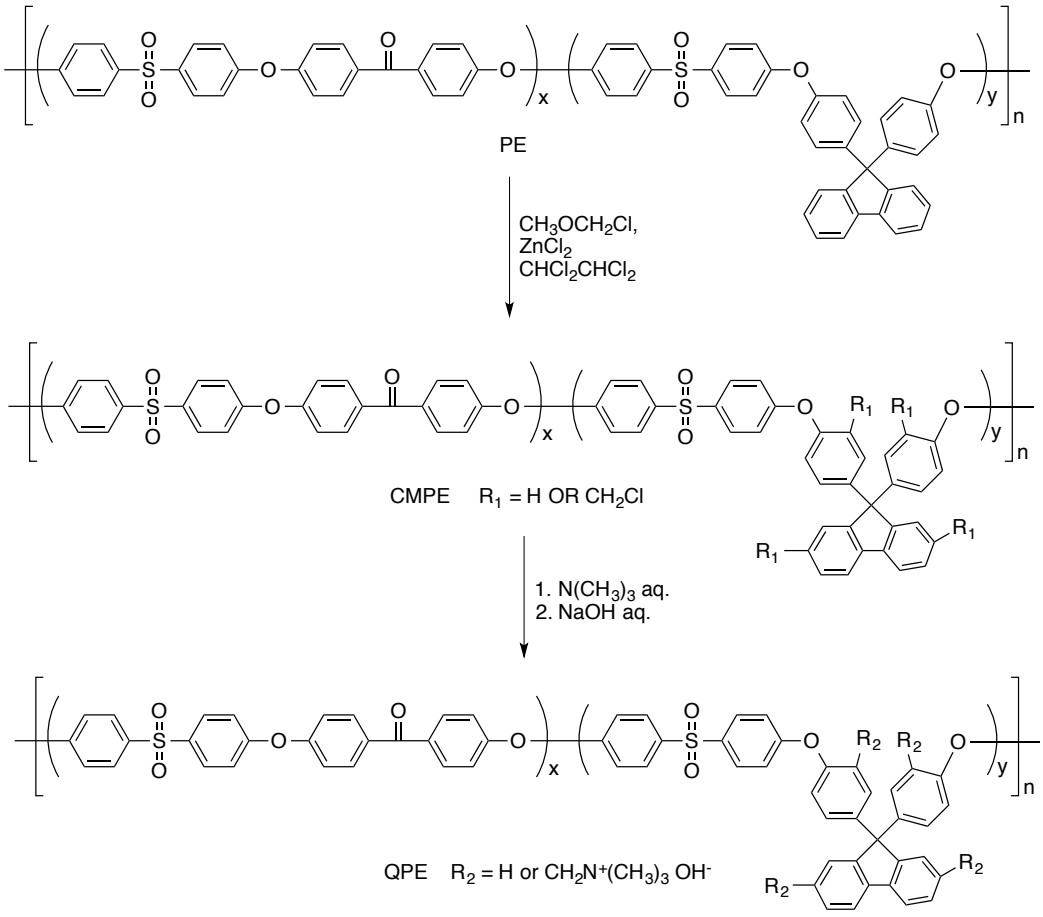

Scheme 1.9 Chloromethylation and quaternization of multiblock poly(arylene ether).

Guiver and coworkers developed multiblock copolymers with pendent quaternized ammonium groups.[61] Previous efforts on proton exchange membrane demonstrated that the pendent side chain connected the polymer chain with the ammonium groups, which could improve the hydrophobic/hydrophilic phase separation and increase ionic conductivity and suppress water uptake.[62-64] Guiver and coworkers synthesized the polysulfone based quaternized

copolymer. The ammonium groups were doubly attached to a pendent group to the polymer chain (Scheme 1.10). This polymer showed low water uptake and low methanol permeability. And the membrane with IEC of 1.74 meq/g and water uptake of 20.8 % at 60 °C showed the highest hydroxide conductivity in this study, which was 58 mS/cm at 80 °C. The obtained high conductivity at the low water uptake and low ion exchange capacity showed the great potential of using multiple cationic sites on side chains from the polymer main chain. However, the phenyltrimethylammonium group was found lacking sufficient stability under alkaline conditions and not suitable to be applied in alkaline fuel cells. However, the concentrated ionic groups at the end of the side chains proved to be efficient for ion conduction from a polymer design perspective.

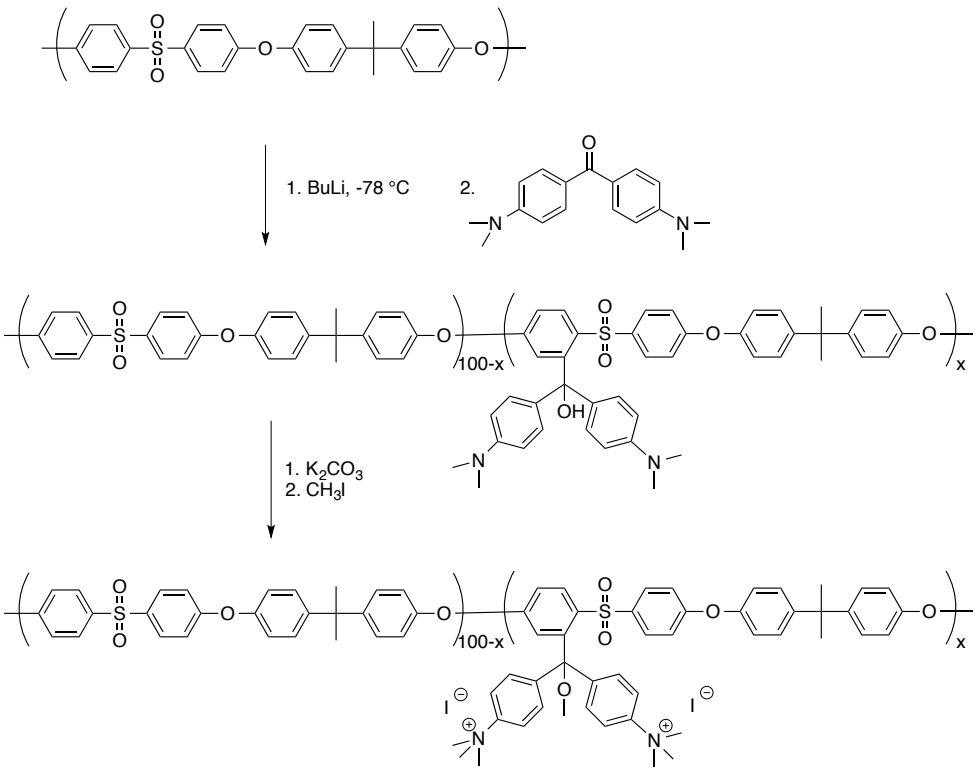

Scheme 1.10. Synthetic route of bis(phenyltrimethylammonium) functionalized copolymer through lithiation chemistry.

Bai and coworkers recently synthesized a triblock copolymer contained a central polysulfone block and two outer poly(2,6-dimethyl-1,4-phenylene oxide) blocks.[65] The structure of the quaternized polymer is presented in Scheme 1.11. The final quaternized AEMs showed promising properties compared to a random quanterized PPO that was also prepared in this study for comparison. While the triblock copolymer poly(phenylene oxide)-*b*-polysulfone-*b*-poly(phenylene oxide) exhibited a water uptake of 53 % with an IEC value of 1.83 meq/g, the quaternized PPO in this study showed a water uptake of 77 % with an IEC value of 1.97 meq/g. Compared to the multiblock copolymer prepared by Watanabe and coworkers,[31] which had a water uptake of 92 % with an IEC value of 1.83 meq/g, the triblock copolymer in this research showed suppressed water uptake. This was explained by the distinct hydrophilic/hydrophobic phase separation in the polymer membrane. The SAXS measurements indicated the quaternized PPO had no characteristic phase separation, while the triblock poly(phenylene oxide)-*b*-polysulfone-*b*-poly(phenylene oxide) copolymers showed phase separation without long-range order. The *d*-spacings of the triblock copolymers were calculated from their SAXS profiles to be around 30 nm. Based on the reduced water uptake for the triblock copolymer compared to the multiblock copolymer, the large size of the hydrophobic phases was proposed to have a positive impact on suppressing water uptake. The conductivity measurement for this triblock copolymer showed the AEM with an IEC value of 1.83 meq/g had hydroxide conductivity as high as 129 mS/cm at 80 °C, revealing potential in fuel cell application.

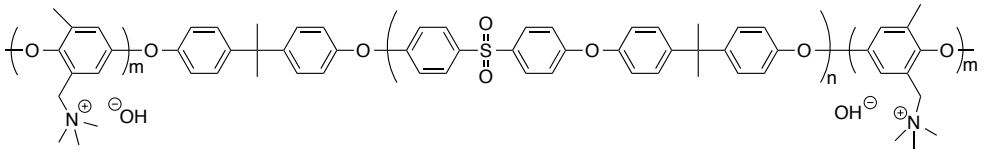

Scheme 1.11. Chemical structure of poly(phenylene oxide)-*b*-polysulfone-*b*-poly(phenylene oxide) triblock copolymer.

1.4.3 Different cations applied in anion exchange membranes

Multiple factors need to be considered in the development of a new anion exchange membrane for alkaline fuel cell applications: high ionic conductivity is crucial to increase the efficiency of the overall fuel cell; good mechanical properties are essential for the handling and assembly for fuel cells; high thermal stability is necessary because higher operation temperature increases the ionic conductivity and fuel cell efficiency accordingly; high chemical stability is vital to the durability and reliability of fuel cell operation. Because higher operation temperature results in higher ionic conductivity and efficiency, it becomes more important to maintain the alkaline stability of the anion exchange membrane at high temperature.

The chemical stability of an anion exchange membrane can be determined by the stability of the polymer backbone, the cationic group that is attached to the polymer backbone, and the chemical linkage between the backbone and the cation. The alkaline stability of the polymer backbone can be controlled by avoiding functional groups that are susceptible to nucleophilic attack by hydroxide ion through proper design and synthesis. In contrast, the cationic groups and the chemical linkages between the polymer backbone and cationic groups are a major concern in current research. The cationic groups in anion exchange membranes are mostly based on ammonium or phosphonium groups, which include the electropositive nitrogens or electropositive phosphorus that are prone to attack by strongly nucleophilic hydroxide ions.

The degradation of quaternized ammonium groups under an alkaline environment can be depicted by two major accepted mechanisms presented in Scheme 1.12: the direct nucleophilic displacement mechanism, and Hofmann elimination mechanism.[19] The former occurs through S_N2 reaction by the direct substitution of hydroxide on the carbon adjacent to the ammonium

group resulting in an amine and an alcohol. The Hofmann elimination mechanism occurs through E2 elimination by the abstraction of the β proton with the products of water, amine, and alkene. Both of the degradation mechanisms exist in the degradation process, resulting in a mixture of products and a loss of the ion conducting cationic groups, resulting in the decrease in ionic conductivity and fuel cell efficiency. However, different alkaline environment conditions and different cationic structures can favor one degradation mechanism over the other. Bulky substitution on the ammonium group can result in Hofmann elimination preferred mechanism. If the β protons are absent in the cation structure, the Hofmann elimination can be prevented. In the design of cation groups for alkaline fuel cell applications, the structures without existing β protons are preferred.

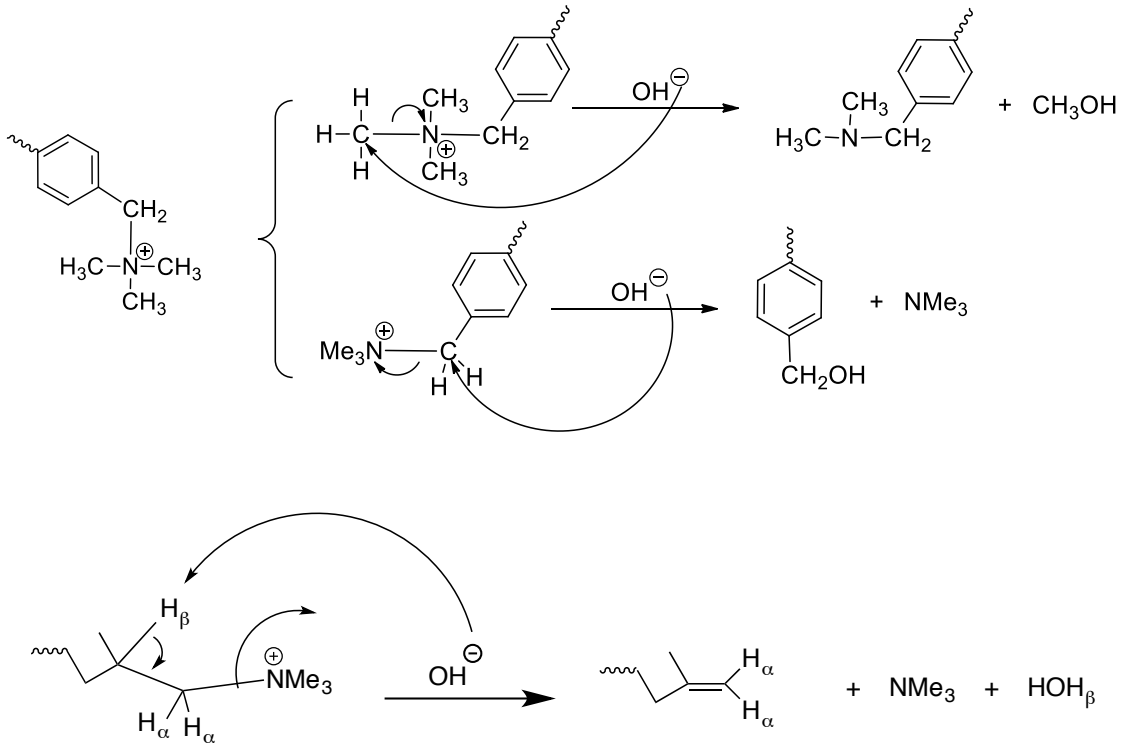

Scheme 1.12. Degradation mechanisms for ammonium groups under alkaline environment.

1.4.3.1 Benzyltrimethylammonium cation

Benzyltrimethylammonium cations are the most often bound cations for anion exchange membranes. One reason is the absence of the β protons in benzyltrimethylammonium, therefore avoiding the Hofmann elimination degradation. Another reason is the facile synthesis by reacting haloalkylated polymeric precursors with trimethylamine. The small size of trimethylamine allows this process at a very high yield by immersing haloalkylated films in aqueous trimethylamine solution.[45,66] This synthetic route provides a convenient method for the situation where the quaternized polymer cannot dissolve in any solvent.

Many of the polymer backbones in current research use aromatic polymers. Choosing aromatic polymers as the backbone is because of the consideration for better mechanical properties and thermal stabilites. Under this situation, benzyltrimethylammonium and phenyltrimethylammonium can be chosen as the cationic groups attached to an aromatic polymer backbone. This choice can also avoid the β protons and the corresponding Hofmann degradation. The stability of benzyltrimethylammonium was compared with phenyltrimethylammonium in a study conducted by Pivovar and coworkers.[67] They conducted stability tests using two model compounds, benzyltrimethylammonium hydroxide and phenyltrimethylammonium hydroxide, at 80 °C to accelerate degradation of the cations. The stability test was conducted in sodium hydroxide solution at three different concentrations. The results revealed that benzyltrimethylammonium was much more stable than phenyltrimethylammonium under all conditions. While benzyltrimethylammonium had 90 % remaining after 29 days under the above conditions, phenyltrimethylammonium had only 20 to 30 % remaining depending on different concentration of sodium hydroxide.

Benzyltrimethylammonium was also compared to tetramethylammonium and tetraethylammonium cations by Herring and coworkers through self-diffusion measurement and simulation.[68] They found that tetramethylammonium had the highest diffusion coefficient, followed by benzyltrimethylammonium and then tetraethylammonium with the same counter ions of chloride. The conductivity measurements showed that benzyltrimethylammonium had the highest conductivity. The difference between diffusivities and conductivity was explained by the difference between the cations with the water around them. This study showed that benzyltrimethylammonium is more suitable compared to simple alkylammonium compounds for alkaline fuel cell applications.

Numerous researchers have utilized benzyltrimethylammonium as the cationic groups. Slade and Varcoe grafted vinylbenzyl chloride onto poly(tetrafluroethylene-co-hexafluoropropylene) (FEP) through radiation grafting to produce FEP-*g*-PVBC copolymer, which was then quaternized by reacting with trimethylamine.[69] The radiation-grafted copolymer has a structure displayed in Scheme 1.13. In this study, they found that the hydration number for AEM was around 28, which was higher than that for the fully hydrated Nafion (λ = 22~23). This phenomenon was explained by two reasons: first, more water molecules could be bound to the larger size of hydroxide ion compared to the size of proton; second, less chance for the AEM with shorter side chains and even distribution of cationic groups to form Nafion-similar ionic cluster model. The activation energy for the AEMs calculated from the conductivity in this research was higher than that for Nafion, due to the hydroxide ion transportation having a stronger dependence on temperature.

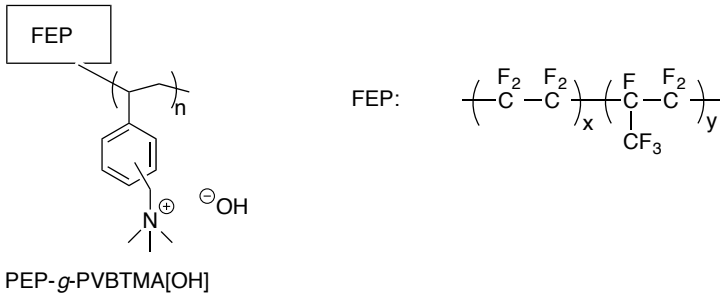

Scheme 1.13. Chemical structure of radiation grafted PVBTMA on FEP substrate.

Benzyltrimethylammonium be used at the end of the pendent group to function as the ion conducting groups, but it can also be used between polymer chains to function as both ion conducting groups and crosslinkers. Coates and coworkers used benzyltrimethylammonium as the crosslinker for a polymer synthesized by ring-opening metathesis polymerization.[70] The synthetic route is presented in Scheme 1.14.

Compound 1 was synthesized to copolymerize with cyclooctene to improve the mechanical properties of the final quaternized films. The crosslinked film swelled in solvents rather than dissolving due to the crosslinking of the film. The TEM image of the AEM showed that the film had a featureless, amorphous morphology, correlating with the random nature of the polymer. Examination of the relationship between mechanical properties and conductivity showed that increased conductivity came with the sacrifice on mechanical properties from the excessive swelling of the film when the crosslinking was not sufficient to resist osmotic pressure. This crosslinked AEM showed ionic conductivity as high as 68 mS/cm at room temperature, and the absence of β proton in the cationic group was expected to provide good chemical stability under alkaline environment.

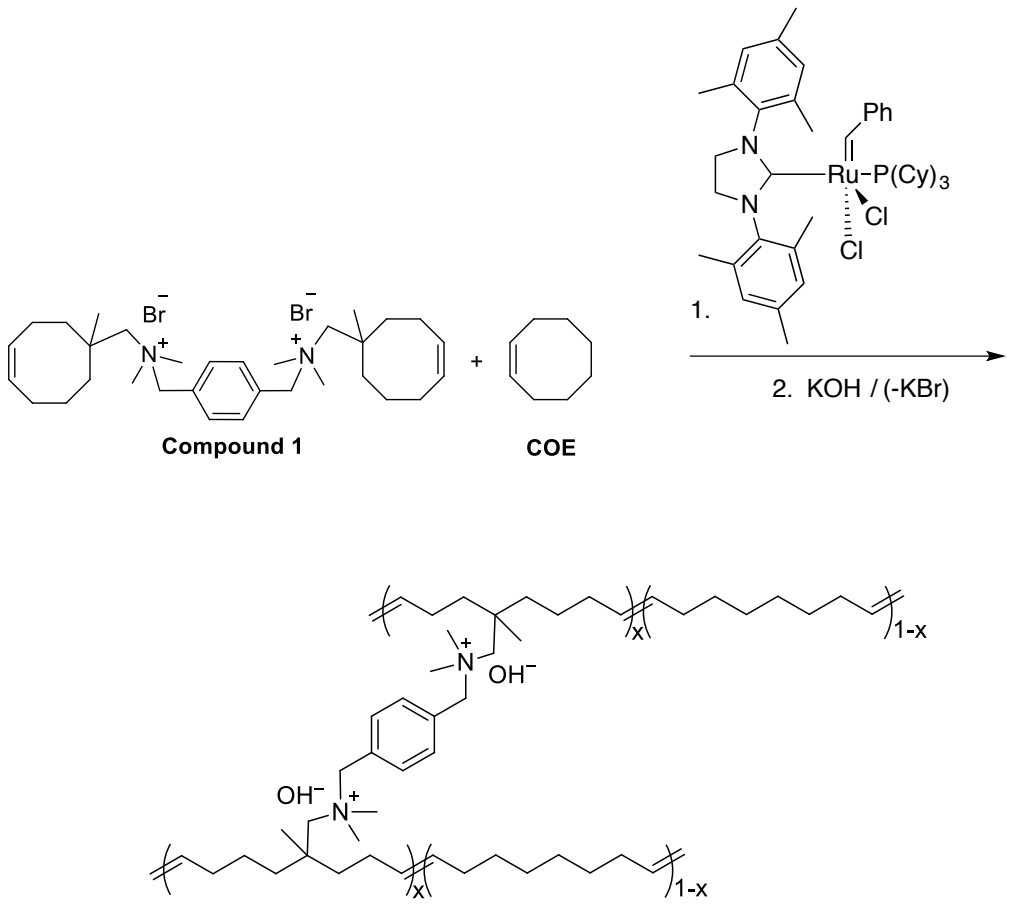

Scheme 1.14. Synthetic route for benzyltrimethylammonium crosslinked AEM.

1.4.3.2 Ammonium groups with spacer chains between benzene ring and quaternary nitrogen

The degradation of benzyltrimethylammonium occurs mainly through direct nucleophilic substitution on either the benzylic or methyl groups (Scheme 1.12). Either substitution results in a loss of the cations and sacrifice of the ion exchange capacity of the anion exchange membrane. The main degradation path is the substitution on the benzylic carbon, which is due to the electron withdrawing effect from the ammonium group and the resonance effect from the benzene ring.[19]

Tomoi and coworkers developed pendent ammonium cations with different alkyl spacer chain lengths between the cation and the phenyl ring.[71] Their structures are displayed in Scheme 1.15. Their research showed that the polymer with propyleneoxymethylene as the spacer chain was less stable than the polymer with benzyltrimethylammonium groups. This decreased stability was due to the accelerated degradation rate through Hofmann elimination. In contrast, polymers with spacers like butylene, heptylene, butyleneoxymethylene, and hexyleneoxymethylene had higher stability than polymers with benzyltrimethylammonium. This was explained by the absence of benzylic carbons that directly connected to the quaternary nitrogen.

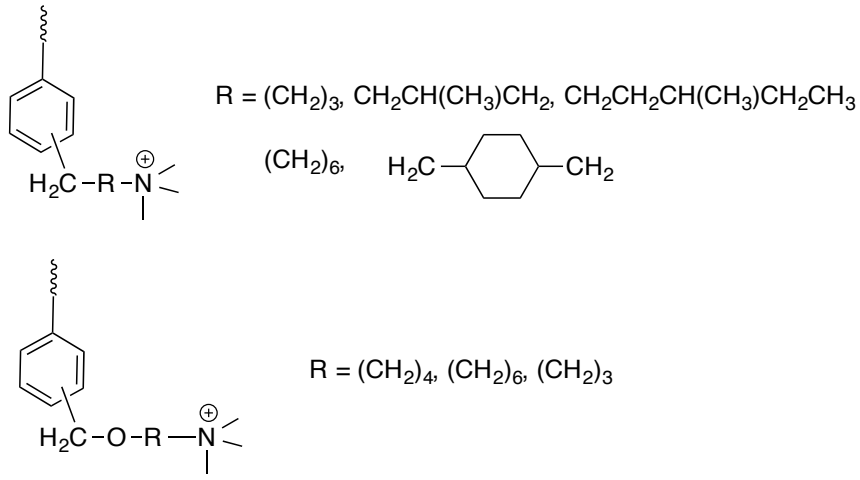

Scheme 1.15. Chemical structures of polymer with spacer inserted ammonium groups.

Wang and coworkers developed comb shaped polymers that also displayed good chemical stability.[25] They also used ammonium groups with a long alkyl chain. Contrary to the work of Tomoi, the alkyl chain was not a spacer between the phenyl ring and quaternary nitrogen, but only connected to the quaternary nitrogen (Scheme 1.16). The amines used in the

synthetic route were N,N'-dimethylhexylamine, N,N'-dimethyldecylamine, and N,N'-dimethyl-1-hexyl-decylamine. The comb shaped polymers all showed low water uptake and dimensional swelling compared to the polymers using the same backbone and benzyltrimethylammonium as the cationic groups. Moreover, the comb shaped polymers also showed higher ionic conductivity compared to the benzyltrimethylammonium polymers with the similar IEC values.

An alkaline stability test at 80 °C showed that the ion exchange capacity of the comb shaped polymer decreased from 2.1 to 1.65 meq/g. In contrast, the ion exchange capacity of the benzyltrimethylammonium polymer decreased from 1.4 to 0.6 meq/g, indicating more than half of the cationic groups degraded. The alkaline stability test showed that the cations with long alkyl chains had higher stability than benzyltrimethylammonium cation. The reason for the good stability was explained by the steric hindrance induced by the long alkyl chains surrounding the ammonium center. In this study, the length of the alkyl chain was also demonstrated to have an impact on the properties of the anion exchange membrane. The polymers with the longest alkyl chains showed better properties than the polymers with the shorter alkyl chains, like lower water uptake, greater ionic domain, and higher hydroxide conductivity.

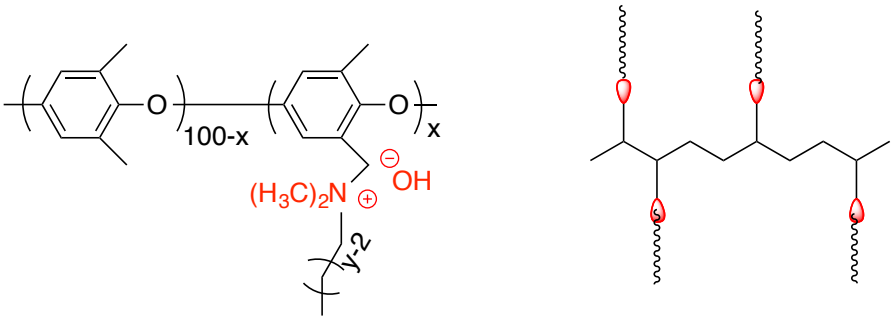

Scheme 1.16. Structure of comb-shaped copolymers.

1.4.3.3 Quaternary phosphonium group

The ionic conductivity of the anion exchange membrane can be increased by several ways: higher ion exchange capacity, higher temperature, and stronger basicity of the pendent cationic groups. The former two methods can be achieved by synthetic procedure and operation conditions modification. The basicity of the cationic group can affect the dissociation of the hydroxide ion, with higher basicity leading to greater dissociation of hydroxide ion and higher ionic conductivity.

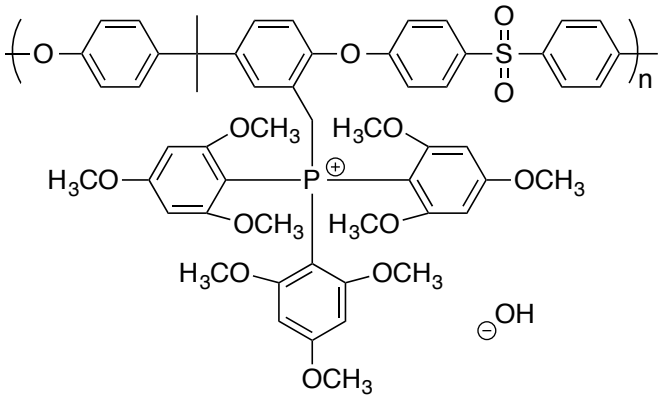

Scheme 1.17. Structure of phosphonium pendent polysulfone.

Yan and coworkers synthesized phosphonium pendent polysulfone as anion exchange membrane (Scheme 1.17).[72] The hydroxide conductivity of phosphonium pendent polysulfone was found to be 27 mS/cm with an IEC value of 1.09 meq/g. The stability of phosphonium cation was studied by conductivity measurement. The conductivity of phosphonium cation was found to be stable in a range of 30 days, indicating the good stability under alkaline environment. The good alkaline stability of the phosphonium cation was explained by the steric hindrance

induced by the tris(2,4,6-trimethoxylphenyl) groups around the center phosphorous atom, and the prevention of hydroxide attack at the α carbon.

Coates and coworkers also developed a new class of phosphonium based cation for anion exchange membranes.[73] The alkaline stability of benzyltrimethylammonium and the tetrakis(dialkylamino)phosphonium cation synthesized in this study were evaluated at 80 °C in 1M NaOD/CH_3OD. The results are presented in Figure 1.5. The stability test showed that under the test conditions, benzyltrimethylammonium had only around 30 % left, while tetrakis(dialkylamino)phosphonium remained stable in the entire stability measurement range, indicating its suitability to be used in anion exchange membranes.

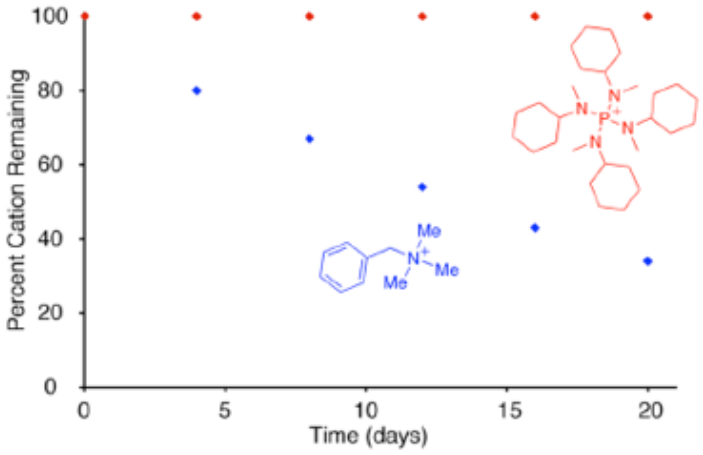

Figure 1.5 Stability of benzyltrimethylammonium and tetrakis(dialkylamino)-phosphonium at 80 °C in 1M NaOD/CH_3OD.

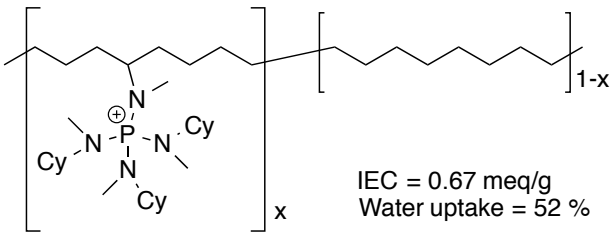

Scheme 1.18. Structure of polyethylene with pendent tetrakis(dialkylamino)-phosphonium.

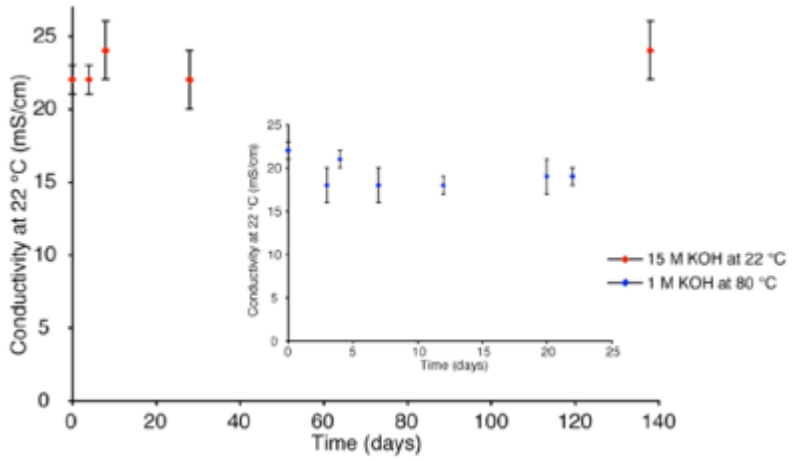

Figure 1.6 Hydroxide conductivity of phosphonium functionalized polyethylene as a function of time in 15M KOH at 22 °C and in 1M KOH at 80 °C (inserted).

The corresponding polymer with tetrakis(dialkylamino)phosphonium cation as the ion conducting group was synthesized through ring-opening metathesis polymerization in this research. The structure of the phosphonium-functionalized polyethylene is presented in Scheme 1.18. The stability of the polymer was studied by immersing in 1M and 15M KOH and then measuring the conductivity periodically. The result in Figure 1.6 showed that the conductivity was kept at a constant level during both measurement conditions: 1M KOH at 80 °C and 15M KOH at 22 °C, indicating the promising potential for tetrakis(dialkylamino)phosphonium to be applied in alkaline fuel cells.

1.4.3.4 Guanidinium group

The guanidinium group was considered as a cationic group for anion exchange membrane to increase the ionic conductivity due to the high basicity of guanidinium groups. Zhang and

coworkers synthesized guanidinium pendent polysulfone and studied the alkaline stability of the cation through conductivity measurement at 60 °C in 1M NaOH.[74] The structure of the guanidinium-functionalized polysulfone is presented in Scheme 1.19. No loss of conductivity was found for the entire measurement over 2 days. The AEM with ion exchange capacity of 1.89 meq/g reportedly had hydroxide conductivity of 45 mS/cm and water uptake of 55 %.

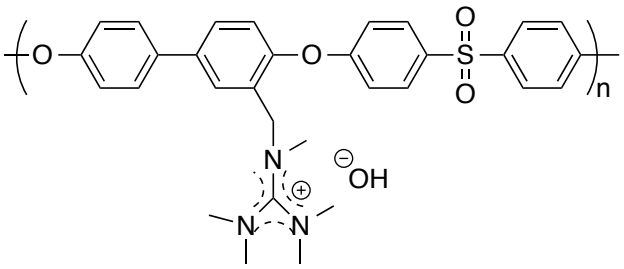

Scheme 1.19. Structure of guanidinium pendent polysulfone.

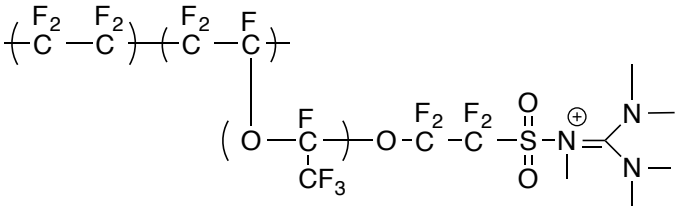

Sulfone-pentamethylguanidinium

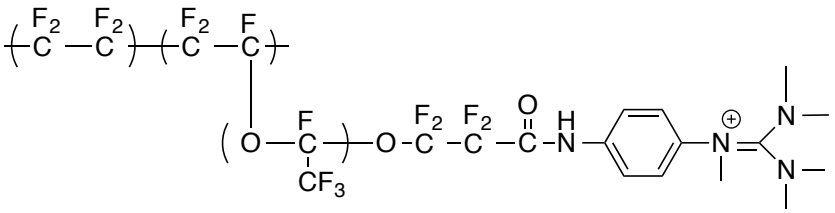

Phenylpentamethylguanidinium

Scheme 1.20 Structures of sulfone-pentamethylguanidinium and phenylpentamethyl-guanidinium functionalized polyfluorinated ionomers.

Kim and coworkers developed resonance stabilized guanidinium cations.[75] The structures of the polymer they designed are displayed in Scheme 1.20. The successful synthesis of sulfone-pentamethylguanidinium and phenylpentamethylguanidinium functionalized polyethylene was confirmed by IR and NMR spectra. By comparing the IR spectra of two products, phenylpentamethylguanidinium was found to be a more charge delocalized structure than sulfone-pentamethylguanidinium. This was due to the lower wavenumber of the C=N stretching peak for the phenyl guanidinium than the sulfone guanidinium, indicating the reduced double bond character of the C=N bond in phenyl guanidinium and its resonance structure. These two guanidinium cations were tested regarding their alkaline stability through IR and NMR spectroscopy. Under a test condition with 0.5 M NaOH treatment at 80 °C, sulfone-guanidinium ionomer showed a fast degradation within 24 hours, phenyl-guanidinium was stable in a 72 hours test range. The degradation reaction pathway was studied theoretically through density function calculations. The sulfone-guanidinium cation was found to be hydrolyzed without an energy barrier. In contrast, the phenyl guanidinium cation had an energy barrier of 23.8 kcal/mol.

1.4.3.5 Imidazolium group

Multiple groups have used imidazolium group as the ion conducting groups in the anion exchange membranes they developed.[30,76-78] Imidazolium has drawn attention because of its different solubility behavior compared to quaternized ammonium cations. Imidazolium pendent ionomers have the potential to dissolve in common solvents, which can promote phase separation and form better connected ion conducting channels, also the ionic contact between polymer electrolyte and catalyst layer can be enhanced in a fuel cell. Since imidazolium also faces the

challenge from stability, research has been done to enhance the alkaline stability of imidazolium cations through protecting the 2-position of imidazolium.

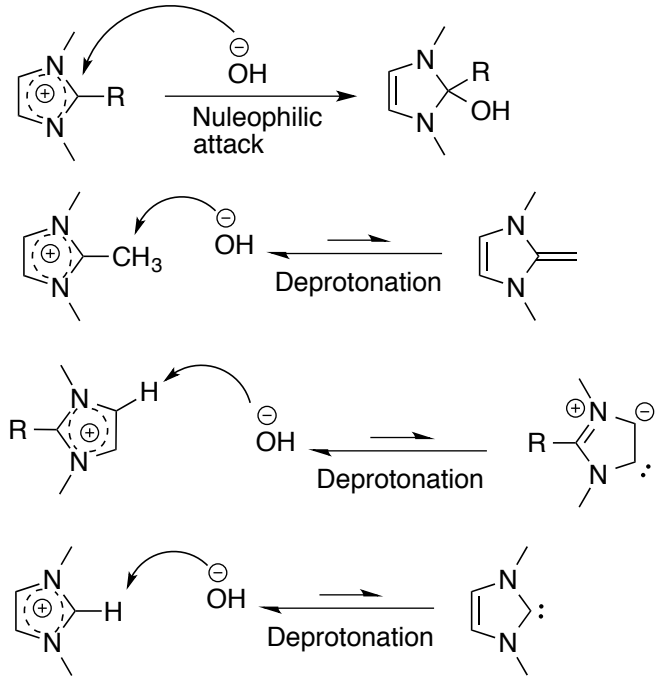

Scheme 1.21. Possible reactions of imidazolium cations in hydroxide solution.

Price and coworkers studied the possible degradation pathways of imidazolium cation and the possible ways to increase the stability of imidazolium.[79] They found that the competing deprotonation between the imidazolium cation with hydroxide ion was the key factor determining the stability of imidazolium under alkaline envoirnment. The possible reactions of imidazolium in hydroxide solution are presented in Scheme 1.21. The competing deprotonation was found to have a larger impact on the alkaline stability of imidazolium cation than steric or resonance effects. This conclusion was drawn from the comparison of alkaline stability between 2-phenyl substituted imidazolium and 2-methyl substituted imidazolium. 2-Phenyl substituted

imidazolium had greater steric hindrance than 2-methyl substituted imidazolium and provided delocalization of electrons through resonance. However, the stability test showed that 2-methyl substituted imidazolium had an order of magnitude greater stability. This phenomenon was explained by the alternative deprotonation pathway provided by 2-methyl substituted imidazolium.

Yan and coworkers further investigated the factors affecting the alkaline stability of imidazolium more systematically.[80] A series of imidazolium cations with different substituents and substitution positions were synthesized and studied experimentally and theoretically. The three imidazolium cations with different substitution positions are presented in Scheme 1.22. Their alkaline stability was studied by proton NMR spectroscopy and the calculation of lowest unoccupied molecular orbital. The results showed that the butyl substitution on 2- position had the lowest stability, which was explained by the stronger electron donation of butyl groups than methyl groups.

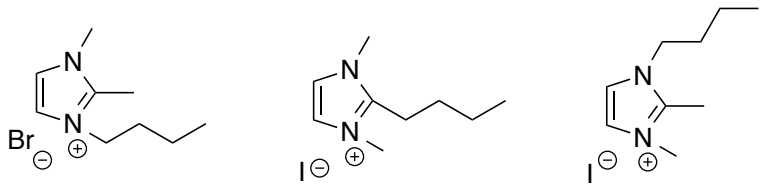

Scheme 1.22 Structures of imidazolium cations with different substitution positions.

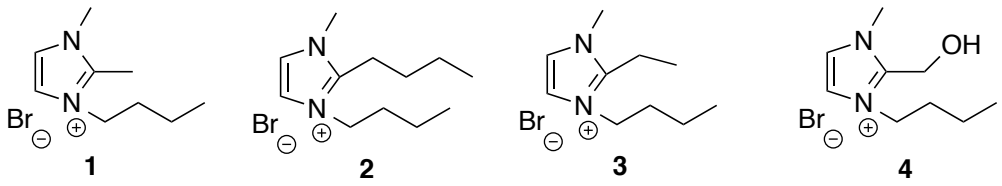

Scheme 1.23 Structures of imidazolium cations with different substituents on 2- position.

Scheme 1.23 showed the imidazolium cations synthesized in this work with different 2-substituent groups. The stability test showed the order of imidazolium cations was: cation 2 > cation 1> cation 3 > cation 4. These studies showed that the strong electron donating groups substituted on nitrogen could improve the alkaline stability of the imidazolium cation greater than that at the 2- position.

1.4.3.6 Metal cation

Tew and coworkers developed ruthenium cation based anion exchange membranes.[81] Ruthenium cation was chosen because of the high thermal stability and pH stability of bis(terpyridine)Ru(II) complexes. Unlike the ammonium or phosphonium with single cation-anion pairs, ruthenium ion has two counter ions per metal center. The structure of the ruthenium pendent anion exchange membrane is displayed in Scheme 1.24. The alkaline stability of this ruthenium cation was studied by UV-Vis spectroscopy through three representative absorption peaks for the ruthenium complex, also from the mass change and the conductivity measurement. The ruthenium complex showed no change from the UV spectrum after immersing in 1M NaOH at room temperature for 6 months, indicating the excellent stability under alkaline enviornment.

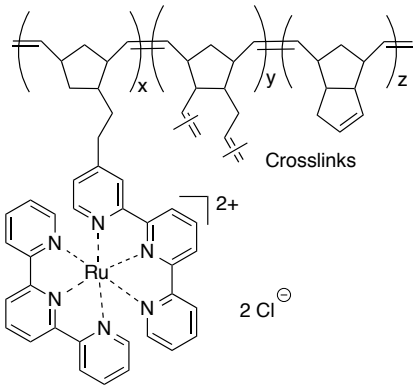

Scheme 1.24 Structure of ruthenium based anion exchange membrane.

1.5 Conclusion

Anion exchange membrane fuel cells can potentially solve some of the problems observed in proton exchange membrane fuel cells. AEMFCs can display enhanced kinetics of oxygen reduction at cathode and less alcohol permeability through the membrane, which could decrease the fuel loss, increase cathode potential and have the potential to use non-precious metals as catalyst such as Ag or Ni, which could greatly reduce the cost of AEMFCs.[15-18] AEMFCs also show improved membrane swelling and water management compared to PEMFCs.[15]

As the most important component in alkaline fuel cells, anion exchange membranes have been studied by numerous groups. However, efforts are still needed to achieve higher conductivities, better mechanical properties, and water uptake for the membranes for large-scale utilization. High conductivity is necessary for reducing the cost and improving the operation of the fuel cell. Easy handling and management of the membranes during assembling of the fuel cell also requires good mechanical properties of the membranes both in the dry and hydrated states. Low water uptake is essential to the fabrication of high performance alkaline fuel cells. The membranes also need to possess high thermal stability and chemical stability to meet the operational temperature of fuel cells and increase the durability of fuel cells. In addition, viable synthetic routes to prepare desirable anion exchange membrane are crucial for producing membranes in large scale for commercialization.

CHAPTER 2 SYNTHESIS, CHARACTERIZATION AND DETERMINATION OF THE CHEMICAL STABILITY OF GUANIDINIUM COMPOUNDS UNDER ALKALINE ENVIRONMENT

2.1 Introduction

Anionic exchange membrane fuel cells (AEMFCs) have received increased attention recently, compared with proton exchange membrane fuel cells (PEMFCs), operating under alkaline environment makes AEMFCs benefiting from: (1) enhanced kinetics of oxygen reduction or fuel oxidation at cathode, which enables the use of high energy density fuel like ethanol and the use of non-precious metals like nickel or silver and therefore reduce the cost of the fuel cell device; [15-18] (2) less alcohol permeability through the membrane due to the opposite direction of electro-osmotic drag to the crossover of the liquid fuel; (3) improved water management resulting from water permeation from cathode to anode caused by electro-osmotic drag.[15]

However, serious challenges for AEMFCs are: (1) relatively low conductivity compared to proton exchange membranes; (2) the degradation of the attached cations in the polymer membrane caused by the attack of hydroxide ion under the alkaline environment.[15,82-84] In order to solve the conductivity problem, increasing the pK_a of the functional cation groups is a way to increase the hydroxide ion conductivity, which is because the increased pK_a could result in increased number of dissociated hydroxide ions and water uptake, therefore enhance the hydroxide ion conductivity under similar humidified conditions.[85-87] To solve the stability

problem, model compounds of cationic groups need to be synthesized and then studied under an alkaline environment.[88]

The guanidinium cation, $C(NH_2)_3^+$, could be a good candidate as cationic groups in AEMFCs because of its high pK_a value (~13.6).[89] The guanidinium ion is stabilized by the multiple resonance structures, which redistribute the electron density of the C=N double bond to three equal carbon-nitrogen bond through p-p interaction between carbon and the lone pair electron on the nitrogen. The high conductivity has already been proven by studies in which pentamethylguanidinium cations were used as pendent groups to poly(arylene ether sulfone) backbone[90] and poly(2,6-dimethylphenylene oxide) backbone[91]. These reports showed that the guanidinium cations were stable under alkaline environment from electrochemical impedance spectroscopy (EIS) measurement, and the guanidinium stability was studied in the polymer film. However, other research using ion exchange capacity titration showed that guanidinium cations were unstable under alkaline environment.[92] With the results showing qualitatively no degradation and different extent of degradation of the cationic polymer, the conflicting research demonstrated very limited result regarding the degradation mechanism and degraded products of the quanidinium cation itself and also quantitative degradation extent under alkaline environment. Because there is a continued interest and need for understanding the stability of the guanidinium cation groups in AEMFCs, we were motivated to study the alkaline stability of the pentamethylguanidinium groups in solutions using model compounds through nuclear magnetic resonance (NMR) spectroscopy. The model compounds were small molecules with similar structure of pendent guanidinium to a polymer backbone. The model compounds tethered the guanidinium cation to benzyl groups for this research. The degradation kinetics of guanidinium

cation can be investigated because of the well-distinguishable signals and excellent resolution resulting from NMR spectroscopy.

In the present work, N-Benzyl-N,N',N',N'',N''-pentamethylguanidinium chloride (BPMGdmCl) and N,N',N''-tribenzyl-N,N',N''-trimethylguanidinium chloride (TBTMGdmCl) were synthesized and investigated as the model compounds. The alkaline stability of guanidinium group was studied in different solvents and under three different temperatures with different molar ratio to sodium hydroxide. The degradation kinetics and the mechanism of degradation were conducted to the model compounds in this research. NMR spectroscopy was employed to simultaneously detect the degradation extent and percentage of the guanidinium cation. The degraded products were characterized by NMR and gas chromatography-mass spectroscopy (GC-MS). The degradation kinetics and mechanism are reported for the first time.

2.2 Experimental Section

The following sections describe the synthesis of the model compounds as well as the materials used for the synthesis and the characterization techniques for the model compounds.

2.2.1 Materials

1,1,3,3-Tetramethylurea (99 %, Aldrich), oxalyl chloride (98 %, Aldrich), anhydrous methylamine (98+ %, Aldrich), 4-vinylbenzyl chloride (90 %, Aldrich), 2,2'-azobis(2-methyl-propionamidine) dihydrochloride (AAPH) (97 %, Aldrich), benzyl chloride (reag., Mallinckrodt), water (HPLC grade, Fisher), deuterium oxide (99.9 %, Aldrich), deuterated dimethyl sulfoxide (99.9 %, Aldrich), deuterated benzene (99.5 %, Cambridge Isotope), deuterated acetonitrile (99.8 %, Cambridge Isotope), N-benzylmethylamine (97 %, Aldrich),

phosgene (Matheson), sodium hydroxide (reag., Baker) were used as received. Acetonitrile was refluxed over CaH_2 then distilled under reduced pressure before use. Toluene was purified by passing through a commercial column system (Innovative Technology).

2.2.2 Characterization

^{1}H and ^{13}C NMR spectroscopy was performed on a JEOL ECA-500 FT-NMR using deuterated water (D_2O), deuterated benzene (C_6D_6), deuterated acetonitrile (CD_3CN), and deuterated dimethyl sulfoxide (DMSO-d_6) as the solvent. Chemical shifts (δ) are reported in ppm, and spin-spin coupling constants (J) are given in hertz. Unless otherwise indicated, all were run at room temperature (~25°C). GC-MS was performed on a Varian 1200 single quadrpole GC/MS with Varian CP 3800 GC.

2.2.3 Synthesis of 1,1,2,3,3-pentamethylguanidine[90,93]

A 250 mL flame-dried flask equipped with a condenser and a nitrogen inlet was charged with tetramethyl urea (10.0 mL, 83.6 mmol), oxalyl chloride (12.0 mL, 139.8 mmol), and dry toluene (106 mL). The flask was heated to 70 °C to let the solution reflux for 5 h. After refluxing, the solvent was removed under vacuum, dry acetonitrile (106 mL) was added to the residue, and excess methylamine gas was bubbled into the flask while cooling in an ice bath. The flask was allowed to warm to room temperature slowly and then stirred at room temperature for 2 h, followed by stirring at 85 °C for 1 h. The solvent was then removed under vacuum and 20 mL 30% NaOH was added to the residue and 30.0 ml diethyl ether was used to extract it three times. The organic layer was collected and the solvent was removed under vacuum. The obtained oil was distilled under 27 °C, 0.2 Torr to afford 9.6 g (74.3 mmol, yield 89%) of 1,1,2,3,3-

pentamethylguanidine as a colorless liquid. GC-MS: *m/z* = 129.1. ^{1}H NMR (500 MHz, C_6D_6): δ 3.04 (s, 3H), 2.48 (s, 3H), 2.43 (s, 3H). ^{13}C NMR (500 MHz, C_6D_6): δ 160.84, 39.32, 39.15, 37.20.

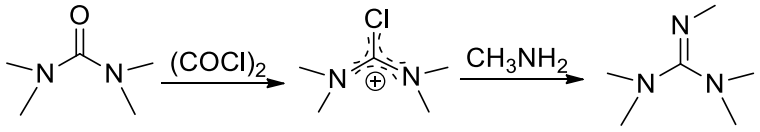

Scheme 2.1 Synthetic route for 1,1,2,3,3-Pentamethylguanidine.

2.2.4 Synthesis of BPMGdmCl

1,1,2,3,3-Pentamethylguanidine (2.0 mL, 13.2 mmol) and benzyl chloride (1.5 mL, 13.2 mmol) were added to a 50 mL flask containing 20 mL dry toluene. The flask was then allowed to stir at room temperature for 12 h. The white precipitate was filtered and washed with cold toluene several times followed by drying in a vacuum oven overnight. The product was obtained in quantitative yield. ^{1}H NMR (500 MHz, D_2O): δ 7.34-7.20 (m, 5H), 4.28 (d, *J* = 13Hz, 1H), 4.03 (d, *J* = 13Hz, 1H), 2.88-2.58 (m, 15H). ^{13}C NMR (500 MHz), D_2O): δ 162.92, 135.27, 129.20, 128.89, 128.60, 55.77, 39.67, 39.59, 39.48, 39.12, 37.40.

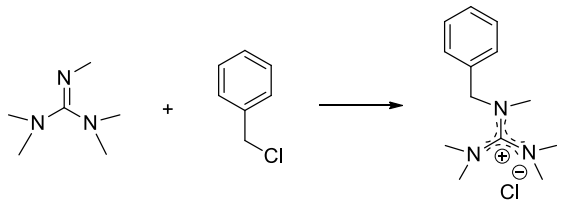

Scheme 2.2 Synthetic route of BPMGdmCl.

2.2.5 Synthesis of N,N'-dibenzyl-N,N'-dimethylurea

A 100 mL three-neck flask equipped with a dry ice condenser, an addition funnel, and a phosgene inlet was charged with N-benzylmethylamine (5.0 mL, 38.7 mmol) and toluene (10.0 mL). The flask was then heated to 55 °C and phosgene (1,72 g, 17.4 mmol) was introduced into the flask at a flow rate of 0.1378 g/min for 12.5 min. After phosgene addition was complete, the flask was heated to 70 °C for 2 h, and then 30 % NaOH (7.0 mL) was added dropwise. The reaction was kept at 70 °C for another 2 h. Residual phosgene was removed by sparging with nitrogen and the flask was allowed to cool to room temperature. The organic phase was then separated and washed with 5 % HCl (20 ml × 3), water (20 mL × 3), brine (20 mL × 2), respectively. The organic phase was then concentrated and distilled under reduced pressure to afford 3.23 g (12.0 mmol, yield 69 %) of N,N'-dibenzyl-N,N'-dimethylurea as a light yellow oil. ^{1}H NMR (500 MHz, CD_3CN): δ 7.36-7.25 (m, 10H), 4.37 (s, 4H), 2.74 (s, 4H). ^{13}C NMR (500 MHz, CD_3CN): δ 139.61, 129.46, 128.66, 128.02, 54.74, 37.17.

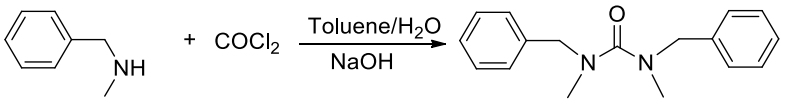

Scheme 2.3 Synthetic route of N, N'-dibenzyl-N, N'-dimethylurea.

2.2.6 Synthesis of 1,3-dibenzyl-1,2,3-trimethylguanidine

A 250 mL flame-dried flask equipped with a condenser and a nitrogen inlet was charged with N,N'-dibenzyl-N,N'-dimethylurea (3.0 g, 11.2 mmol), oxalyl chloride (1.9 mL, 22.4 mmol), and dry toluene (12 mL). The flask was then refluxing at 70 °C for 5 h, followed by cooling the

flask and concentrating the residue. Dry acetonitrile was then added in the flask before bubbling in excess methylamine gas at 0 °C. The flask was brought to room temperature to react for 2 h and then react at 85 °C for 1 h. The residue was concentrated at reduced pressure followed by adding 20 mL 30 % NaOH in the flask and extracting with diethyl ether (30 mL × 3). The extracted ether layer was combined and concentrated under vacuum. The obtained residue was distilled under reduced pressure to afford 1.93 g (6.86 mmol, yield 61%) of 1,3-dibenzyl-1,2,3-trimethylguanidine as yellow oil. ^{1}H NMR (500 MHz, $(CD_3)_2SO$): δ 7.35-7.23 (m, 10H), 4.19 (d, J= 3 Hz , 4H), 2.89 (s, 3H), 2.60 (s, 3H), 2.50 (s, 3H). ^{13}C NMR (500 MHz, $(CD_3)_2SO$): δ 159.52, 139.04, 138.80, 128.41, 128.26, 128.04, 127.63, 127.11, 126.66, 55.27, 54.13, 37.22, 36.34, 36.28.

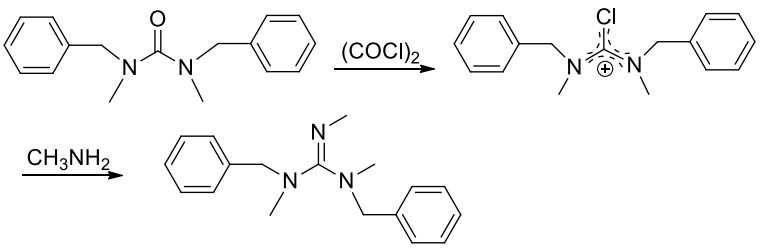

Scheme 2.4 Synthetic route of 1,3-dibenzyl-1,2,3-trimethylguanidine.

2.2.7 Synthesis of TBTMGdmCl

1,3-Dibenzyl-1,2,3-trimethylguanidine (2.4 g, 8.53 mmol) and benzyl chloride (1.2 mL, 8.53 mmol) were added to a 50 mL flask containing 15 mL dry toluene. The flask was then allowed to stir at room temperature for 12 h. The white precipitate was filtered and washed with cold toluene several times followed by drying in a vacuum oven overnight. The product was obtained in quantitative yield. ^{1}H NMR (500 MHz, D_2O): δ 7.43-7.15 (m, 15H), 4.84-4.12 (m,

6H), 2.95-2.30 (m, 9H). ^{13}C NMR (500 MHz, D_2O): δ 163.95, 136.05, 135.81, 135.31, 130.28-130.06 (m, 6C), 129.75-129.65 (m, 6C), 129.38, 128.83, 128.67, 57.47, 56.85.

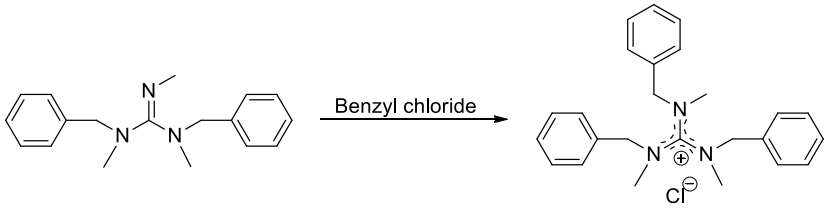

Scheme 2.5 Synthetic route of TBTMGdmCl.

2.2.8 Kinetic study of BPMGdmCl under alkaline environment

Representative procedure for preparing 1 M BPMGdmCl in 1 M NaOH using D_2O as solvent: BPMGdmCl was dissolved in 1 M sodium hydroxide/ D_2O solution to also achieve a concentration of 1 M so that the ratio of the cations to hydroxide ions is 1 : 1. The solution was then added into three NMR tubes, each with 0.7 mL. The three NMR tubes were placed at 20 °C, 60 °C, 80 °C, respectively. ^{1}H NMR analysis was performed every 6 h in the first 24 h, then every 24 h thereafter. The water peak was used as a standard to integrate the other peaks.

Similar procedure as above was used to prepare 1 M BPMGdmCl in 3 M NaOH/ D_2O solution; 1 M BPMGdmCl was dissolved in 1 M NaOH/ DMSO-D_2O solution; 1 M TBTMGdmCl in 1 M NaOH/ D_2O solution.

2.3 Results and Discussion

The following sections discuss the temperature dependence feature of the ^{1}H NMR spectra of the model compounds and the degradation behavior of the model compounds.

2.3.1 ^{1}H NMR spectra of BPMGdmCl and TBTMGdmCl at room temperature and elevated temperature.

The ^{1}H NMR spectra of BPMGdmCl at room temperature and 80 °C are shown in Figure 2.1. From the structure of BPMGdmCl, the *d* protons should be chemically equivalent, as are the *f* protons. However, from the ^{1}H NMR spectrum at room temperature, *d* protons split into double doublets, *f* protons split into one doublet and two singlets. After increasing the NMR testing temperature to 80 °C, the ^{1}H NMR spectrum corresponds with the expected structure of the compound. A similar pattern was found in the ^{1}H NMR spectra at room temperature and 100 °C of TBTMGdmCl. This temperature dependence on proton splitting is consistent with the study of Santoro and Mickevicius on hindered rotation in hexasubstituted guanidinium salts: 2,2-dibenzyl-1,1,3,3-tetramethylguanidine chloride and 2,2-dixylyl-1,1,3,3-tetramethylguanidine chloride.[94] From their study, these two compounds exhibited temperature dependent resonances for both the $-N(CH_3)_3$ and $-N(CH_2Ar)_2$ protons, which is proposed due to the restricted rotation about the C=N bond, which results in that the $-N(CH_2Ar)_2$ group is not in, nor perpendicular to, the plane of the guanidine nucleus. As suggested by Santoro, this will induce the non-equivalence of the benzyl protons and then a broad AB pattern spectrum should arise at lower temperature. As the temperature increases, the free energy of activation barriers should be overcome and the benzyl protons show a broadened singlet. Later NMR studies done by Azumaya[95], Butschies[96], Sundermeyer[97] all showed that as long as the elevated temperature could overcome the energy barrier for the sterically and electronically hindered rotation around the central C=N bonds, the chemical shift of the same substituent groups around C=N bonds will become a single peak. From the study of Christe on the crystal structure of the guanidinium salt,[98] the propeller conformation of guanidinium salt was determined by X-ray, and its geometry

was further calculated, showing that the propeller arrangement is the minimum energy structure of the free ion. This could result in the formation of the isomers of the guanidinium salt.[99] In the cases when steric hindrance of the guanidinium salt is too strong to invert isomers in solution, the NMR spectrum will show several sets of peaks corresponding to each isomer.

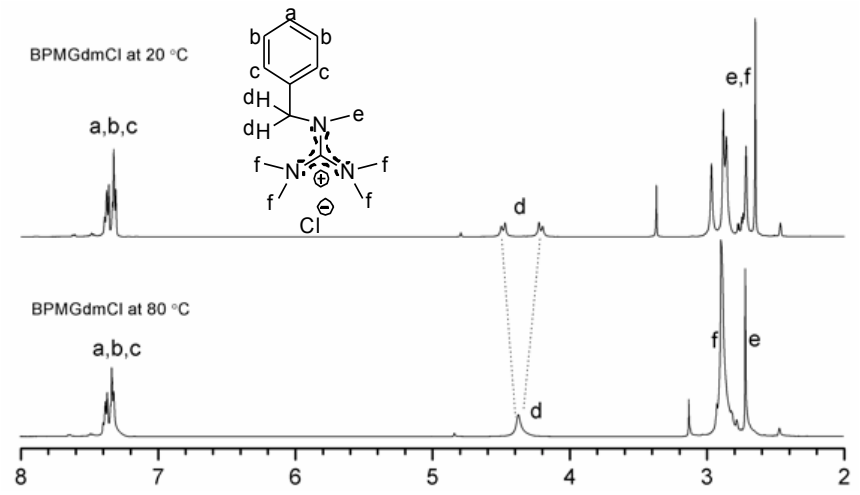

Figure 2.1 ^{1}H NMR spectra of BPMGdmCl at 20 °C and 80 °C in DMSO-d_6.

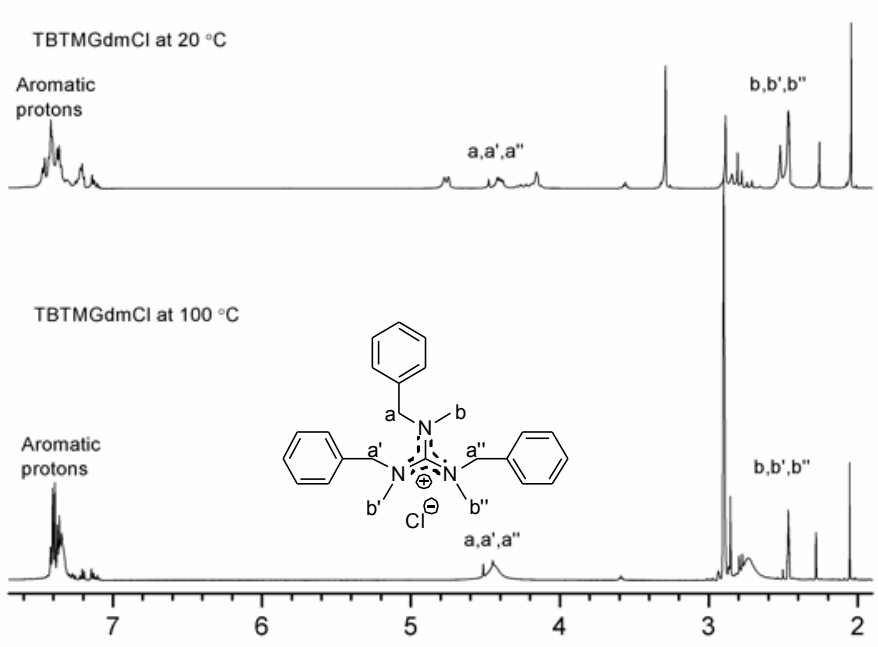

Figure 2.2 ^{1}H NMR spectra of TBTMGdmCl at 20 °C and 100 °C in DMSO-d_6.

From our study, BPMGdmCl has a lower energy barrier for isomerization then TBTMGdmCl because the former has a lower steric hinderance. This also can be easily seen from the NMR spectra: the *f* peaks become a single peak at 80 °C in Figure 2.1 for BPMGdmCl, whereas in contrast, the *b* peaks in Figure 2.2 for TBTMGdmCl are still several sets even at 100 °C.

2.3.2 Degradation of BPMGdmCl in alkaline environment

A stability test of the guanidinium group in an alkaline environment was performed by NMR spectroscopy using 1M and 4 M BPMGdmCl in sodium hydroxide solution at 20 °C, 60 °C, 80 °C, respectively.

After 96 h at 20 °C, 60 °C and 80 °C, all six samples generated a layer of yellow oil on top of the D_2O. This oil was examined separately by GC-MS and ^1H NMR spectroscopy. GC-MS showed that the m/z calculated for $C_{11}H_{16}N_2O$ is 192.1263, found 192.1, indicating the formation of 1-benzyl-1,3,3-trimethylurea.

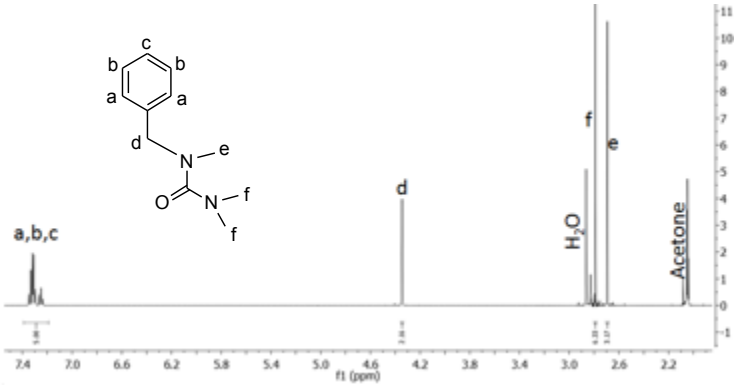

Figure 2.3 ^1H NMR spectrum of the oil layer generated in NMR tube after 288 h. The peaks correlate with 1-benzyl-1,3,3-trimethylurea.

The degradation mechanism is proposed as below:

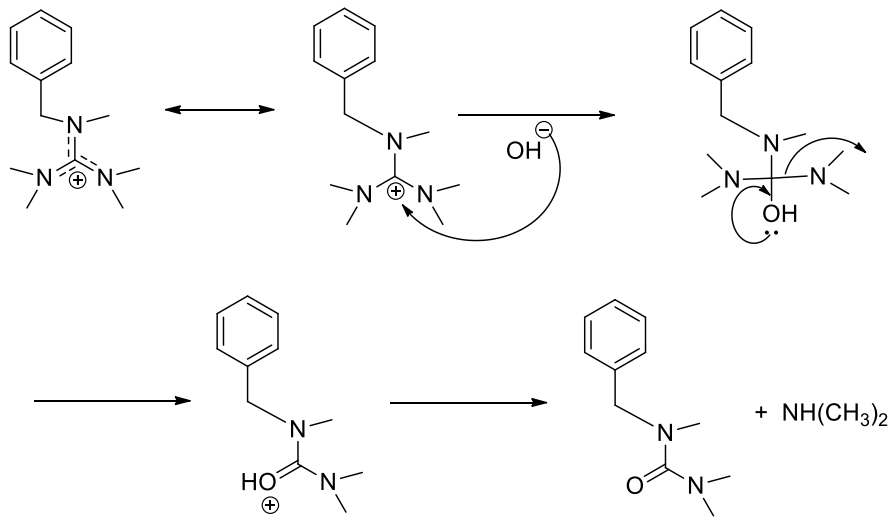

Figure 2.4 Degradation mechanism of BPMGdmCl in 4M NaOH.

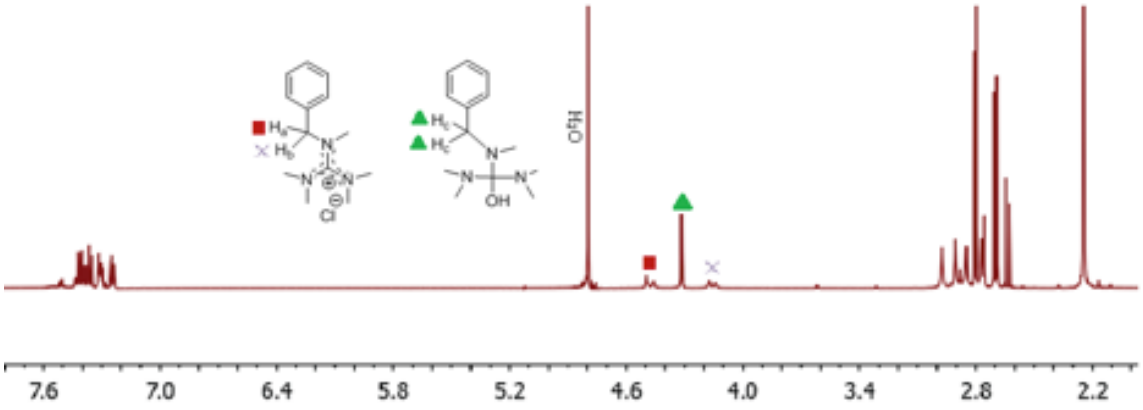

Figure 2.5 ^{1}H NMR spectrum of BPMGdmCl in 4M NaOH at 60 °C after 72 h. The peaks (■, 4.49 ppm) and (×, 4.16 ppm) belong to the two protons on the methylene group of BPMGdmCl. The peak (▲, 4.3071 ppm) is a new peak belonging to the intermediate: benzylmethylamino-bis(dimethylamino)-methanol, from degradation of BPMGdmCl.

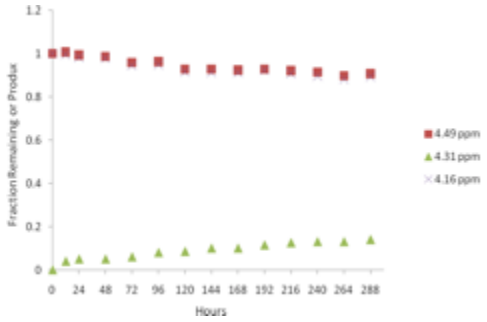

Figure 2.6 Degradation curve of 4 M BPMGdmCl in 4 M NaOH at 20 °C in 288 h. The curve was obtained from the integration of each peak in the ^{1}H NMR spectra that measured every 24 h. Water peak was used as reference for integration.

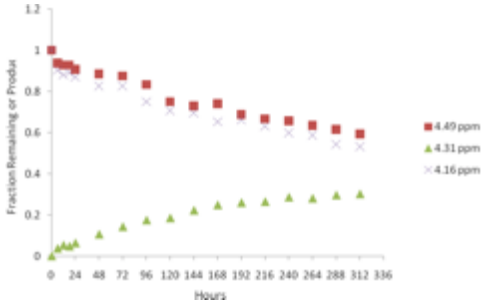

Figure 2.7. Degradation curve of 1 M BPMGdmCl in 1 M NaOH at 20 °C in 312 h. The curve was obtained from the integration of each peak in the ^{1}H NMR spectra that measured every 24 h. Water peak was used as reference for integration.

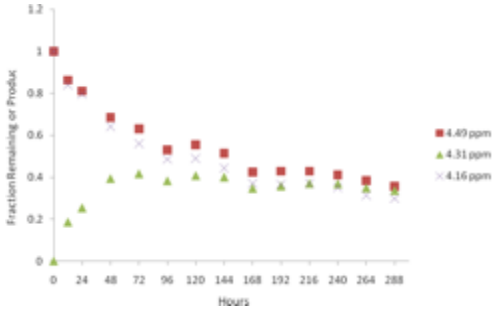

Figure 2.8 Degradation curve of 4 M BPMGdmCl in 4 M NaOH at 60 °C in 288 h. The curve was obtained from the integration of each peak in the ^{1}H NMR spectra that measured every 24 h. Water peak was used as reference for integration.

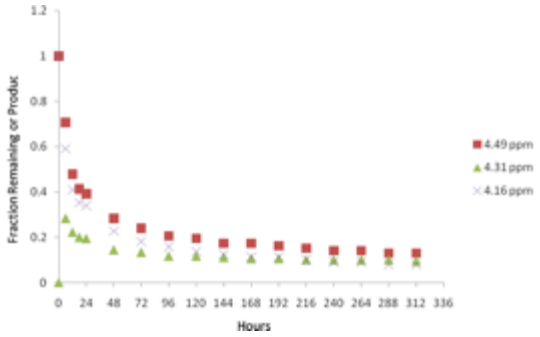

Figure 2.9 Degradation curve of 1 M BPMGdmCl in 1 M NaOH at 60 °C in 312 h. The curve was obtained from the integration of each peak in the ^{1}H NMR spectra that measured every 24 h. Water peak was used as reference for integration.

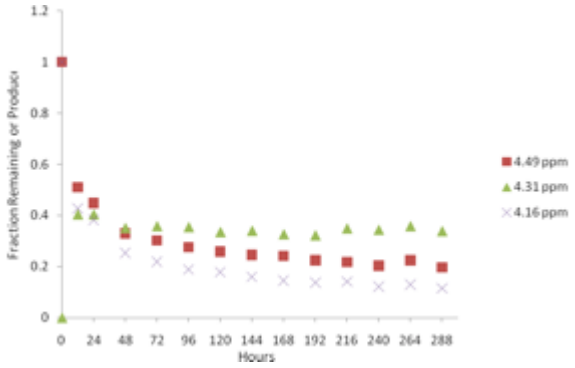

Figure 2.10 Degradation curve of 4 M BPMGdmCl in 4 M NaOH at 80 °C in 288 h. The curve was obtained from the integration of each peak in the ^{1}H NMR spectra that measured every 24 h. Water peak was used as a standard to integrate the other peaks.

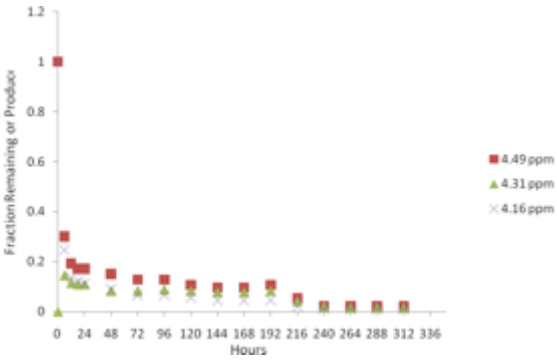

Figure 2.11 Degradation curve of 1 M BPMGdmCl in 1 M NaOH at 80 °C in 312 h. The curve was obtained from the integration of each peak in the ^{1}H NMR spectra that measured every 24 h. Water peak was used as a standard to integrate the other peaks.

From the degradation curves above, the higher the temperature, the faster the degradation. In each degradation curve, an equilibrium in both the decrease of the old peaks and the increase of the new peak is observed. Using Figure 2.8 as an example, the fraction remaining of the methylene protons in BPMGdmCl in 4M NaOH at 60 °C as a function of time was displayed, as well as the fraction produced of the methylene protons in BPMGdmCl. The degradation of proton H_a (■, 4.49 ppm) is quite rapid in first 96 h, after which a slow decrease in the fraction remaining was observed in the degradation curve and relatively maintained at 0.4, as shown in Figure 2.8. A similar behavior is observed for proton H_b (×, 4.16 ppm). The protons H_c (▲, 4.31 ppm) corresponds with the two protons in the methylene group in BPMGdmCl, the integration of which was divided by two to maintain the uniformity. The fraction produced of proton H_c (▲, 4.31 ppm) and the fraction remaining of the protons H_a (■, 4.49 ppm) and H_b (×, 4.16 ppm) unified after 96 h, which indicates that the degradation until this step become an equilibrium. The degradation results in a product, 1-benzyl-1,3,3-trimethylurea, which cannot dissolve in water and forms a layer of oil on the top of the water layer. The separation of the product from the reaction mixture drives the degradation of BPMGdmCl toward completion. The similar pattern can be found in the 60 °C and 80 °C experiment for both 1 M and 4 M concentration. The 20 °C experiments are still on the way to equilibrium because of the slower rate of reaction.

One unexpected feature from these degradation curves is that at the same temperature, the lower concentration (1 M for both BPMGdmCl and NaOH) experiment achieves the equilibrium in a shorter time and more complete comparing to higher concentration (4 M for both BPMGdmCl and NaOH) experiment even though the former one has a much lower hydroxide concentration. However, it is reasonable when dielectric constant is taken into account. For the measurements of the dielectric constants of aqueous solutions, an increase of the dielectric

constant is always observed with an increase of concentration.[100,101] From the study of Pivovar on the relationship between reaction barrier, free energy change and dielectric constant, it was found that both reaction barrier and free energy change decrease with decreasing dielectric constant.[102] In our study, for the 1 M solution, the dielectric constant is lower than that of the 4 M solution, which will result in a lower reaction barrier and free energy change, and then a faster degradation will be observed.

2.3.3 Degradation of TBTMGdmCl in alkaline environment

A stability test of the guanidinium group in an alkaline environment was performed by NMR spectroscopy using 1 M N,N',N''-tribenzyl-N,N'-N''trimethylguanidinium chloride in 1 M sodium hydroxide solution at 20 °C.

In the end of the stability test, all three samples generated a layer of yellow oil on top of the D_2O. This oil was examined separately by GC-MS and ^1H NMR spectroscopy. GC-MS showed that the m/z calculated for $C_{17}H_{20}N_2O$ is 268.16, found 268.2. The results indicate the formation of N,N'-dibenzyl-N,N'-dimethylurea.

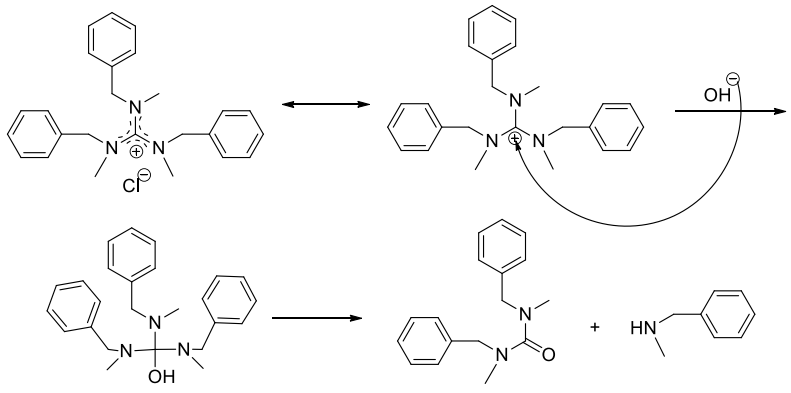

Scheme 2.6 Proposed degradation mechanism for TBTMGdmCl.

The study on the stability of TBTMGdmCl was motivated by the degradation pattern of BPMGdmCl, which degraded exclusively to dimethylamine and N-benzyl-N,N',N'-trimethylurea with no benzylmethylamine or tetramethylurea produced. This interesting phenomenon brought up our hypothesis: benzyl substituted amino group on the guanidinium cation could further stabilize the entity because of the electron donating nature of the benzyl group. Furthermore, benzyl substituted amino group has a greater steric hindrance then methyl substituted amino group, which could also result in a better alkaline stability since the nucleophilic substitution is more difficult for hydroxide ion to attack the center carbon in the guanidinium group. To test this hypothesis, TBTMGdmCl was designed and synthesized to study the stability. In order to compare with the stability of BPMGdmCl under similar condition, 1 M TBTMGdmCl in D_2O with 1 M NaOH was prepared. Contrary to our hypothesis, TBTMGdmCl degraded even faster than BPMGdmCl under alkaline condition. The degraded products were benzylmethylamine and N,N'-dibenzyl-N,N'-dimethylurea. The produced N,N'-dibenzyl-N,N'-dimethylurea was also proven by GC-MS. One of the possible reasons is that the intermolecular strain in TBTMGdmCl is greater than that in BPMGdmCl, because of its bulkier substituted benzyl groups. But this brings up another question: why there is no benzylmethylamine produced during the degradation of BPMGdmCl? A possible reason is that the intermediate during the degradation, benzylmethylamino-bis(dimethylamino)methanol, needed to have a intermolecular proton transfer from the hydroxyl group to one of the amino groups, to produce an ammonium group and a oxy-anion. During this process, dimethylamino groups had greater chance to provide the lone pair electrons to the proton to form ammonium group because the smaller steric hindrance than benzylmethylamino groups. Whereas, when it comes to TBTMGdmCl, only benzylmethylamino groups were present in the molecule, in order to release the intermolecular

strain, the proton had to settle down to one of the amino groups to form ammonium groups to be removed from the guanidinium cation as a leaving neutral amine, specifically as benzylmethylamine.

2.4 Conclusions

Comparison of the ^{1}H NMR spectra of BMGdmCl at room temperature and 80 °C showed that the split peaks belong to either the methylene group protons or the five methyl groups protons in the ^{1}H NMR spectrum at room temperature have the tendency to merge into one peak in the ^{1}H NMR spectrum at 80 °C, which indicates that the structurally equivalent protons are in different chemical environment at room temperature, which was caused by the hindered rotation around C=N bonds in propeller conformed guanidinium salt. When the temperature goes up high enough to overcome the energy barrier, the central C=N bonds can rotate freely to form a chemically equivalent environment, which then presented in the ^{1}H NMR spectrum as a single peak. Similar phenomena was found in the ^{1}H NMR study of TBTMGdmCl at room temperature and 100 °C. Stability test was done to BPMGdmCl at three different temperature and two different concentrations. BPMGdmCl was found decomposing into one molecule of dimethylamine and one molecule of benzyltrimethylurea, indicating the guanidinium group has minimal stability under an alkaline environment. TPTMGdmCl showed similar instability under alkaline environment, which decomposed into one molecule of benzylmethylamine and one molecule of dibenzyldimethylurea. The stability results showed negative tendency of guanidinium group to be applied in alkaline fuel cells.

Acknowledgement

Funding was provided by the Army Research Office MURI grant (W911NF-10-1-0520). The NMR spectroscopy was possible with a grant from the NSF-MRI CHE-0923537.

CHAPTER 3 DIBLOCK COPOLYMERS BASED ON POLY(2,6-DIMETHYL-1,4-PHENYLENE OXIDE) FOR ANION EXCHANGE MEMBRANE APPLICATIONS

3.1 Introduction

Solid anion exchange membranes (AEMs) are critical components for alkaline fuel cells, functioning as an electrolyte to transport anions between the electrodes while serving as a barrier to both fuel and electrons. AEMs should be designed to have high ionic conductivity so that useful current can be achieved.[20] In addition, AEMs should possess good mechanical properties and have high thermal and chemical stabilities to withstand the alkaline, humid, and elevated temperature operating conditions in a fuel cell.[23,103] The challenge to making an ideal anion exchange membrane is to balance a high ion exchange capacity and water content with sufficient mechanical properties. Mechanical properties tend to be compromised by excessive water uptake that accompanies increasing the number of cationic pendent groups in the pursuit of higher ionic conductivity.[104]

Research has investigated anion exchange membranes with different polymer backbone structures including poly(arylene ether)s,[25,31,61,105-107] poly(olefin)s,[46,70,73,108] polystyrene,[32,71,109-111] and polyphenylene.[26,92] The engineering polymer, poly(2,6-dimethyl-1,4-phenylene oxide) (PPO), displays good mechanical properties and outstanding chemical and thermal stability[34,112,113] and anion exchange membranes based on PPO have been recently studied.[91,114-117] The interest in using PPO to prepare AEMs is in part because the benzylic methyl groups of PPO can be readily functionalized to cationic groups and a number of different cations can be anchored to PPO including benzyltrimethylammonium,[118] methylimidazolium,[76]

dimethylimidazolium,[115] benzimidazolium,[119] and guanidinium.[91] Recently, AEMs have been developed using quaternized PPO with long alkyl side chains pendent to the nitrogen-centered cation.[25] The resulting comb-shaped AEMs exhibited organized ionic domains and good hydroxide conductivity (43 mS/cm at room temperature).[25] Other modifications to PPO have been done to prepare AEMs. A PPO-silica hybrid anion exchange membrane was investigated and exhibited good swelling resistance and thermal stability, and also showed reasonable hydroxide conductivity (11 mS/cm at room temperature).[40] A crosslinked membrane was prepared through blending chloroacetylated PPO and brominated PPO followed by heat treatment and quaternization, and the resulting AEM displayed good conductivity (32 mS/cm at 25 °C) while the crosslinking was reported to improve tensile strength and increase the initial degradation temperature.[120]

The above studies all took advantage of the benzylic methyl groups on the PPO backbone to attach cationic groups by post-polymerization bromination and subsequent quaternization. This synthetic method is convenient, but can only provide randomly distributed cationic groups on the PPO backbone without the capability to control the bromination position along the polymer chain. Multiple research groups have demonstrated that micro-phase separation through the formation of diblock copolymers effectively improves the membrane performance with increased ionic conductivity and better mechanical properties.[31,58,121,122,48] For example, our group has developed both random and block copolymers containing a quaternized PPO moiety and a hydrophobic poly(2,6-diphenyl-1,4-phenylene oxide) moiety.[123] The diblock copolymer showed higher conductivities than random copolymers with similar ion exchange capacities.

We designed a diblock copolymer of PPO and poly(vinylbenzyltrimethylammonium hydroxide) (PVBTMAOH) to thoroughly exploit the beneficial properties of PPO and direct the

phase separation between hydrophilic and hydrophobic phases. We took advantage of the hydroxyl terminal group of PPO to attach a TEMPO functional group for nitroxide mediated polymerization and grow a poly(vinylbenzyl chloride) (PVBC) block from the chain end of PPO. The PVBC block was then conveniently converted to a PVBTMA block by reacting with trimethylamine through the Menshutkin reaction. With this design, we can tune the IEC of the polymer electrolyte by changing the length of the PVBTMA block while maintaining the PPO block intact; therefore, benefiting from the mechanical properties and the chemical and thermal stability of the unaltered PPO chain. The quaternized PPO-*b*-PVBTMA membranes were evaluated for their application as anion exchange membranes by examining thermal stability, water uptake, morphology, and ionic conductivity.

3.2 Experimental section

The following section describes the materials used for the synthesis of the diblock copolymers and the end-capping agent. The purity and the source of these materials are also presented.

3.2.1 Materials

4-Vinylbenzylchloride (Sigma-Aldrich, 90%) was distilled from calcium hydride (Sigma-Aldrich, 95 %) under reduced pressure prior to the block copolymer synthesis. For the alkoxyamine synthesis, 4-vinylbenzyl chloride was passed through a silica gel column before use. 1-[1-(4-chloromethylphenyl)ethoxy]-2,2,6,6-tetramethylpiperidine (Cl-BzEt-TEMPO) was synthesized according to the reported method[124] from manganese acetate (Matheson Co. Inc.),

N,N'-disalicylidene-1,2-ethanediamine (Sigma-Aldrich), and 2,2,6,6-tetramethylpiperidine (TEMPO) (Sigma-Aldrich). Poly(2,6-dimethyl-1,4-phenylene oxide) (PPO) (Sigma-Aldrich) was dried under vacuum at room temperature overnight before use. Tetrabutylammonium hydroxide (TBAH) (1.0 M in methanol) (Sigma-Aldrich) was diluted to 0.1 M with chloroform before use. Trimethylamine (45 % in water), anhydrous 1,2-dichlorobenzene and all solvents were used as received from Sigma-Aldrich. Homopolymer of PVBC (20 kg/mol) was synthesized through nitroxide mediated polymerization. A PPO/PVBC blend sample was prepared by precipitating the blend solution in chloroform into methanol and drying the precipitate under vacuum for 24 h.

3.3 Synthetic process

The following sections describe the synthesis of the diblock copolymers as well as the synthesis of the end-capping agent. The characterization of the end-capping agent and the copolymers are also discussed.

3.3.1 Synthesis of end capped poly(2.6-dimethyl-1,4-phenylene oxide) (PPO-BzEt-TEMPO).

PPO (5.0 g, 0.25 mmol) was dissolved in 120 mL 1,2-dichlorobenzene in a 250 mL single-neck flask equipped with a nitrogen inlet and a magnetic stir bar. Sodium hydride (0.18 g, 7.5 mmol) was then added and the mixture was heated to 50 °C and stirred for one hour. Cl-BzEt-TEMPO (0.93 g, 3.0 mmol) was introduced and the mixture allowed to react under magnetic stirring for 48 h at 50 °C. The mixture was cooled to room temperature and then

poured into 1200 mL methanol. The precipitate was collected by filtration through a glass fritted funnel and washed several times with fresh methanol. The polymer was re-dissolved in chloroform and precipitated into methanol two more times before drying under vacuum at 50 °C overnight.

3.3.2 General procedure to synthesize PPO-*b*-PVBC diblock copolymers.

The PPO-*b*-PVBC diblock copolymers were synthesized by employing PPO-BzEt-TEMPO as a macroinitiator for nitroxide mediated polymerization. In a typical synthesis of PPO-*b*-PVBC diblock copolymers, PPO-BzEt-TEMPO macroinitiator (0.50 g, 0.025mmol) was added to 4-vinylbenzylchloride (10 mL, 71.0 mmol) in a 15 mL single neck, round bottom flask. The flask was sealed with a rubber septum and purged for 30 min with nitrogen. The flask was then immersed in a 125 °C oil bath to initiate the polymerization. The size of the PVBC block was controlled by the reaction time. The polymerization was terminated at specific time intervals by cooling the flask in a dry ice/acetone bath. After the solution was warmed to room temperature, chloroform was added to dilute the reaction mixture. The diluted solution was precipitated twice from methanol. The precipitated polymer was collected by filtration and washed with fresh methanol several times before drying under vacuum at 50 °C overnight.

3.3.3 Membrane preparation and quaternization.

The PPO-*b*-PVBC copolymer powder was melt pressed for 20 min. between two Teflon sheets in a Carver 3912 press with home-made heated/water cooled platens at 240 °C and 20000 pounds. Films were obtained after melt pressing with film thickness ranging from 50 to 90 μm.

The films were immersed in 45 % aqueous trimethylamine solution to convert benzyl chloride groups to quaternized benzyltrimethylammonium chloride groups. Conversion from chloride to the bicarbonate form was done by soaking the chloride form film in 1 M potassium bicarbonate for 48 h, followed by removing any excess salt by rinsing and subsequently soaking the film in fresh DI water for 12 h and changing the water every two hours. Similarly, the film was converted to the hydroxide form by immersing the benzyltrimethylammonium chloride film in 1 M potassium hydroxide for 48 h. The film was then rinsed with nitrogen purged DI water and then soaked in DI water for 12 h with constant nitrogen purge and changing the water every two hours.

3.4 Characterization and Measurements.

Proton nuclear magnetic resonance (^{1}H NMR) spectra were recorded using a JEOL ECA-500 FT-NMR at room temperature with $CDCl_3$ as solvent. Chemical shift values (d) are reported downfield from tetramethylsilane at 0 ppm.

The thermal stability of membranes was investigated by thermogravimetric analysis (TGA) using a Seiko TG/DTA 320 Thermal Analyzer with a RT Instruments software upgrade. Polymer samples were dried under vacuum at 60 °C overnight before the TGA measurement and were run under a nitrogen atmosphere with a heating rate of 10 °C per minute. Differential scanning calorimetry (DSC) was performed with a TA Instruments Q20 DSC. Samples were measured in aluminum pans over a temperature range of 20 to 250 °C with a heating rate of 10 °C/min and a cooling rate of 40 °C/min. The second and third cycles were used to determine the glass transition temperature (T_g), which was measured by the midpoint of the slope change in

the heat flow plot.

Molecular weights were determined relative to polystyrene standards by gel permeation chromatography (GPC) using a Waters 600-MS pump coupled with a Wyatt Technology Mini Dawn and Optilab DSP interferometric refractometer as detectors. GPC was performed using two PLgel 5 μm mixed D columns with THF as eluent at a flow rate of 1 mL/min.

Ultraviolet-visible spectroscopy was done in quartz cuvettes from 200 nm to 600 nm with a Thermo Electron Corporation Evolution 300 PC spectrophotometer. Samples were prepared to 3 mL with concentrations of 500 ppm in chloroform, which was followed by adding 10 μL 0.1 M TBAH. The analysis was conducted by running chloroform as background, followed by recording the sample. The presence of phenoxide groups were detected by the absorption between 310 nm to 380 nm.[125]

Attenuated total reflectance Fourier transform infra-red spectroscopy was performed with a Thermo Electron Nicolet 4700 spectrometer in a range of frequencies between 400 cm^{-1} and 4000 cm^{-1}. Samples were measured in their powder forms for PPO, end capped PPO, and PPO-*b*-PVBC. PPO-*b*-PVBTMA was measured as a film.

The percentage of water uptake of the PPO-*b*-PVBTMA copolymers was measured in the chloride form and calculated based on the following equation:

$$\text{Water uptake (\%)} = \frac{W_{wet} - W_{dry}}{W_{dry}} \times 100$$

The dry membrane weight (W_{dry}) was determined by drying the membrane at 60 °C under vacuum for 24 h. The wet membrane weight (W_{wet}) was measured after the membranes were

fully hydrated by soaking the dry membranes in DI water until a constant weight was obtained.

The ion exchange capacity values (IEC) of the membranes were determined by standard back-titration methods.[73,110,126] The hydroxide form membranes were each immersed in 9.00 mL of standardized HCl solution (0.01 M) for 24 h to fully neutralize the hydroxide ions in the membrane. The residual HCl was titrated by a standardized NaOH solution (0.01 M) using an automatic titrator (Company: Mettler Toledo; Model: G20). The titrated samples were then dried under vacuum at 60 °C overnight before measuring the mass of the dry sample in the chloride form. The IEC value of each membrane was calculated from the following equation.

$$\text{IEC} = \frac{V_{HCl} * c_{\square Cl} - V_{NaOH} * c_{NaOH}}{W_{dry}}$$

where V_{HCl} and c_{HCl} represent the volume and concentration of the standardized HCl solution; V_{NaOH} and c_{NaOH} represent the volume and concentration of the standardized NaOH solution; W_{dry} represents the weight of the dry membrane.

In-plane conductivity was measured by electrochemical impedance spectroscopy (EIS) using a 4-probe Teflon cell with Pt electrodes connected to a BioLogic VMP3 Potentiostat in a frequency range from 1 Hz to 100 kHz. The chloride conductivity at 95 % relative humidity was determined in a TestEquity® (Solatron 1007H Model) environmental chamber to control the temperature and percentage of relative humidity for measurement. The hydroxide and bicarbonate conductivity under fully hydrated conditions was performed with the same Teflon cell immersed in deionized ultra pure water (18 MΩ resistance). A control cell with a Teflon film was running as background while measuring the polymer samples. The ionic conductivity was obtained from the following equation:

$$\sigma = \frac{d}{L_s W_s R}$$

where σ is the ionic conductivity of the membrane (S cm^{-1}), d is the distance between reference electrodes (mm), L_s and W_s are the thickness (mm) and width (mm) of the membrane, and R is the ohmic resistance of the membrane (Ω).

Small angle X-ray scattering (SAXS) profiles were acquired at the Advanced Photon Source at Argonne National Lab. The measurements were carried out with a 12 keV beam (λ = 1 Å) using a Pliatus 2 M SAXS detector and a Pliatus WAXS detector. The samples were measured at 60 °C from dry to 95 % relative humidity. The relative humidity was controlled by a combination of wet and dry nitrogen. Kapton tape was used to mount the film samples on samples holders for measurement. The scattering intensity was normalized for background scattering and beam transmission.

Transmission electron microscopy (TEM) experiments were imaged with an FEI Tecnai F20 electron microscope (FEI Corp, Hillsboro, OR) operating at 200 kV. TEM samples were prepared by embedding the quaternized polymer sample in epoxy and sectioning into ~100 nm thick sections at room temerature using a Leica Ultracut UCT ultramicrotome (Leica Microsystems, Buffalo Grove, IL). The sections were collected onto 200 mesh copper EM grids, followed by staining for 3 h with osmium tetroxide vapor from a 4 % aqueous solution.

ImageJ analysis was conducted to the histograms based on the TEM micrographs. The dark/bright area percentages in the TEM micrographs were calculated to determine which phase was darkened after exposing to OsO_4.

3.5 Results and Discussion

The objective of this research was to develop highly conductive AEMs while maintaining robust membranes with suppressed water uptake. We designed diblock copolymers with PPO blocks to provide mechanical properties and PVBTMA blocks to provide a hydrophilic medium for ionic conductivity. PPO was chosen because of its outstanding chemical and thermal stability and its expected ability to form robust films. PVBTMA was chosen as the hydrophilic domain due to the reasonable alkaline stability of benzyltrimethylammonium ion[67] and the ease of polymerization and quaternization resulting from the bifunctionality of 4-vinylbenzyl chloride.

Similarly designed block copolymers of PPO and poly(vinylbenzyl phosphonic acid) have prewviously been prepared as proton exchange membranes.[127] Atom transfer radical polymerization (ATRP) was employed to attach the poly(vinylbenzyl phosphonic acid) block to the PPO block. The resulting proton exchange membranes exhibited promising proton conductivity, good thermal stability and mechanical properties. More recent research has investigated phase-separated copolymers incorporating PPO for AEM applications. Our group developed a block copolymer system with quaternized PPO as the hydrophilic block and poly(2,6-diphenyl-1,4-phenylene oxide) as the hydrophobic block.[123] The hydroxide conductivity for the best sample reached 84 mS/cm under 95 % relative humidity at 80 °C. Bai and coworkers recently prepared a series of triblock copolymers with quaternized PPO as the hydrophilic end block and polysulfone as the hydrophobic middle block that showed promising hydroxide conductivity,[65] while Xu and coworkers synthesized graft copolymers with PPO as the backbone and PVBTMA as grafted side chains.[128] Low water uptake and encouraging hydroxide conductivity were observed in the graft copolymers.

3.5.1 Synthesis and Characterization of PPO-BzEt-TEMPO.

In the work described here, diblock copolymers of PPO-*b*-PVBTMA were designed to combine the mechanically supportive PPO block with the ion conductive PVBTMA block. The first step was to end cap the phenol end group of PPO with the benzylmethyl TEMPO moiety (Scheme 3.1). The PPO phenol end groups were deprotonated with sodium hydride at 50 °C before adding Cl-BzEt-TEMPO. The deprotonated phenoxide substituted for chloride on the benzylic carbon of Cl-BzEt-TEMPO to synthesize the PPO-BzEt-TEMPO. End group analysis of the phenol in the phenoxide form was conducted using ultraviolet/visible (UV/Vis) spectroscopy, showing the phenoxide group at an absorbance between 310nm to 380 nm.[125] UV-Vis spectra of the PPO are shown in Figure 3.1, before and after the introduction of the BzEt-TEMPO moiety. The lower spectrum shows the end capped PPO with no absorbance in the region of 310 nm to 380 nm, indicating the successful nucleophilic substitution between PPO and Cl-BzEt-TEMPO.

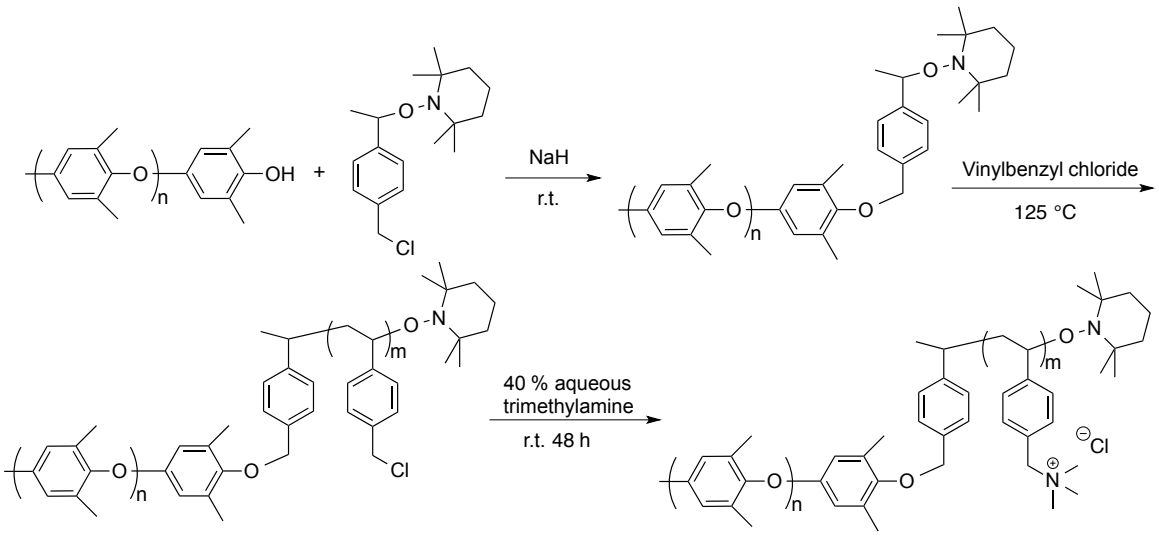

Scheme 3.1 Synthetic route of PPO-*b*-PVBTMA copolymers.

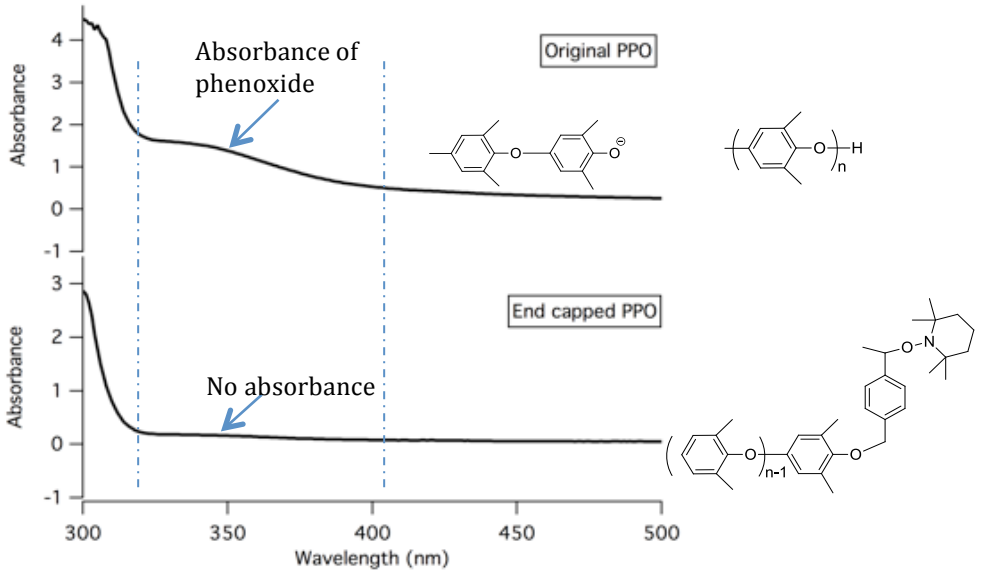

Figure 3.1 UV spectra of PPO (upper) and end capped PPO with BzEt-TEMPO moiety after nucleophilic substitution with Cl-BzEt-TEMPO (lower).

3.5.2 Nitroxide mediated polymerization of PPO-*b*-PVBC block copolymer.

PPO-BzEt-TEMPO was employed as an initiator for nitroxide mediated polymerization of vinylbenzyl chloride to synthesize the PPO-*b*-PVBC block copolymers. The polymerization was carried out in bulk vinylbenzyl chloride at 125 °C for different reaction times, and a series of block copolymers with different PVBC block lengths was synthesized in this research.

The PPO-*b*-PVBC block copolymers were characterized by various techniques. The GPC traces are displayed in Figure 3.2 including the original PPO, the end capped PPO, and two representative PPO-*b*-PVBC copolymers with different PVBC block lengths. The PPO M_n was determined to be 20 kg/mole relative to polystyrene stndards. The GPC traces of the original PPO and the end capped PPO almost exactly overlapped due to the negligible effect of the small end group on the molecular weight of the end-capped PPO. The clear shifts of the

chromatograms to lower elution volume from the PPO macroinitiator to the block copolymers demonstrate the formation of the higher molecular weight copolymer, suggesting the successful synthesis of PPO-*b*-PVBC copolymers. The lower elution volume of PPO-*b*-PVBC10 than PPO-*b*-PVBC6 indicated the higher molecular weight of PPO-*b*-PVBC10 and its longer PVBC blocks. Also the unimodal appearance of the chromatograms of the copolymers indicated the absence of unreacted PPO or self-initiated polymerization of VBC.

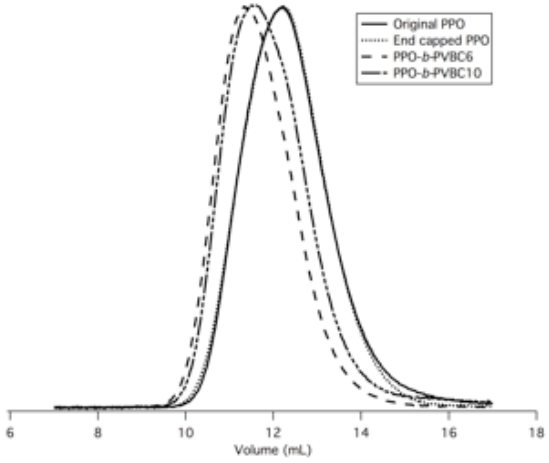

Figure 3.2 GPC curves of original PPO, PPO macroinitiator and two PPO-*b*-PVBC block copolymers.

The PPO-*b*-PVBC copolymers were characterized by ^{1}H NMR spectroscopy, from which the fraction of PVBC can be calculated based on the distinguishable peaks from each block. The proton NMR spectrum of PPO-*b*-PVBC6 is illustrated in Figure 3.3 as a representative example. The NMR spectra exhibit characteristic peaks at δ = 4.5 ppm (a) from protons on the benzylic carbon of PVBC, as well as peaks at δ = 2.1 ppm (b) representing protons from the methyl groups of PPO. The quantitative ratio of PVBC block to PPO block was calculated from the integration of the "a" and "b" peaks. The repeat unit ratio of PVBC block to PPO block was

calculated, and the total molecular weight of each block copolymer was then calculated based on the repeat unit ratio of the two blocks and the number-average molecular weight of PPO (20 kg/mol). The number-average molecular weights of the PPO-*b*-PVBC copolymers are displayed in Table 3.1 along with the weight percentage of PVBC. The weight percentage of PVBC in the block copolymers varied from 16 % to 74 % with the concomitant increase in number average molecular weight of the PVBC.

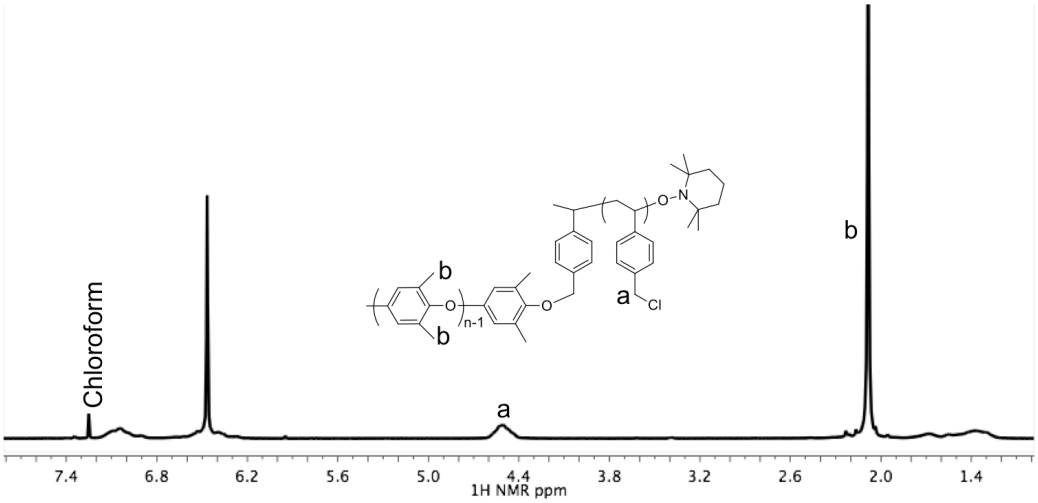

Figure 3.3 ^{1}H NMR spectrum of PPO-b-PVBC6 in $CDCl_3$.

Table 3.1 Molecular weight of each PPO-*b*-PVBC block copolymer

Sample	M_n (NMR)[a]		Weight percentage of PVBC[a] (%)	M_n of PPO-*b*-PVBC (GPC)[b] (kg/mol)	M_w/M_n[b]
	M_n of PVBC block (kg/mol)	M_n of PPO-*b*-PVBC (kg/mol)			
PPO-*b*-PVBC1	3.7	23.7	16	27	1.74
PPO-*b*-PVBC2	6.2	26.2	24	28	1.64
PPO-*b*-PVBC3	7.6	27.6	28	28	1.83

PPO-*b*-PVBC4	9.3	29	32	31	1.81
PPO-*b*-PVBC5	12	32	37	34	1.61
PPO-*b*-PVBC6	13	33	39	36	1.59
PPO-*b*-PVBC7	18	38	47	39	1.69
PPO-*b*-PVBC8	20	40	50	42	1.65
PPO-*b*-PVBC9	23	43	53	46	1.97
PPO-*b*-PVBC10	28	48	58	52	1.78
PPO-*b*-PVBC11	33	53	62	59	1.66
PPO-*b*-PVBC12	57	77	74	85	1.74

[a]m : n depicts the block ratio of PPO to PVBC. [b]Determined by proton NMR from the integrations of methylgroups of PPO and benzylic methylene groups of PVBC. [c]Determined by GPC against polystyrene standard.

3.5.3 Thermal properties of PPO-*b*-PVBC copolymers.

The copolymers were ultimately to be converted from PVBC to an ammonium salt form PVBTMA to form block polyelectrolyte membranes. Because of the solubility differences of PPO and the PVBTMA, processing from a common solvent is a difficult endeavor. It is desirable to develop a thermal process for preparing membranes, however melt processing of the polyelectrolyte block copolymers is also precluded. We have had good success with solvent casting of block copolymer films in the benzyl halide form and then subsequently converting to the ammonium salt form by reacting the films with aqueous trimethylamine.[123,129] In this case, we expected to be able to melt process the block copolymers into films while in the benzyl chloride form and then convert into ionic block copolymers.

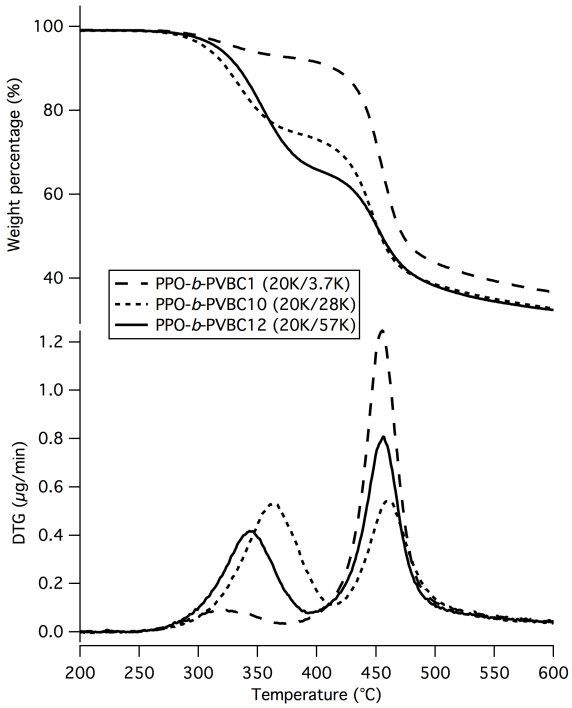

Figure 3.4 TGA and DTG thermograms of PPO-*b*-PVBC1, PPO-*b*-PVBC10 and PPO-*b*-PVBC12 under flowing nitrogen at a heating rate of 10 °C/min. The two numbers in each pair of parentheses after the sample name represent the molecular weight of the PPO segment and PVBC segment, respectively.

Melt pressing of the films required the PPO-*b*-PVBC copolymers to be stable at the melt pressing temperature. Thermal gravimetric analysis (TGA) was used to determine the highest temperature that PPO-*b*-PVBC remained stable before degradation. The TGA thermograms and derivative thermogravimetry (DTG) curves are shown in Figure 3.4 for PPO-*b*-PVBC1, PPO-*b*-PVBC10, and PPO-*b*-PVBC12 recorded between 200 °C and 600 °C. These three copolymers were chosen as representative cases because they possess the lowest, middle, and the highest weight percentage of the PVBC segment, respectively. The copolymers exhibited stabilities up to 250 °C, beyond which there were two stages of degradation. Based on the TGA trace of the PVBC homopolymer, the first weight loss, occurring between 255 °C and 400 °C, was associated

with the decomposition of the benzyl chloride groups. The TGA and DTG curves showed that a longer PVBC segment block resulted in a greater weight loss in the first degradation stage. The second weight loss above 400 °C revealed the degradation of the copolymer backbone, which was not affected by the PVBC segment length but resulted in similar weight percentage of the degradation residue. The three samples exhibited the same onset decomposition temperatures at approximately 255 °C. The results indicate that melt processing of the films could be accomplished below 255 °C.

The block copolymers were synthesized in order to have phase separated blocks with the PPO providing good film properties and the PVBTMA to provide for the ionic conductivity in a hydrophilic medium. While it is expected that the PPO and PVBTMA would be well phase separated because of the distinct difference between the PPO and a cationic block, our processing of the films as the PPO-*b*-PVBC copolymers requires that the materials are phase separated prior to conversion to PVBTMA. The miscibility of many blends of PPO and styrenic polymers and copolymers have been studied,[130,131] however the miscibility of PPO and PVBC have not been reported.

DSC analysis was employed to characterize the miscibility of the block copolymers, Figure 3.5 depicts DSC results for PPO homopolymer, PVBC homopolymer, a 50/50 blend of the two homopolymers and representative PPO-*b*-PVBC copolymer. The PVBC and PPO homopolymers are found to have T_gs at 109 °C and 213 °C, respectively. A 50/50 blend of the two homopolymers shows two T_gs at close to the same relative temperatures of the pure homopolymers, indicating immiscibility of the blend. The diblock copolymers, however, show a distinct increase in the lower T_g while the higher T_g corresponds well with that of the PPO homopolymer. The increase in the lower T_g can be attributed to a number of possible factors:

The attachment of one chain end to the PPO in the formation of the block copolymer can increase the T_g; some phase mixing between the PPO and PVBC to form a PVBC-rich phase rather than a pure PVBC phase; and the constraint of segmental motion from the glassy PPO in the dispersed system could increase the T_g of the PVBC phase. In addition, crosslinking can occur from the benzyl chloride groups,[132] that could increase the T_g.

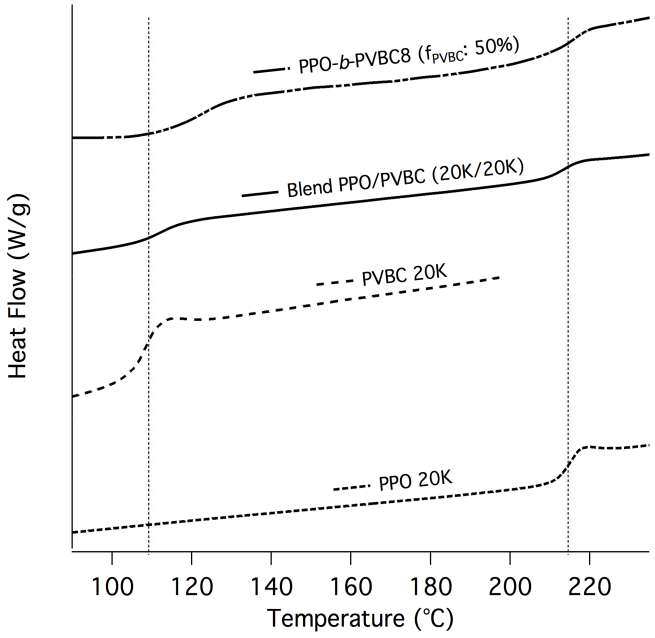

Figure 3.5 DSC thermograms of PPO-*b*-PVBC8 with a weight percentage of PVBC 50 %, blended PPO and PVBC with a weight percentage of PVBC of 50 %, homopolymer PVBC (20 kg/mol) and homopolymer PPO (20 kg/mol). Vertical dash lines were added for clarification.

Further analysis of DSC thermograms are shown in Figure 3.6 for six diblock copolymers with weight percentages of PVBC ranging from 16 % to 74 %. The copolymers with weight percentage between 37 % and 58 % showed two T_gs, indicating phase separation between PPO phase and PVBC phase. The T_g of the PVBC block cannot be found in the DSC thermograms of PPO-*b*-PVBC1 and PPO-*b*-PVBC3, and so as the T_g of the PPO block in PPO-*b*-PVBC12, in

part due to instrument sensitivity and also because the size of the dispersion phase was below a critical value for DSC identification.[133]

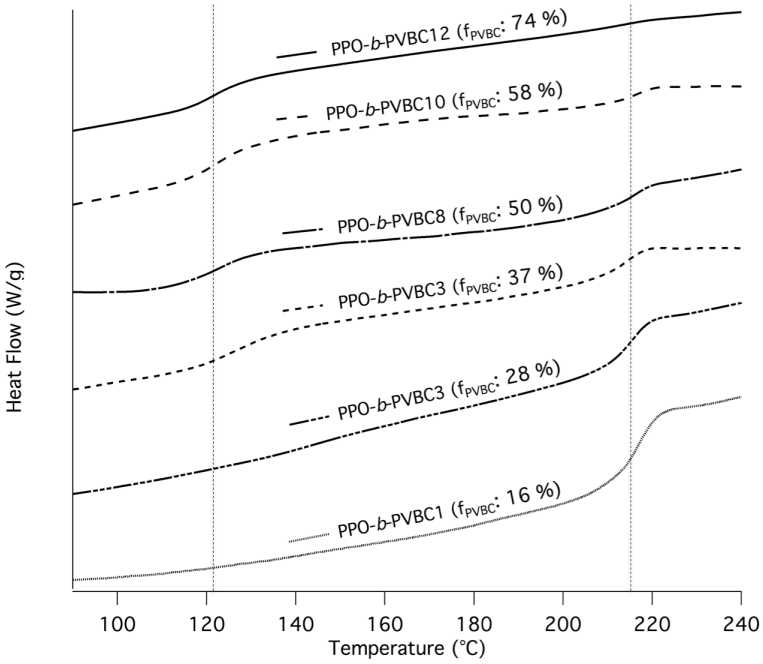

Figure 3.6 DSC thermograms of copolymers PPO-*b*-PVBC1, PPO-*b*-PVBC3, PPO-*b*-PVBC8, PPO-*b*-PVBC10 and PPO-*b*-PVBC12 with weight percentages of PVBC of 16 %, 28 %, 50 %, 58 % and 74 %. Vertical dash lines were added for clarification.

PPO-*b*-PVBC films were prepared by pressing the copolymer powders at 240 °C for 20 minutes. The press temperature was determined from TGA and DSC measurements to exceed the T_gs of both the PVBC and the PPO phases yet avoid themal degradation. At this temperature some crosslinking of the PVBC does occur[132] and the PPO-*b*-PVBC copolymer films were found to be insoluble but swelled in the solvents that were good solvents prior to melt pressing the films.

3.5.4 Film preparation and quaternization.

The melt-pressed films were immersed in 45 % aqueous trimethylamine solution to obtain quaternized films. The generation of benzyltrimethylammonium groups can be demonstrated by FT-IR spectroscopy. The FT-IR spectra of the PPO macroinitiator, PPO-*b*-PVBC8 and PPO-*b*-PVBTMA8 are displayed in Figure 3.7 as representative samples. In the IR spectrum of copolymer PPO-*b*-PVBC8, the presence of the absorption peak around 650 cm^{-1} was characteristic of C-Cl stretching, indicating the successful attachment of the PVBC block to the PPO block.[134] After the quaternization, the disappearance of C-Cl stretching implied an effective substitution of chloride groups to form an ammonium group. A new absorption appeared at approximately 3400 cm^{-1} in the IR spectrum of the quaternized copolymer as a result of moisture absorbed by the hygroscopic ammonium groups.

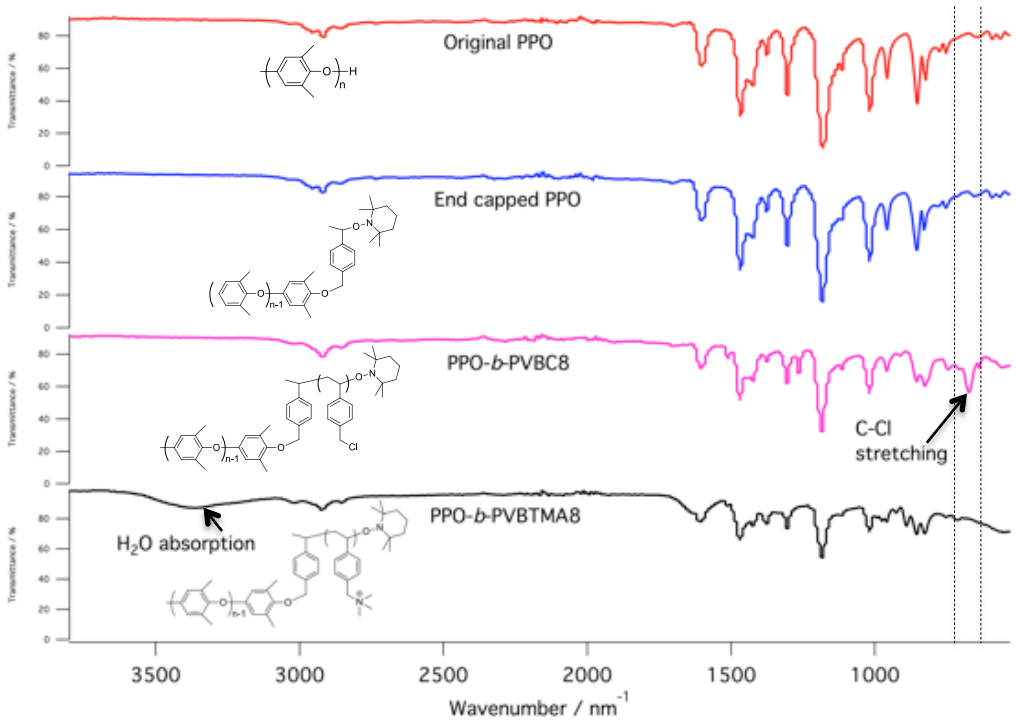

Figure 3.7 FT-IR spectra of original PPO, end capped PPO, copolymer PPO-*b*-PVBC8 and quaternized copolymer PPO-*b*-PVBTMA8.

Solubility test was performed on polymers before and after hot press and quaternization. The result is summarized in Table 3.2. The pressed PPO-*b*-PVBCx films could not dissolve but only swelled in solvents, resulting from the crosslinking between benzyl chloride groups during hot pressing. The pressed films were then immersed in 45 % aqueous trimethylamine solution to obtain quaternized films, whose solubility was also studied, and the result is presented in Table 3.2. The result shows that the PPO-*b*-PVBCx powders before hot pressing have good solubility in the chlorinated solvents, while the pressed PPO-*b*-PVBCx films lose the solubility but only swell in the chlorinated solvents. The quaternized films were insoluble but swelling in the chlorinated solvents with additional swelling in water and methanol occurred because of the hydrophilic PVBTMA block.

Table 3.2 Solubility Test for PPO-*b*-PVBCx Powder, Pressed PPO-*b*-PVBCx Films and PPO-*b*-PVBTMA quaternized Films

	$CHCl_3$	1,2-dichloro-benzene	1,1,2,2-tetrachloro-ethane	trichloro-ethylene	DCM	THF	MeOH	toluene	DMF	H_2O
PPO-*b*-PVBCx powder	+	+	+	+	+	+	–	–	–	–
Pressed PPO-*b*-PVBCx films	–/swell	–/swell	–/swell	–/swell	–/swell	–/swell	–	–	–	–
PPO-*b*-PVBTMA	–/swell	–/swell	–/swell	–/swell	–/swell	–/swell	–/swell	–	–	–/swell

"+" = soluble, "– " = insoluble, "–/swell" = insoluble but swelling.

3.5.5 Water uptake, ion exchange capacity, and ionic conductivity.

The candidacy of AEMs for alkaline fuel cell application can be evaluated by determining the ionic exchange capacity (IEC), water uptake. The water uptake and IEC relative to the weight percentage of the PVBTMA block is summarized in Table 3.3 for the PPO-*b*-PVBTMA films in the chloride counterion form in water at 20 °C. As expected, water uptake increased proportionally with increasing fraction of the ionic component PVBTMA block and the concomitant increase in IEC. The titrated IEC values of the melt-pressed PPO-*b*-PVBTMA films were found to be lower than that calculated from the NMR spectra of the PPO-*b*-PVBC powder. The IEC difference between theoretical IEC and titrated IEC was attributed in part to the crosslinking of the benzyl chloride groups that occurred during melt-pressing of the films. The crosslinking reduced the total number of benzyl chloride groups available for conversion to ammonium chloride groups. However, the crosslinking of what has been converted into the ionic portion of the membranes ensures that the material cannot dissolve in aqueous solutions and inhibits the water uptake during hydration. The quaternized PPO-*b*-PVBTMA films in this study were found to remain intact with IECs as high as 3.2 meq/g because of the crosslinking in the hydrophilic portion. The PPO-*b*-PVBTMA membranes were able to support more charge carrier groups (higher IEC values) to afford higher conductivity compared to reported AEMs with similar water uptake and the same pendent cations. For example, PPO-*b*-PVBTMA11 had a water uptake of 50 % and an IEC of 2.4 meq/g. For comparison, recently reported values for other materials show water uptake of 50 % for IECs of 1.54 meq/g;[31] water uptake of 73 % for IEC of 0.82 meq/g;[110] water uptake of 53 % for IEC of 1.83 meq/g,[65] and water uptake of 50 % for IEC of 1.23 meq/g.[105] Compared to the published values, the water uptake of PPO-*b*-

PVBTMA membranes was significantly lower than that found for other materials with the same IEC values.

The number of water molecules per cationic group, hydration number (λ), is an important parameter for AEMs. λ was measured for the different membranes and was determined to be around 4-5 when the PVBTMA weight percentage was below 40 weight percent. A distinct change occurred as the PVBTMA weight percentage increase above 40 % with the hydration number increasing along with the weight percentage as the PVBTMA becomes the major component and allowing a greater water uptake.

Table 3.3. Weight Percentage of PVBTMA(OH), IEC, Water Uptake and λ of PPO-*b*-PVBTMA Membranes

sample	weight percentage of PVBTMA[Cl][a] (%)	IEC[a] (meq/g)	IEC[b] (meq/g)	water uptake (%)	λ[c]
PPO-*b*-PVBTMA1	20	1.0	0.7	5	4.0
PPO-*b*-PVBTMA2	30	1.4	1.4	11	4.4
PPO-*b*-PVBTMA3	35	1.6	1.4	13	5.2
PPO-*b*-PVBTMA4	39	1.8	1.6	13	4.5
PPO-*b*-PVBTMA5	45	2.1	1.7	32	10.4
PPO-*b*-PVBTMA6	48	2.2	1.7	33	10.8
PPO-*b*-PVBTMA7	55	2.6	2.4	50	11.6
PPO-*b*-	58	2.7	2.5	64	14.2

PVBTMA8					
PPO-*b*-PVBTMA9	62	2.9	2.6	70	15.0
PPO-*b*-PVBTMA10	65	3.1	2.8	87	17.2
PPO-*b*-PVBTMA11	69	3.3	2.9	95	18.2
PPO-*b*-PVBTMA12	80	3.8	3.2	174	30.2

[a]Calculated from ^{1}H NMR spectra of PPO-*b*-PVBCx samples. [b]Titrated values. [c]Number of surrounded water molecules per ammonium group.

3.5.6 Morphological study of PPO-*b*-PVBTMA membranes.

The PPO-*b*-PVBTMA membranes were investigated by TEM to observe the morphology with different weight percentage of PVBTMA. Typical cross-sectional TEM micrographs are presented in Figure 3.8 for the dry membranes of PPO-*b*-PVBTMA1, PPO-*b*-PVBTMA10, and PPO-*b*-PVBTMA12. Distinct phase separation was observed in each case. ImageJ analysis showed that the percentage of the darkened domains corresponded reasonably to the weight percentage of PVBTMA and therefore indicated the PVBTMA phase was stained after the exposure to OsO_4 (Table 3.4).

Table 3.4 ImageJ analysis of the TEM images of PPO-*b*-PVBTMA1, PPO-*b*-PVBTMA10, and PPO-*b*-PVBTMA12

sample	mean-to-max ratio/%
PPO-*b*-PVBTMA1	22
PPO-*b*-PVBTMA10	61
PPO-*b*-PVBTMA12	73

The membranes exhibited phase separation without long-range ordering in all TEM micrographs. PPO-*b*-PVBTMA1 with the lowest fraction of PVBTMA showed the PVBTMA phase dispersed in the PPO matrix as spherical shapes (Figure 3.8a). An increase in the weight percentage of PVBTMA to 65 % for PPO-*b*-PVBTMA10 the TEM image showed that the PVBTMA phase becomes the major and continuous phase (Figure 3.8b). When the weight percentage of PVBTMA[Cl] reached 80 %, PPO became the dispersed phase in the PVBTMA phase (Figure 3.8c). The larger domain size for the dispersed PPO in Figure 3.8 (c) than the PVBTMA in Figure 3.8 (a) was due to the longer chain length of PPO in PPO-*b*-PVBTMA12 than that of PVBTMA in PPO-*b*-PVBTMA1, and the fact that PPO chain was more extended resulting from its inherent stiffness. The TEM micrographs for the three membranes revealed that better-connected PVBTMA phases were achieved in the samples with higher weight percentage and longer length of PVBTMA blocks.

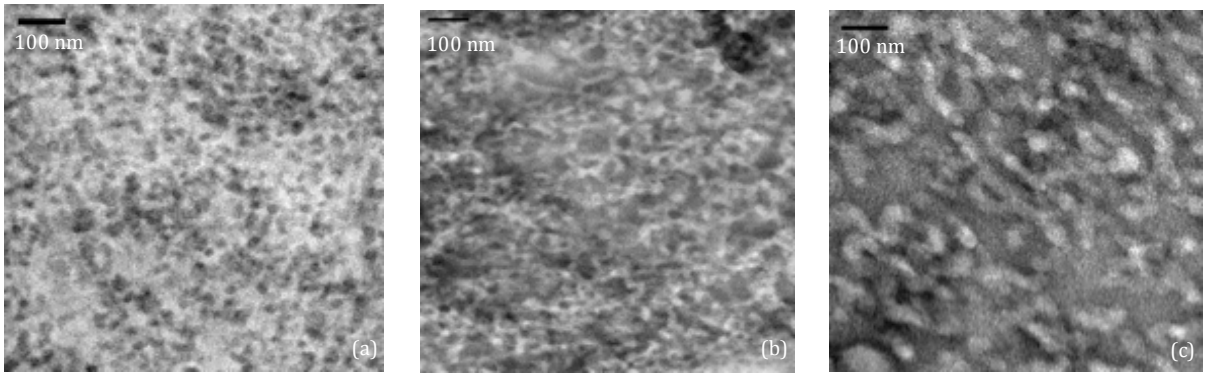

Figure 3.8 Cross-sectional TEM micrographs of dry membranes of PPO-*b*-PVBTMA1 (a), PPO-*b*-PVBTMA10 (b), and PPO-*b*-PVBTMA12 (c).

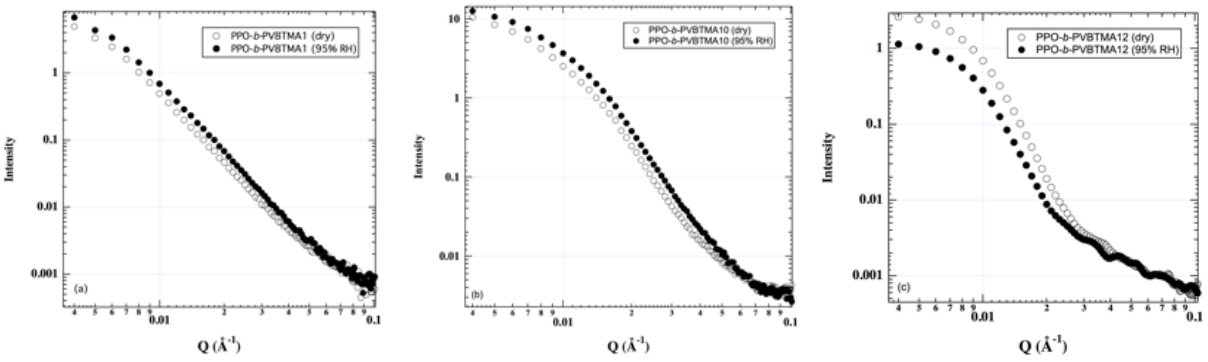

Figure 3.9 SAXS profiles of PPO-*b*-PVBTMA1 (a), PPO-*b*-PVBTMA10 (b), and PPO-*b*-PVBTMA12 (c) under dry condition and 95 % relative humidity at 60 °C.

The lack of long-range ordering was also observed in the SAXS profiles of PPO-*b*-PVBTMA1, PPO-*b*-PVBTMA10, and PPO-*b*-PVBTMA12 from the absence of scattering peaks (Figure 3.9).

3.5.7 Ionic conductivity of PPO-*b*-PVBTMA membranes in their hydroxide form and bicarbonate form in water.

The ionic conductivities of the PPO-*b*-PVBTMA membranes were evaluated in their hydroxide and bicarbonate form in water. The bar chart in Figure 3.10 displays the hydroxide conductivity and bicarbonate conductivity measured in water at 20 °C. The hydroxide conductivity was higher than the bicarbonate conductivity for each PPO-*b*-PVBTMA sample due to the higher aqueous diffusion coefficient of the hydroxide ion.[135,136] The copolymers PPO-*b*-PVBTMA5 and PPO-*b*-PVBTMA6 had the same values for ion exchange capacity and similar water absorption extent, the ionic conductivity of PPO-*b*-PVBTMA5 was slightly higher than that of PPO-*b*-PVBTMA6, presumably deriving from a better-connected ion conducting network in PPO-*b*-PVBTMA5.

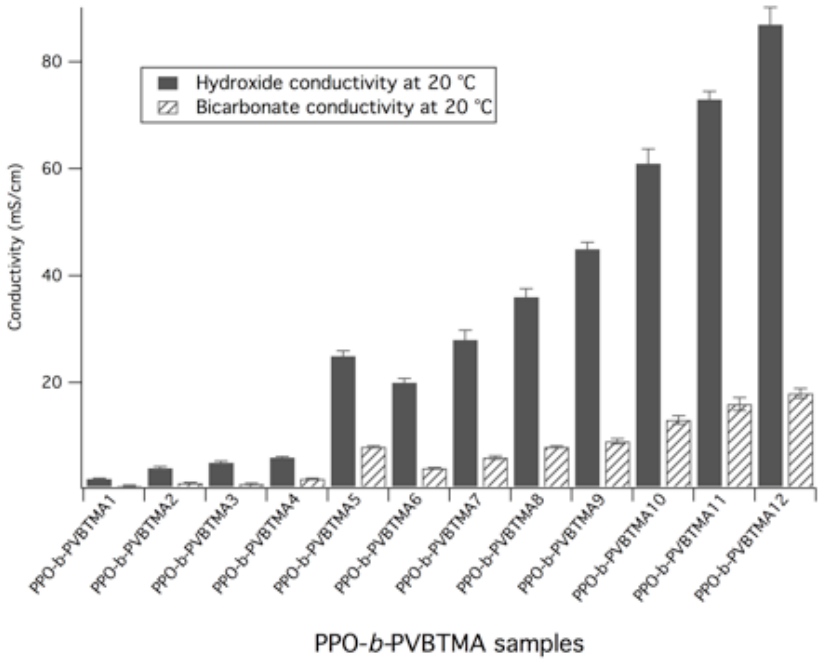

Figure 3.100 Ionic conductivity comparison of the PPO-*b*-PVBTMA series membranes under fully hydrated condition in their hydroxide forms (solid black) and bicarbonate forms (black stripe) at 20 °C. Errors were calculated based on three replica of each sample.

The plot of the conductivity at 60 °C versus water uptake shown in Figure 3.11 (a) demonstrates elevated ionic conductivity along with increased water uptake. A similar trend was also found in Figure 3.11 (b) between the relationship of ionic conductivity and ion exchange capacity. This phenomenon can be rationalized by the factors assisting to increase conductivity: higher water content induced better connected ion pathways and more conductive sites. More conductive sites usually lead to higher water uptake because of the higher content of the hydrophilic part. In the PPO-*b*-PVBTMA membranes, PPO-*b*-PVBTMA4 and PPO-*b*-PVBTMA5 had similar IEC values, 1.6 meq/g for the former one and 1.7 meq/g for the latter one, while the water absorption of PPO-*b*-PVBTMA5 reached 32 % when PPO-*b*-PVBTMA4 has only 13 %. Research has shown that sudden upsurge of water uptake was due to the

percolation threshold, where the isolated ionic clusters started to percolate to form continuous networks throughout the membrane after the percolation threshold.[48] The sudden increase of water uptake from PPO-*b*-PVBTMA4 to PPO-*b*-PVBTMA5 indicated that the percolation threshold of the PPO-*b*-PVBTMA membranes for the IEC was around 1.7 meq/g, where the hydration number was calculated to be 10 water molecules per ammonium group.

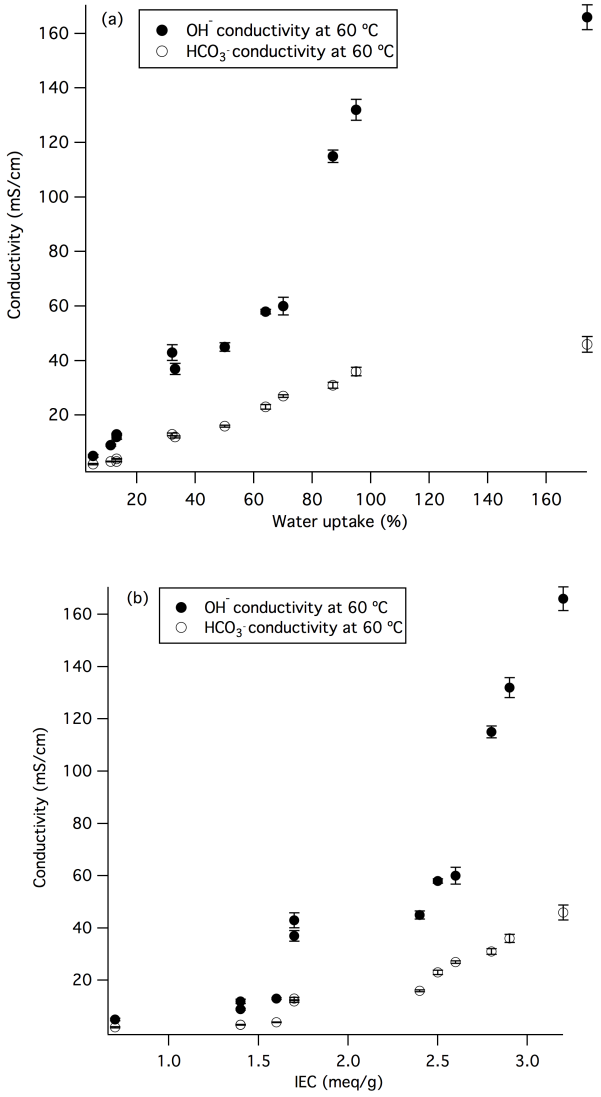

Figure 3.11 Ionic conductivity of the PPO-*b*-PVBTMA series membranes under fully hydrated condition in their hydroxide forms (solid shape) and bicarbonate forms (hollow shape) at 20 °C and 60 °C as a function of (a) water uptake and (b) ion exchange capacity.

The relationship between conductivity and IEC in Figure 3.11 (b) illustrates a small conductivity increase at IEC lower than 2.4 meq/g, and then a larger increase at IECs higher than 2.5 meq/g, indicating the formation of a continuous ion-conducting network at higher IEC values. The plot of conductivity against water uptake in Figure 3.11 (a) shows an almost linear conductivity increase with increased water uptake for the former 11 membranes in both counter ions except PPO-*b*-PVBTMA12, indicating a strong dependence of conductivity on water uptake, also suggesting an excessive swelling in the PPO-*b*-PVBTMA12 membrane which diluted the charge carrier concentration therefore resulting in compromised conductivity. The PPO-*b*-PVBTMA11 membrane exhibited the overall optimized properties considering the high conductivity, the suppressed water uptake. The hydroxide conductivity reached 73 ± 1.5 mS/cm at 20 °C and 132 ± 3.8 mS/cm at 60 °C, comparable with the highest reported conductivity to date.[31] At the same time PPO-*b*-PVBTMA11 membrane remained qualitatively tough and flexible under both dry and hydrated conditions. The low water uptake warrants further study for this material in fuel cell applications.

The temperature dependence of chloride conductivity was studied at 95 % relative humidity for the PPO-*b*-PVBTMA membranes (Figure 3.12). Arrhenius behavior was found in a plot of log conductivity versus temperature and the activation energy for each membrane was calculated through the slope, resulting in the range of 6 to 11 kJ/mol independent of the IEC or water uptake. The activation energy values for the PPO-*b*-PVBTMA membranes were similar to that reported for other anionic exchange membranes.[137]

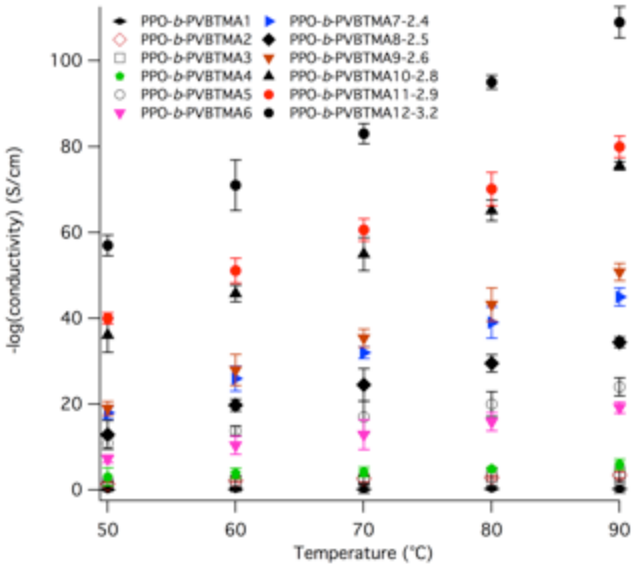

Figure 3.12 Temperature dependence of chloride conductivity of PPO-*b*-PVBTMA membranes under 95 % relative humidity. The number after each membrane name depicts the titrated IEC value.

3.6 Conclusion

A series of PPO-*b*-PVBC diblock copolymers was synthesized with different PVBC length in this research. Thermoforming by melt-pressing was employed to press the PPO-*b*-PVBC powder into films while a crosslinking side reaction of the benzyl chloride groups provide extra mechanical support. The PPO-*b*-PVBTMA12 membrane with IEC as high as 3.2 meq/g was obtained as a flexible film under hydrated conditions. The PPO-*b*-PVBTMA membranes exhibited constrained water uptake compared to other membranes with the same IEC values. The PPO-*b*-PVBTMA11 membrane showed high hydroxide conductivity at 60 °C (132 ± 3.8 mS/cm) while behaving as a flexible film under both dry and wet conditions.

Acknowledgement

Funding was provided by the Army Research Office MURI grant (W911NF-10-1-0520). The NMR spectroscopy was possible with a grant from the NSF-MRI CHE-0923537.

CHAPTER 4 POLYSULFONE BASED TRIBLOCK COPOLYMER FOR ANION EXCHANGE MEMBRANE APPLICATIONS

4.1 Introduction

Alkaline fuel cells (AFCs) have attracted significant attention because the alkaline environment operation provides AFCs with the advantages of using non-precious metals as electrodes, stemming from facile fuel oxidation and oxygen reduction, as well as reduced metal oxidation due to decreased standard potential on the electrodes.[19,20,138] As an important component in AFCs, the anion exchange membrane acts as a hydroxide ion conductor in frequent start/stop cycles during fuel cell operation. With the demand to supply adequate ionic conductivity and retain extended durability under thermal and mechanical stress in fuel cell operation, the fabrication of anion exchange membranes (AEMs) faces serious challenges in achieving high hydroxide conductivity and reliable mechanical properties.

Numerous AEMs have been developed based on polystyrene,[33,80,110,139] polyethylene,[46,108,140] polynorborene,[81,141] polybenzimidazole,[142,143] and poly(arylene ether).[25,31,77,105,106] Among these materials, polysulfone stands out to be an excellent supporting matrix because of its strong film forming ability, thermal and mechanical properties, and its solvent processability.[144] In previous research for alkaline fuel cell application, polysulfone was either chloromethylated on the aromatic backbone and then quaternized by reacting with trimethylamine,[44,126,145,146] or brominated at the benzylic position followed by quaternization,[106,147] or modified by means of lithiation chemistry with amine groups and then quaternized,[61] or functionalized through a combination of iridium catalyzed C-H bond borylation

and Suzuki-Miyaura cross-coupling reaction.[105] The aforementioned research mainly involved random or multiblock copolymers. Recently, a series of triblock copolymers was synthesized by Bai and coworkers containing quaternized poly(2,6-dimethyl-1,4-phenylene oxide) (PPO) as the hydrophilic outer blocks and polysulfone as the hydrophobic middle block.[65]

Our current research started by synthesizing dihydroxyl terminated polysulfone, followed by end capping the hydroxyl groups with alkoxyamine to act as macroinitiator to grow poly(vinylbenzyl chloride) (PVBC) through nitroxide mediated polymerization. The polycondensation produced polysulfone was connected with living polymerization produced PVBC to keep the integrity of polysulfone and simplify the synthetic procedure by using functional monomer while avoiding bromination and chloromethylation. With this design, we can tune the IEC of the polymer electrolyte by changing the length of the PVBC block and readily quaternizing it into the PVBTMA block in aqueous trimethylamine solution. The polysulfone block was the hydrophobic matrix and served as mechanical support, while the hydrophilic PVBTMA block was employed to deliver hydroxide ions from the cathode to the anode and direct phase separation. The quaternized membranes were thoroughly investigated on their ion exchange capacity, water uptake, and conductivity in different counter ions.

4.2 Experimental section

The following section describes the chemicals and solvents used to synthesize the end-capping agent and triblock copolymers.

4.2.1 Materials

Bisphenol A was obtained from Sigma-Aldrich and recrystallized from toluene, followed by drying under vacuum at room temperature overnight before use. 4,4'-Dichlorodiphenyl

sulfone was obtained from Solvay Advanced Polymers and used without any purification. Potassium carbonate (anhydrous) was obtained from Fisher and pulverized in a mortar and pestle, then dried overnight in a vacuum oven before use. N-Methyl-2-pyrrolidone (Sigma-Aldrich, HPLC grade) was distilled from calcium hydride under reduced pressure before use. Toluene was passed through a commercial column system for purification (Innovative Technology). 4-Vinylbenzylchloride (90%, Sigma-Aldrich) was distilled from calcium hydride (Sigma-Aldrich, 95 %) under reduced pressure before block copolymer synthesis. For alkoxyamine synthesis, 4-vinylbenzyl chloride was passed through a silica gel column before use. 1-[1-(4-Chloromethylphenyl)ethoxy]-2,2,6,6-tetramethylpiperidine (Cl-BzEt-TMEPO) was synthesized using Mn(salen)Cl as a catalyst. Synthesis of Cl-BzEt-TEMPO and Mn(salen)Cl were both prepared according to the literature.[148] Tetrabutylammonium hydroxide (TBAH) (1.0 M in methanol) was purchased from Sigma-Aldrich and diluted to 0.1 M with chloroform before use. Homopolymers of PVBC (8 kg/mol and 20 kg/mol) were synthesized through nitroxide mediated polymerization. Blended polysulfsone and PVBC was prepared by dissolving the two homopolymers in a targeted ratio followed by precipitation. The precipitate was collected and dried under vacuum for 24 h.

4.3 Synthetic process

The following sections describe the synthesis of polysulfone, end-capping agent, and triblock copolymers. The characterization techniques for the copolymers and membranes are discussed.

4.3.1 Synthesis of dihydroxy-terminated polysulfone.

Bisphenol A (5.00 g, 21.9 mmol), 4,4'-dichlorodiphenyl sulfone (6.21 g, 21.6 mmol) and potassium carbonate (4.54 g, 32.8 mmol) were weighed into a two-neck round bottom flask equipped with a condenser, a Dean-Stark trap, and a nitrogen inlet. NMP (45.0 mL) and toluene (15.0 mL) were added to the flask. The flask was then heated to 140 °C to react for 6 h before increasing the temperature to 170 °C. After 15 h, the flask was cooled to room temperature, chloroform was added to dilute the viscous solution, and then precipitated into a large excess of methanol. The precipitate was collected through filtration using a glass fritted funnel, and then the islated polymer powder was boiled in water for 30 min to remove potassium carbonate salt residue. The polymer was then filtered and washed several times with fresh methanol before drying in a vacuum oven overnight at 60 °C.

4.3.2 Synthesis of end capped polysulfone (PSf-BzEt-TEMPO).

Polysulfone (5 g, 0.17 mmol) was dissolved in 120 mL NMP, followed by the addition of NaH (0.24 g, 10 mmol). The mixture was heated to 50 °C and stirred for one hour. 1-[1-(4-Chloromethylphenyl)ethoxy]-2,2,6,6-tetramethylpiperidine (1.3 g, 4.1 mmol) was then added and stirred for 72 h at 50 °C. The mixture was cooled to room temperature and then precipitated into 1200 mL methanol. The precipitate was collected by filtration through a glass fritted funnel and washed several times with fresh methanol. The polymer was then dissolved in chloroform and precipitated in methanol two more times before drying under vacuum at 60 °C overnight.

4.3.3 General procedure to synthesize PSf-PVBC triblock copolymers.

The PSf-PVBC triblock copolymers were synthesized by employing PSf-BzEt-TEMPO as the macroinitiator to initiate nitroxide mediated polymerization of vinylbenzyl chloride. In a typical synthesis of PSf-PVBC triblock copolymers, PSf-BzEt-TEMPO macroinitiator (0.50 g, 0.017mmol) was added to 4-vinylbenzyl chloride (10.0 mL, 71.0 mmol) in a 15 mL single neck, round bottom flask. The flask was sealed with a rubber septum and purged for 30 min with nitrogen. The flask was then immersed in a 125 °C oil bath to initiate the polymerization. The size of the PVBC block was controlled by the reaction time. After reacting for fixed time intervals, the polymerization was terminated by cooling the flask in a dry ice/acetone bath. After the flask was warmed to room temperature, chloroform was added to dilute the reaction residue. The diluted solution was precipitated twice from methanol. The precipitated polymer was collected by filtration and washed with fresh methanol several times before drying under vacuum at 50 °C overnight.

4.3.4 Membrane preparation and quaternization.

The PSf-PVBC copolymer films were prepared through two methods: casting and melt pressing. The casting method was accomplished by dissolving the PSf-PVBC copolymer in chloroform to form a 10 wt.% solution, followed by filtering the solution through filter with pore size of 0.2 μm, and then drop casting the solution on a microscope glass slide. The glass slide was then left at room temperature for 3 h before drying in a vacuum oven at 60 °C for 24 h. The melt pressing was accomplished by pressing PSf-PVBC copolymer powder between two Teflon sheets in a Carver 3912 press at 200 °C and 20000 pounds for 20 min. The temperature of the press was controlled by homemade heated and water-cooled platens. The thicknesses of the melt

pressed films were in a range from 50 to 90 μm. The quaternized films from both methods were obtained by immersing the PSf-PVBC films in 45 % aqueous trimethylamine solution to convert benzyl chloride groups to quaternized ammonium chloride forms. The corresponding bicarbonate form was obtained by soaking the chloride form film in 1 M potassium bicarbonate for 48 h, followed by washing off the excess salt through rinsing and soaking the film in fresh DI water for 12 h with a change in water every two hours. The hydroxide form film was achieved by immersing the chloride form film in 1 M potassium hydroxide for 48 h. Degassed water was used to rinse the film and soak the film for 12 h with bubbling nitrogen. The water was changed every two hours.

4.4 Characterization and Measurements

JEOL ECA-500 FT-NMR was used to record ^{1}H NMR spectra at room temperature. $CDCl_3$ was used as the solvent, and chemical shifts (δ) are reported in ppm relative to tetramethylsilane at 0 ppm.

Thermogravimetric analysis (TGA) was conducted using a Seiko TG/DTA 320 thermal analyzer with upgraded RT instrument software. The measuring temperature range was from 25 °C to 1000 °C with a heating rate of 10 °C min^{-1}. The polymer samples were dried under vacuum at 60 °C overnight before the TGA measurement. Differential scanning calorimetry (DSC) was conducted with Q20 DSC (TA instruments) in a temperature range from 20 °C to 250 °C, heating at 10 °C/min and cooling at 40 °C/min. The samples were in aluminum pans hermetically sealed for measurement. The glass transition temperatures (T_g) were determined at the midpoints of the heat flow changes in the second and third cycles.

Gel permeation chromatography (GPC) (Waters 600-MS) was employed to determine

molecular weights coupled with a Wyatt Technology Mini Dawn detector and an Optilab DSP interferometric refractometer. PLgel 5 μm mixed D columns were used and THF was employed as an eluent at 35 °C and at a flow rate of 1 mL/min. Linear polystyrene standards were used for calibration.

Ultraviolet-visible spectra were acquired in quartz cuvettes with an Evolution 300 PC spectrophotometer (Thermo Electron Corporation) from 200 nm to 600 nm with sample concentrations of 500 ppm in chloroform. 10 μL TBAH was then added. The analysis was conducted by running chloroform as the background then followed by recording the spectra of the samples.

Attenuated total reflectance Fourier transform infra-red (ATR-FTIR) spectra were recorded in the range between 4000 cm^{-1} and 400 cm^{-1} with Thermo Electron Nicolet 4700 spectrometer. Polysulfone, end-capped polysulfone, and PSf-PVBC were measured in powder form. Quaternized samples were measured in membrane form.

Percentage water uptake of quaternized block copolymers were calculated based on the following equation:

$$\text{Water uptake (\%)} = \frac{W_{wet} - W_{dry}}{W_{dry}} \times 100$$

Chloride form membranes were dried at 60 °C under vacuum for 24 h before measuring the dry membrane weight (W_{dry}). The wet membrane weight (W_{wet}) was measured after soaking the dry membranes in DI water until a constant weight was obtained.

The well-established back-titration method[70,149] was used to titrate ion exchange capacity

values (IEC) of the quaternized membranes. Before the measurement, the hydroxide form membranes were each immersed in 9.00 mL of standardized HCl solution (0.01 M) for 24 h to completely neutralize the hydroxide ions in the membrane. Then standardized NaOH solution (0.01 M) was used to titrate the residue HCl by an automatic titrator (Company: Mettler Toledo; Model: G20). After the titration, the chloride-form membranes were dried under vacuum at 60 °C overnight before measuring the mass. The IEC value of each membrane was then calculated from the following equation.

$$\text{IEC} = \frac{V_{HCl} * c_{HCl} - V_{NaOH} * c_{NaOH}}{W_{dry}}$$

where V_{HCl} and c_{HCl} represent the volume and concentration of the standardized HCl solution; V_{NaOH} and c_{NaOH} represent the volume and concentration of standardized NaOH solution; W_{dry} represents the weight of the dry membrane.

For transmission electron microscopy (TEM) experiments, the samples were dried under vacuum overnight before embeding in epoxy resin and sectioned into ~100 nm at room temerature using a Leica Ultracut UCT ultramicrotome (Leica Microsystems, Buffalo Grove, IL). The sections were collected onto 200 mesh copper EM grids. The electron density contrast between hydrophobic and hydrophilic blocks were enhanced by staining for 3 h with osmium tetroxide vapor from a 4 % aqueous solution. The transmission electron micrographs were obtained with an FEI Tecnai F20 electron microscope (FEI Corp, Hillsboro, OR) operated using an accelerating voltage of 200 kV.

Histograms based on TEM micrographs were analyzed by ImageJ. Dark area and bright area percentages were calculated to determine the stained phase after OsO_4 exposure.

Small angle X-ray scattering (SAXS) measurements were carried out at the Advanced Photon Source at Argonne National Lab with a Pliatus 2M SAXS detector and a Pliatus WAXS detector that provided a 12 keV beam with a 1 Å wavelength. The measurement condition was 60 °C with changing relative humidity from dry to 95 % controlled by a combination of wet and dry nitrogen. A film sample was mounted to a sample holder using Kapton tape and the sample holder was positioned perpendicular to the direction of the incident beam so that the beam could pass through the sample. The scattering intensity was normalized for background scattering and beam transmission.

Electrochemical impedance spectroscopy (EIS) was used to measure in-plane conductivity. The membranes were clamped in 4-probe Teflon cells with Pt electrodes, which were measured in a frequency range from 1 Hz to 100 kHz using a BioLogic VMP3 Potentiostat. A TestEquity® (Solatron 1007H Model) environmental chamber was employed to control the temperature and percent relative humidity for chloride conductivity measurement at 95 % relative humidity. The hydroxide and bicarbonate conductivity was measured in deionized ultra pure water (18 MΩ resistance) with a Teflon film as background. The ionic conductivity was obtained from the following equation:

$$\sigma = \frac{d}{L_s W_s R}$$

where σ is the ionic conductivity of the membrane (S cm^{-1}), d is the distance between reference electrodes (mm), L_s and W_s are the thickness (mm) and width (mm) of the membrane, and R is the ohmic resistance of the membrane (Ω).

The activation energy (E_a) was calculated from the linear Arrhenius relationship between -log(σ) and 1000/T:

$$E_a = b \times R$$

where R is the gas constant, b is the slope of the linear regression of $-\log(\sigma) \sim 1000/T$ relationship.

4.5 Results and Discussion

We took advantage of the terminating hydroxyl groups of polysulfone to grow PVBC blocks. The anion exchange membranes were then obtained through quaternizing the PVBC blocks. This design can afford AEMs without chloromethylation on the polysulfone chains, and in the same time avoid damaging the polysulfone backbone under alkaline environment.[150]

4.5.1 Synthesis and characterization of dihydroxy-terminated polysulfone.

The excellent properties of polysulfone, like high chemical and thermal stability, film-forming ability, and mechanical properties, have made it an ideal candidate to mechanically support anion exchange membranes. Dihydroxy-terminated polysulfone was prepared by reaction of bisphenol A with 4,4'-dichlorophenylsulfone using potassium carbonate as depicted in Scheme 4.1. The molecular weight and desired end groups were controlled by off-setting the molar ratio of the two monomers based on the Carothers Equation. Bisphenol A was calculated and used as the excess monomer to ensure the hydroxyl functionality. The number-average molecular weight of polysulfone was determined by GPC with polystyrene standards calibration. The obtained molecular weight was calculated to be 30 kg/mol, which reasonably agreed with the target molecular weight, 35 kg/mol.

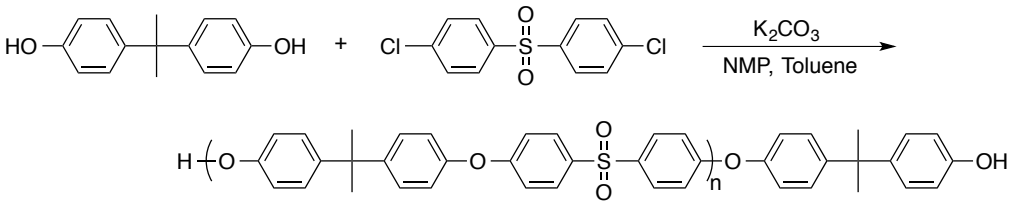

Scheme 4.1 Synthetic route of dihydroxy-terminated polysulfone.

4.5.2 Synthesis and Characterization of PSf-BzEt-TEMPO.

We designed a copolymer to exploit the advantages of polysulfone by growing hydrophilic blocks from the ends of the polysulfone chains. This process started by end capping the hydroxyl end group of polysulfone with TEMPO moiety to serve as a macroinitiator to initiate polymerization with 4-vinylbenzyl chloride. The synthetic route for the end-capped polysulfone is depicted in Scheme 4.2. The phenoxide groups were prepared using sodium hydride at 50 °C followed by adding Cl-BzEt-TEMPO to make PSf-BzEt-TEMPO through the nucleophilic substitution between phenoxide groups and Cl-BzEt-TEMPO. The successful attachment of the end group to polysulfone was validated by the appearance of the "a" peaks and the "b" peak from ^{1}H NMR spectra shown in Figure 4.1, where the "a" peaks corresponding to methyl protons on TEMPO and the "b" peak stemming from the protons on the CH group that is connected to the TEMPO moiety. Also noticeably, the "c" peak belonged to benzyl protons shifted to a lower field because of the ether linkage substitution of the chloride group.

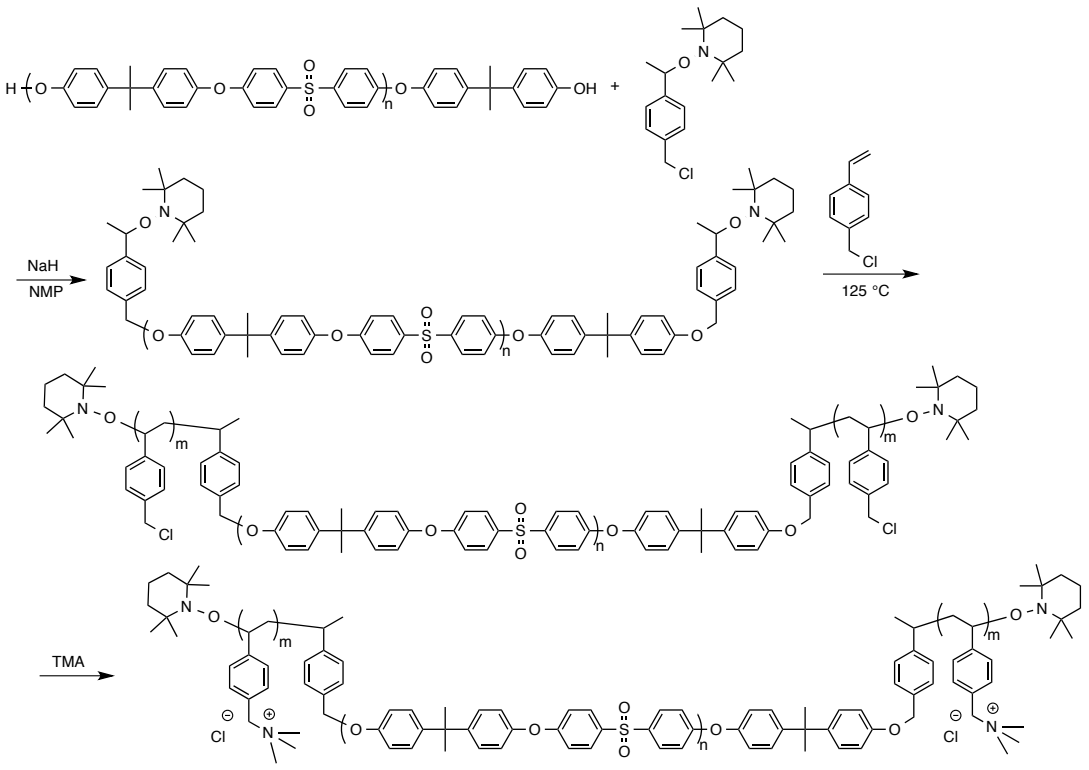

Scheme 4.2 Synthetic route of PSf-PVBTMA triblock copolymers.

The complete end capping was confirmed by ultraviolet/visible (UV/Vis) spectroscopy based on the phenoxide group absorbance between 310nm to 340 nm (Figure 4.2).[125] The upper spectrum shows the original polysulfone before end capping, which has a clear absorbance between 310 nm to 340 nm stemming from the phenoxide groups. While no absorbance in the region of 310 nm to 340 nm in the lower spectrum for the end capped polysulfone demonstrated the successful substitution and fully end capping. The molecular weight of the end capped polysulfone was characterized by GPC in Figure 4.3. The GPC traces showed a negligible shift from the original polysulfone to the end capped polysulfone due to the small additional size of the TEMPO groups.

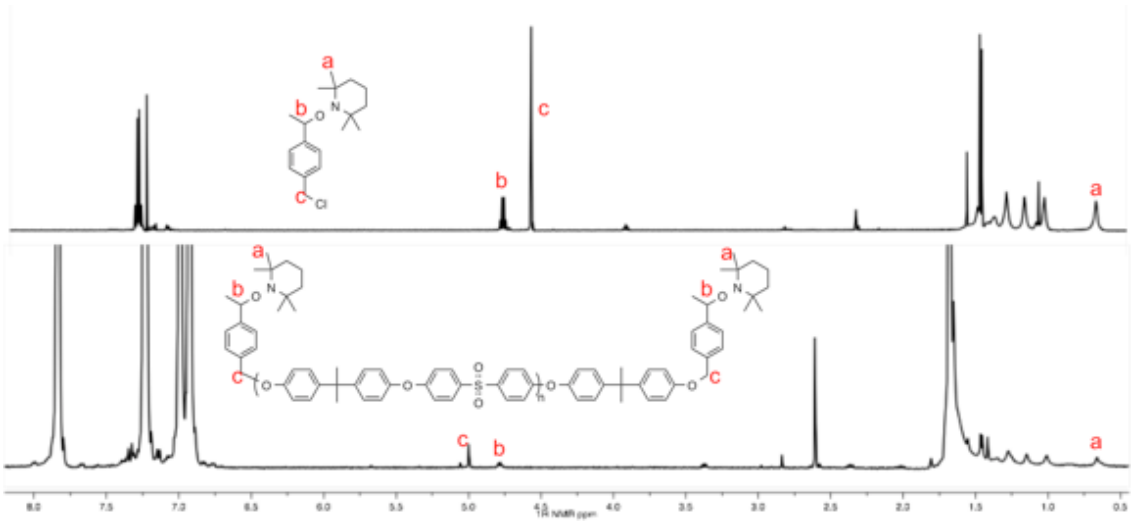

Figure 4.1. ^{1}H NMR spectra of Cl-BzEt-TEMPO (upper) and end-capped polysulfone (lower) measured in $CDCl_3$.

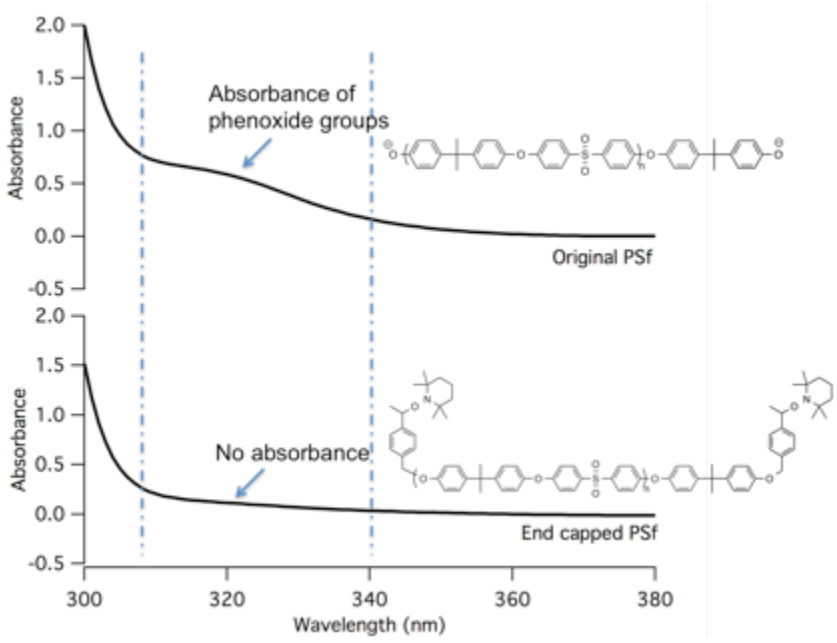

Figure 4.2. UV-Vis spectra of basified original polysulfone (upper) and end capped polysulfone (lower).

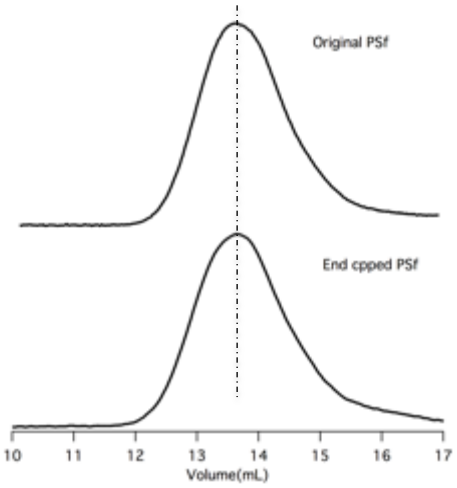

Figure 4.3. GPC traces of the original polysulfone(upper) and end capped polysulfone (lower).

4.5.3 Nitroxide mediated polymerization of PSf-PVBC triblock copolymer.

The synthesis in this study produced the copolymers by combining nitroxide mediated polymerization with a polysulfone produced by polycondensation. The dihydroxyl-terminated polysulfone chains were end capped with TEMPO moieties on both ends so a triblock copolymer was produced. A series of block copolymers with different PVBC block lengths were synthesized in this research. The PVBC block length was controlled by reaction time while the polymerization carried out in bulk vinylbenzyl chloride at 125 °C. Figure 4.4 displays the GPC traces of the end-capped polysulfone and five PSf-PVBC triblock copolymers with different PVBC lengths. Due to larger hydrodynamic volumes induced by their higher molecular weights, the block copolymers have lower elution volume compared to the end-capped polysulfone. Both end capped polysulfone and the copolymers exhibited unimodal and narrow shape of the chromatograms, indicating the absence of unreacted PPO or self-initiating polymerization of VBC. The molecular weight obtained from GPC of PSf-PVBC copolymers are shown in Table 4.1.

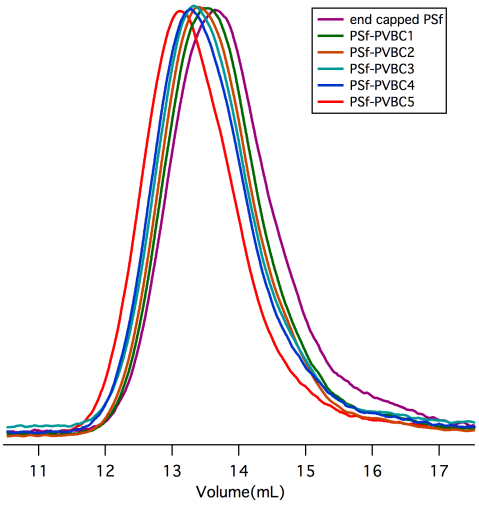

Figure 4.4. GPC traces of end capped polysulfone and five PSf-PVBC triblock copolymers.

^{1}H NMR spectroscopy was employed to characterize the block ratio in PSf-PVBC triblock copolymers and therefore calculating the weight percentage of PVBC blocks. The proton NMR spectrum of a representative triblock copolymer, PSf-PVBC5, is displayed in Figure 4.5, from which the characteristic peaks for polysulfone block and PVBC block can be found. Peak "a" with a chemical shift of 7.8 ppm stemmed from aromatic protons adjacent to sulfone groups in the polysulfone block. Peak "b" with a chemical shift of 4.5 ppm was derived from protons on the benzylic carbon in PVBC block. The quantitative ratio of PVBC block to polysulfone block was calculated from the integration of these two peaks by normalizing the integration of one proton from the polysulfone block and one from the PVBC block. Based on the number-average molecular weight of polysulfone of 30 kg/mol determined by GPC and the block ratios obtained from the NMR spectra, the molecular weight of the PVBC blocks were calculated. Table 4.1 displays the molecular weight of each block copolymer calculated from NMR spectra. A series of PSf-PVBC triblock copolymers was synthesized in this study, and the weight percentage of the PVBC in the block copolymers ranged from 27 % to 58 %.

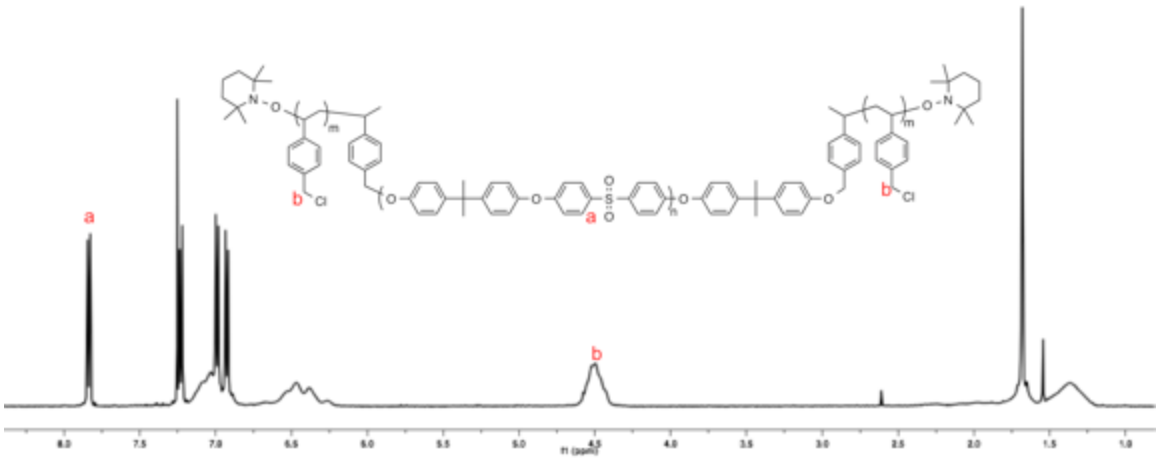

Figure 4.5. ^{1}H NMR spectrum of PSf-PVBC5 in $CDCl_3$.

Table 4.1. Characterizations of PSf-PVBC triblock copolymers

Sample	M_n (NMR)[a]		Weight percentage of PVBC[a] (%)	M_n of PSf-PVBC (GPC)[b] (kg/mol)	M_w/M_n[b]	DP_n[a] of PVBC
	M_n of PVBC block (kg/mol)	M_n of PSf-PVBC (kg/mol)				
PSf-PVBC1	11	41	27	40	1.84	73
PSf-PVBC2	17	47	36	45	1.73	111
PSf-PVBC3	25	55	45	53	1.71	161
PSf-PVBC4	28	58	48	54	1.78	181
PSf-PVBC5	42	72	58	68	1.70	276

[a]m : n depicts the block ratio of Polysulfone to PVBC. [b]Determined by proton NMR from the integrations of methylgroups of PPO and benzylic methylene groups of PVBC. [c]Determined by GPC against polystyrene standard.

4.5.4 Thermal properties of PSf-PVBC triblock copolymers.

The PSf-PVBC copolymers were processed through solvent casting and melt pressing to compare the properties of the cast membranes and pressed membranes. In order to melt press

films, the copolymers needed to fulfill the thermal stability requirement at the pressing temperature. Therefore, the thermal stabilities of PSf-PVBC copolymers were investigated by TGA. Because the linkage and block structure was the same in all copolymers and the only difference was the PVBC block length, a representative copolymer was chosen for the thermal stability study. The TGA thermograms and DTG curves are shown in Figure 4.6 for the highest weight percentage of the PVBC block among all the copolymers, PSf-PVBC5. The TGA measurement was between 20 °C to 1000 °C with flowing nitrogen at a heating rate of 10 °C/min. The copolymer exhibits stability up to 250 °C beyond which there are two thermal degradation steps. Referenced with the thermal behavior of homopolymer PVBC, the first weight loss occurring between 250 °C to 430 °C was attributed to the decomposition of the PVBC block.

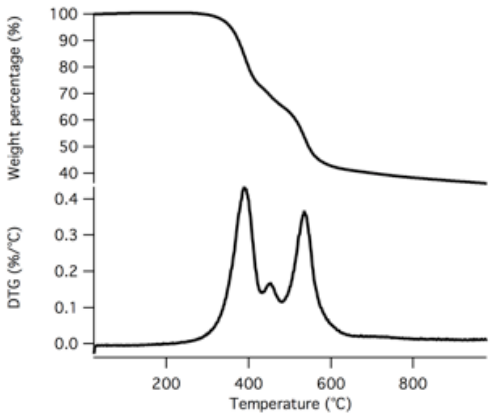

Figure 4.6. TGA (upper) and DTG (lower) thermograms of PSf-PVBC5 (f_{PVBC}: 58 %) under flowing nitrogen at a heating rate of 10 °C/min.

The design in this research was to prepare AEMs with the ability to direct phase separation between hydrophobic phase and hydrophilic phase. Since both the cast films and pressed films were prepared from the PSf-PVBC, phase separated AEMs can only be obtained if PSf phase separated from PVBC phase. DSC was employed to determine whether phase

separation was present in PSf-PVBC copolymers. The comparison of DSC thermograms is presented in Figure 4.7 for triblock copolymers, the PSf/PVBC blended systems, polysulfone homopolymer, and PVBC homopolymers. Each blended PSf/PVBC system had the blended PSf and PVBC homopolymers with the same molecular weight and weight percentage as the corresponding block copolymer. Phase separation was indicated from the two T_g transitions oberved in the DSC thermograms of the block and blended PSf/PVBC samples in Figure 4.7. Block copolymer PSf-PVBC2 and blend $PSf_{30K}/PVBC_{8K}$ have the same weight percentage as $PVBC_{8K}$. Compared to the T_g of homopolymer $PVBC_{8K}$, the PVBC segments in both the block copolymer and the blend system showed higher T_g values. In contrast, the T_g values for the polysulfone part in the block copolymer and blend system were found reduced when compared to the T_g for polysulfone homopolymer. Partial mixing between the PVBC phase and PSf phase is proposed to cause the increases in T_g of PVBC phase and the reduced T_g value of PSf phase as suggested by previous studies on other polymers.[151,152] The increase of the T_g value of PVBC phase can also be due to some crosslinking within the PVBC phase during DSC measurement, where the mobility of the PVBC chains was restricted resulting in an increased T_g. In previous research conducted by Song on the thermal treatment of PVBC, the occurrence of crosslinking was proven by FT-IR.[132] The crosslinking was found only existing inside the PVBC phase because pressed PSf/PVBC blend system only had PSf leaching out of the system by solvent extraction. Furthermore, an isothermal experiment was conducted on PSf-PVBC5 at 200 °C for 30 minutes (Figure 4.8). An irreversible exothermic peak was observed, indicating the occurrence of the crosslinking reaction. The similar phenomenon was also noticed in the block copolymer PSf-PVBC5, the $PSf_{30K}/PVBC_{20K}$ blend, and the homopolymer $PVBC_{20K}$ group. Both of the T_gs of PVBC and PSf phase are higher for the block copolymer compared to the

corresponding blend system, this was possibly associating with the tied chain ends between both PSf chain ends and one PVBC chain end in block copolymers.

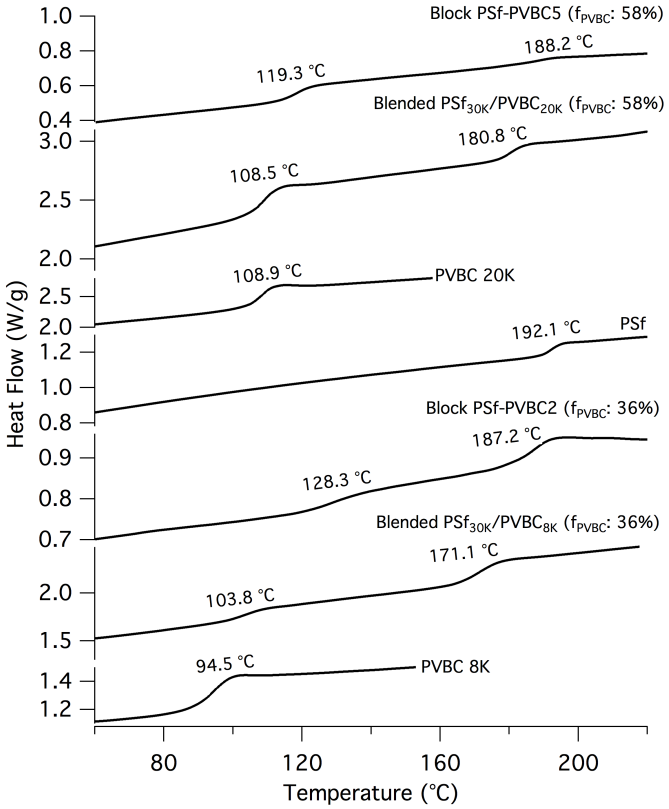

Figure 4.7. DSC thermograms of block copolymers PSf-PVBC2 and PSf-PVBC5, blended polysulfone and PVBC (8 kg/mol) with 36 % weight percentage of PVBC, blended polysulfone and PVBC (20 kg/mol) with 58 % weight percentage of PVBC, homopolymer PVBC (8 kg/mol), PVBC (20 kg/mol) and homopolymer polysulfone (30 kg/mol).

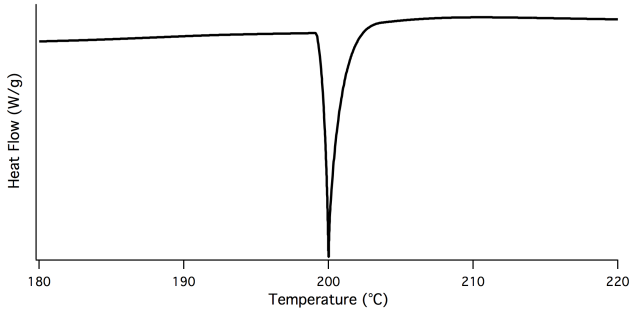

Figure 4.8. Isothermal DSC measurement of PSf-PVBC5 at 200 °C for 30 min.

The DSC thermograms are presented in Figure 4.9 for the PSf-PVBC triblock copolymers, ranging from the lowest weight percentage of PVBC (PSf-PVBC1) to the highest weight percentage of PVBC (PSf-PVBC5). These copolymers all presented two T_g values except for PSf-PVBC1, which showed one T_g at 187 °C for the polysulfone block. This was probably because at a low weight percentage of PVBC, the dispersion size of PVBC in the polysulfone matrix was below a critical value for DSC identification.[133]

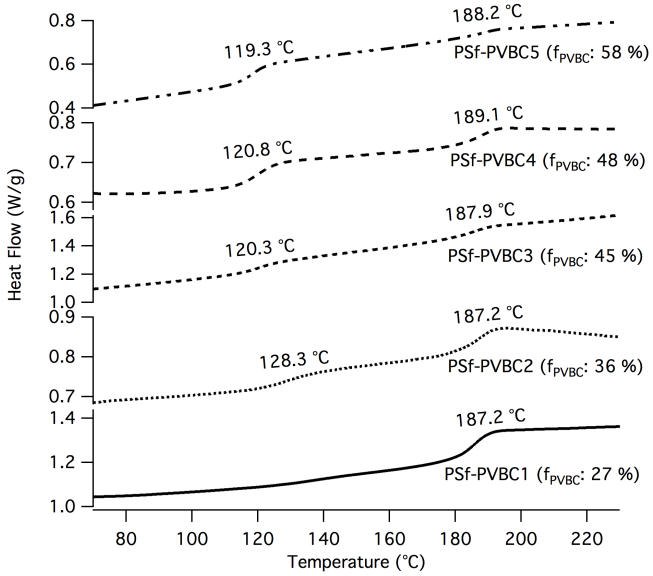

Figure 4.9. DSC thermograms of block copolymers PSf-PVBC1, PSf-PVBC2, PSf-PVBC3, PSf-PVBC4 and PSf-PVBC5 with weight percentages of PVBC of 27 %, 36 %, 45 %, 48 % and 58 %, respectively.

4.5.5 Film preparation and quaternization.

Different film processing methods were studied in this research to compare the effect of film processing on the performance of the quaternized PSf-PVBTMA membranes. The PSf-PVBC triblock copolymers were processed into films before quaternization using two methods: solvent casting and melt pressing. Solvent cast films were prepared by drop casting 10 wt. % polymer solutions in chloroform onto a clean microscope glass slide. The glass slide was then

left at room temperature for a couple of hours before drying in vacuum oven overnight at 50 °C. Melt pressed films were prepared by pressing the copolymer powders into films at 200 °C in a hot press. The press temperature was determined from TGA and DSC measurement, exceeding the T_gs of both the PVBC and polysulfone phase, yet avoiding degradation. The solvent cast and melt pressed films were then immersed in 45 % aqueous trimethylamine solution to generate quaternized films.

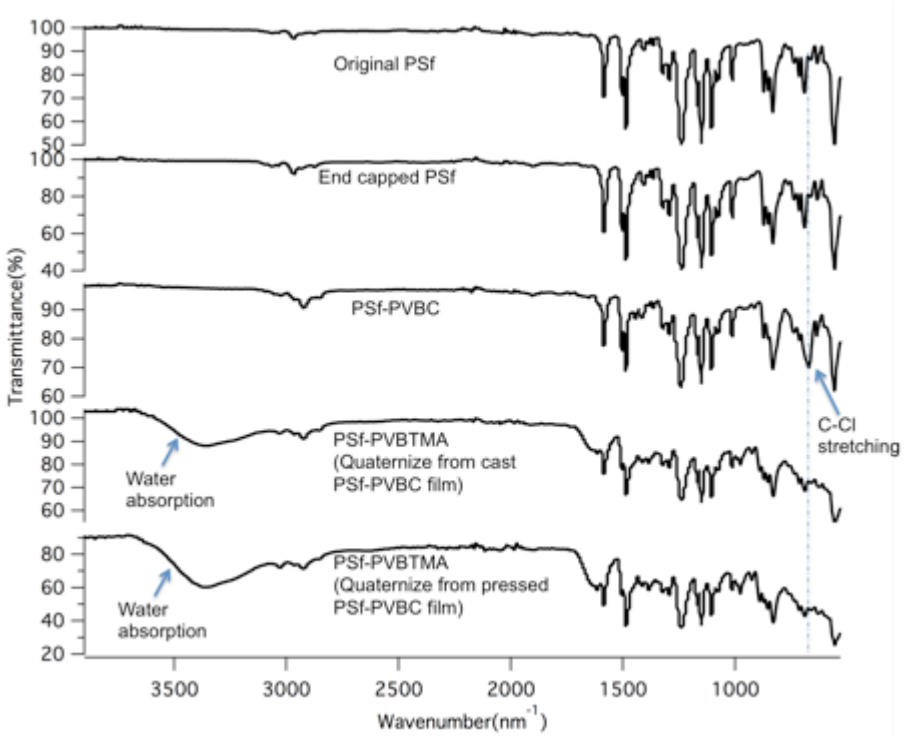

Figure 4.10. IR spectra of polysulfone, end capped polysulfone, PSf-PVBC and PSf-PVBTMA prepared from both solvent casting and melt pressing.

FT-IR spectroscopy was employed to verify the generation of benzyltrimethylammonium groups in the quaternized polymer. Figure 4.10 displays the FT-IR spectra of the original polysulfone, polysulfone macroinitiator, PSf-PVBC5, and PSf-PVBTMA5 originating from both solvent casting and melt pressing. PSf-PVBC5 was chosen as a representative case because the higher weight percentage of PVBC would induce stronger absorption for comparison. The IR

spectra of the original polysulfone and the end-capped polysulfone are essentially the same because the terminal groups in the end capped polysulfone are too small to be observed. In the IR spectrum of the PSf-PVBC5 copolymer, the presence of the absorption peak around 670 cm^{-1} is characteristic C-Cl stretching, indicating the successful attachment of the PVBC block to the polysulfone block.[134] Quaternized PSf-PVBTMA5 shows that the C-Cl stretching disappears, indicating complete conversion from PVBC to PVBTMA. The absorption at 3400 cm^{-1} in the IR spectrum of PSf-PVBTMA5 was due to the hygroscopic ammonium groups absorption of atmospheric water.

The solvent cast films and melt pressed films were studied for their solubility differences and the results summarized in Table 4.2. The PSf-PVBC powder and solvent pressed PSf-PVBC films had the same solubility, while the melt pressed PSf-PVBC films could not dissolve in any solvents but only swell in the solvents that could dissolve PSf-PVBC powder. This was attributed to the crosslinking between benzyl chloride groups during hot pressing. The solution cast and melt pressed films were immersed in 45 % aqueous trimethylamine solution to obtain quaternized films and their solubility was also studied (Table 4.2). The results shows the quaternized films from solvent casting and melt pressing are both insoluble but swelled in all the solvents. Swelling in water and methanol was attributed to the hydrophilic PVBTMA blocks.

Table 4.2. Solubility test to PSf-PVBC powder, the solvent casted PSf-PVBC films and the corresponding PSf-PVBTMA films, melt pressed PSf-PVBC films and the corresponding PSf-PVBTMA films

	$CHCl_3$	1,2-dichloro-benzene	1,1,2,2-tetrachloro-ethane	THF	toluene	DMF	NMP	MeOH	H_2O

PSf-PVBC (powder)	+	+	+	+	+	+	+	–	–
PSf-PVBC films (solvent cast)	+	+	+	+	+	+	+	–	–
PSf-PVBC films (melt press)	–/swell	–/swell	–/swell	–/swell	–/swell	–/swell	–/swell	–	–
PSf-PVBTMA films (solvent cast)	–/swell	–/swell	–/swell	–/swell	–/swell	–/swell	–/swell	–/swell	–/swell
PSf-PVBTMA films (melt press)	–/swell	–/swell	–/swell	–/swell	–/swell	–/swell	–/swell	–/swell	–/swell

"+" = soluble, "– " = insoluble, "–/swell" = insoluble but swelling.

4.5.6 Water uptake, ion exchange capacity

The properties as AEMs for PSf-PVBTMA films were characterized by the water uptake and ion exchange capacity (IEC) relative to the weight percentages of PVBTMA blocks and the method of film preparation. The properties were measured for the PSf-PVBTMA films with chloride counterions in water at 20 °C (Table 4.3). The results show that increasing weight percentage of PVBTMA and the corresponding IEC values led to increased water uptake because of the higher weight percentage of the PVBTMA blocks. The IEC values were determined by titration for the membranes made from the different methods. For the same PSf-PVBTMA sample, the titrated IEC for the solvent cast membranes showed similar values to the theoretical IEC that was calculated from the ^{1}H NMR spectra of PSf-PVBC samples with the error below 5%, suggesting complete quaternization in the solvent cast membranes. Whereas the titrated IEC values for the melt pressed membranes differed from the theoretical IEC values in a range from 7% to 13%, attributed to crosslinking during hot pressing of the films. The crosslinked films had fewer remaining benzyl chloride groups available for quaternization. The solubility test, IR

spectra comparison in Figure 4.9, and isothermal DSC measurement in Figure 4.10 all support the occurrence of the crosslinking reaction, while the IEC determination provides some measure of the crosslinking extent.

Both the pressed membranes and cast membranes revealed comparably lower water uptake with similar IEC from other published research.[31,110,65,105] The pressed membrane PSf-PVBTMA2 showed an IEC of 1.9 mequiv/g with a water uptake of 32 %. The cast membrane PSf-PVBTMA2 showed an IEC of 2.0 mequiv/g with a water uptake of 58 %. While the recently reported values are: water uptake of 112 % for IEC of 2.05 meq/g; water uptake of 13 % for IEC of 1.65 meq/g; water uptake of 53 % for IEC of 1.83 meq/g; and water uptake of 75 % for IEC of 2.02 meq/g. Pressed and cast PSf-PVBTMA2 clearly showed lower water uptake compared to the research with either similar or lower IEC membranes. Moreover, the cast membranes in this research retained good film quality (the dry membrane was flexible) with IEC as high as 2.5 mequiv/g and water uptake of 120 %. While the pressed membranes were all flexible, even when IEC was 2.9 mequiv/g and water uptake was 125 %.

Compared to the water uptake for the solvent cast membranes, the melt pressed membranes with the same PSf-PVBC precursor showed lower IEC values and water uptake. The lower IEC values of melt pressed films resulted from the crosslinking and the accompanied consumption of benzyl chloride groups during melt pressing. A lower IEC and the crosslinking network in melt pressed membranes further lead to lower water uptake compared to solvent cast membranes. Figure 4.11 showed the relationship between water uptake and titrated IEC for pressed membranes and cast membranes, exhibiting a lower water uptake with increasing IEC in pressed membranes.

Table 4.3. Weight Percentage of PVBTMA(OH), IEC and Water Uptake of PSf-PVBTMA Membranes

	Weight percentage of PVBTMA(OH)	IEC (meq/g)[a]	Melt pressed films (Solvent cast films)[d]		
			IEC[b]	Water uptake/%	λ[c]
PSf-PVBTMA1	32	1.6	1.4 (1.6)	12 (35)	5 (12)
PSf-PVBTMA2	42	2.1	1.9 (2.0)	32 (58)	9 (16)
PSf-PVBTMA3	50	2.5	2.3 (2.5)	53 (98)	13 (20)
PSf-PVBTMA4	54	2.6	2.4 (2.5)	71 (120)	17 (26)
PSf-PVBTMA5	64	3.1	2.9 (3.0)	125 (238)	24 (44)

[a]Theoretical IEC calculated from ^{1}H NMR spectra of PSf-PVBC polymers. [b]Titrated IEC. [c]Number of surrounded water molecules per ammonium group. [d]The values in parentheses represent the titrated IEC, water uptake and hydration number of solvent cast membranes.

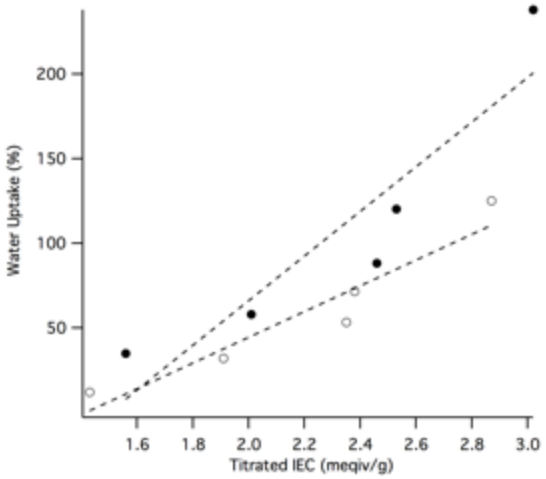

Figure 4.11. Water uptake as a function of titrated IEC for solvent cast membranes (solid cycles) and melt pressed membranes (open cycles). Linear trends are showed in dashed lines.

4.5.7 Morphological characterization of PSf-PVBTMA membranes.

The SAXS profiles of the cast and pressed membranes of PSf-PVBTMA1 were showed in Figure 4.12. The membranes were measured at 60 °C under dry and 95 % RH conditions. PSf-PVBTMA1 was chosen as a representative case to compare the SAXS pattern for cast membranes and pressed membranes. The PSf-PVBTMA1 cast membrane showed a strong scattering peak at 0.014 $Å^{-1}$ under dry conditions, corresponding to a domain spacing of 44.8 nm. Under 95% RH the PSf-PVBTMA1 cast membrane showed a peak at 0.011 $Å^{-1}$ matching with a domain spacing of 57.1 nm. The shift of the scattering peak to a lower angle at higher humidity indicates the ionic domain expansion after water absorption. A single scattering peak suggests the presence of a periodic but lack of long range ordering within the membrane. Another diffuse scattering peak at 0.032 $Å^{-1}$ only appeared in the wet condition but not dry condition, corresponding to the secondary peak and demonstrating more ordered configuration under higher relative humidity. In contrast, the PSf-PVBTMA1 pressed membrane showed a weak and broad scattering peak (where the arrow labels) under both the dry and wet conditions. This was because of the weakened ionic domain correlation in the pressed membrane resulting from the crosslinking within the membrane, which constrained the mobility of polymer chains and interrupted the orderly arrangement.

The SAXS profiles are presented in Figure 4.13 for the cast membranes of PSf-PVBTMA2, PSf-PVBTMA4, and PSf-PVBTMA5 under dry and wet conditions. The SAXS profiles of PSf-PVBTMA3 are not shown because of the identical appearances to the SAXS profiles of PSf-PVBTMA4, presumably due to the close weight percentage of PSf-PVBTMA3 to PSf-PVBTMA4. The scattering peaks in the samples indicated phase separation between the hydrophobic phase and the hydrophilic phase. The positions of the scattering peaks demonstrated

that the domain spacing were between 50 nm and 70 nm for the samples. The absence of any derivative peaks in the SAXS profiles implied that the samples lack long-range ordering.

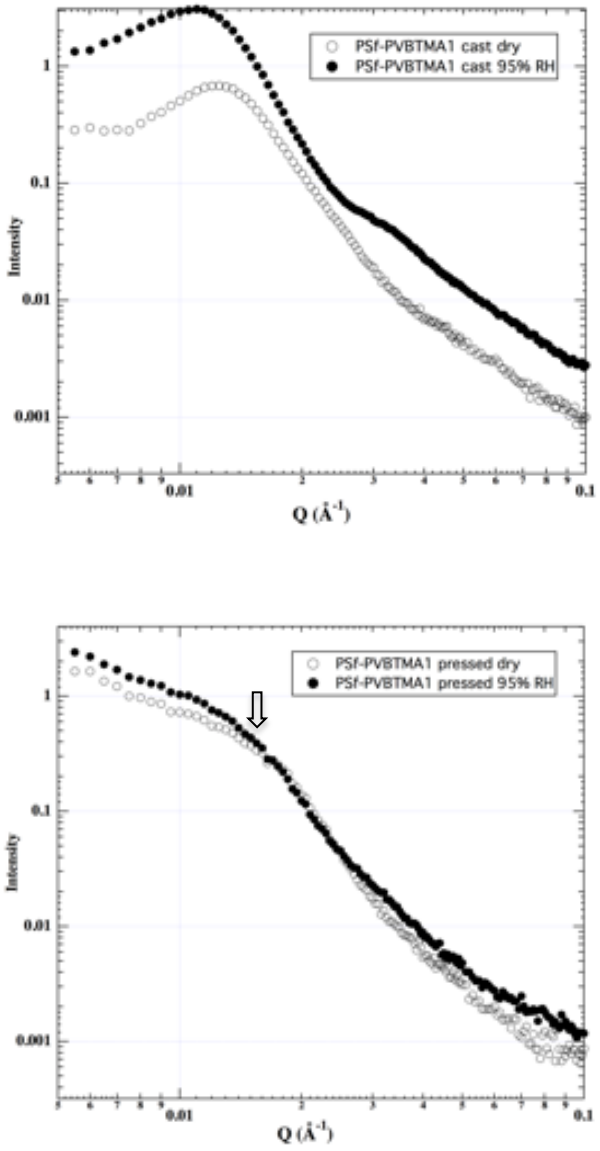

Figure 4.12. SAXS profiles of PSf-PVBTMA1 membrane (a) in chloride form prepared from cast PSf-PVBC1 film(a) and pressed PSf-PVBC1 film (b). The open dots stand for dry membrane at 0 % RH and the solid circles represent the humidified membrane at 95 % RH.

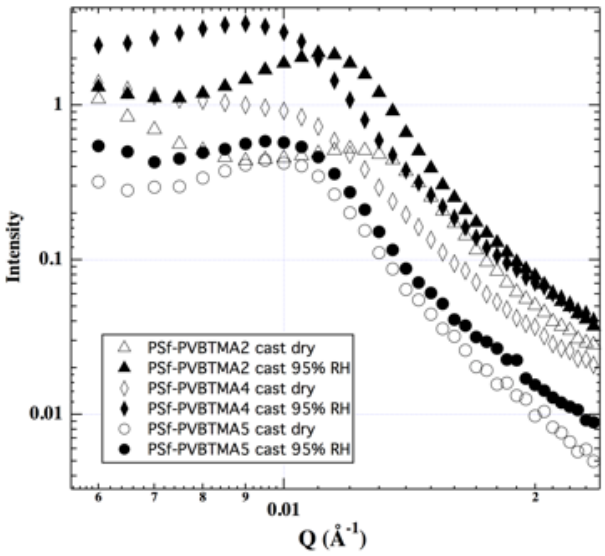

Figure 4.13. SAXS profiles of PSf-PVBTMA2, PSf-PVBTMA4, PSf-PVBTMA5 membranes (a) in chloride forms prepared from cast PSf-PVBC1 film(a) and pressed PSf-PVBC1 film (b). The open dots stand for dry membrane at 0 % RH and the solid circles represent the humidified membrane at 95 % RH.

The morphology of the membranes was also investigated by TEM. The cross-sectional TEM micrographs are shown for each cast membrane (Figure 4.14a, c-f) and a representative pressed membrane of PSf-PVBTMA1 (Figure 4.14b). ImageJ analysis was conducted to the TEM micrographs to determine the stained phase after exposing to OsO_4. The result showed that PVBTMA was the stained phase because of the well-correlated weight percentage of PVBTMA with the darkened domain percentage calculated from ImageJ (Table 4.4). Phase separation between hydrophobic and hydrophilic domains was observed in both the cast membranes and pressed membrane of PSf-PVBTMA1. Long-range ordering was not found in the TEM micrographs. The pressed membrane of PSf-PVBTMA1 exhibited less clear phase boundaries compared to the cast membrane of PSf-PVBTMA1, stemming from the weaker segregations due to the crosslinking induced restrained chain mobility.

Table 4.4 ImageJ analysis to the TEM micrographs of the cast PSf-PVBTMA membranes

cast membranes	mean-to-max ratio/%
PSf-PVBTMA1	36
PSf-PVBTMA2	43
PSf-PVBTMA3	50
PSf-PVBTMA4	52
PSf-PVBTMA5	63

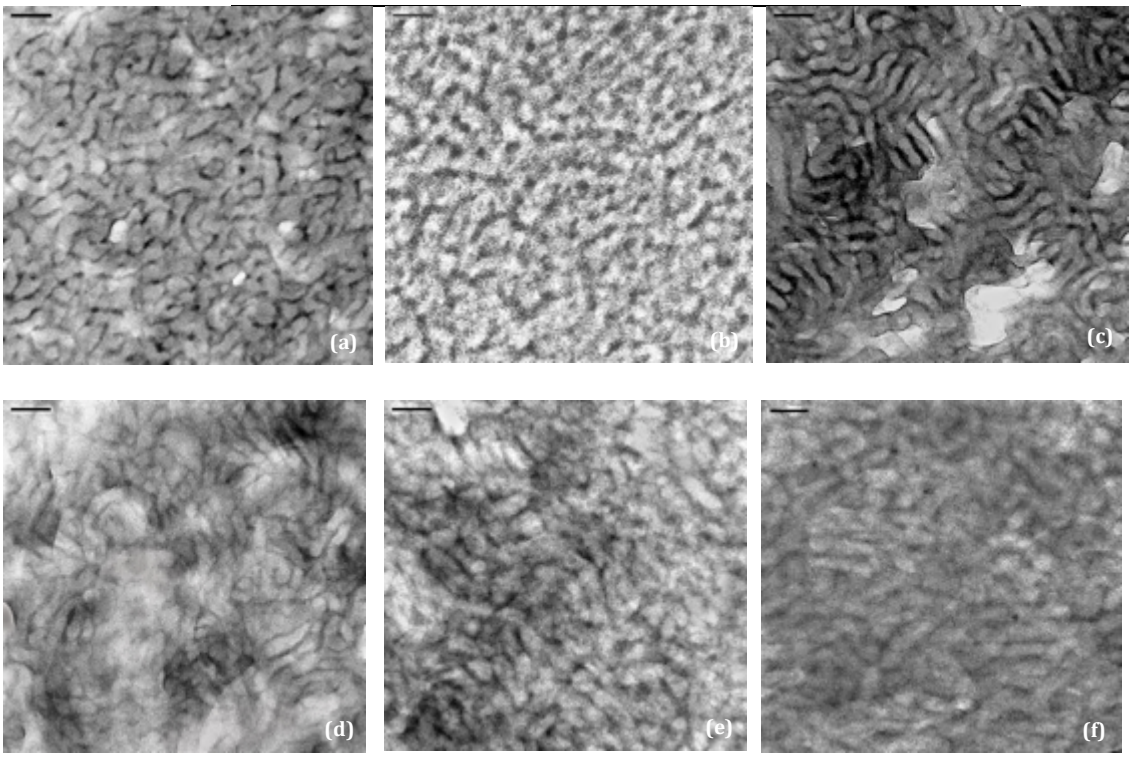

Figure 4.14 Cross-sectional TEM micrographs of dry membranes of cast PSf-PVBTMA1 (a), pressed PSf-PVBTMA1 (b), cast PSf-PVBTMA2 (c), cast PSf-PVBTMA3 (d), cast PSf-PVBTMA4 (e), cast PSf-PVBTMA5 (f). Scale bar on each TEM micrographs represents 100 nm.

Phase separation was also perceived in the rest of the cast membranes of PSf-PVBTMA2, PSf-PVBTMA3, PSf-PVBTMA4, and PSf-PVBTMA5 (Figure 4.14c-f). It should be noted that the PSf-PVBC cast films were dried within a couple of hours not allowing the formation of equilibrium phase separation, precluding any long-range ordering.

4.5.8 Ionic conductivity of PSf-PVBTMA membranes in their chloride forms, hydroxide forms and bicarbonate forms in water.

The conductivity in chloride, hydroxide, and bicarbonate forms is displayed in Figure 4.15 for the PSf-PVBTMA membranes (solvent casting and melt pressing prepared) measured in water at 20 °C, 60 °C, and 80 °C. The conductivities of different counter ions all increased with increased temperature. Because of the higher aqueous diffusion coefficient of hydroxide ions,[135,136] the hydroxide conductivity showed higher values than the chloride and bicarbonate conductivity for each PSf-PVBTMA sample. The chloride conductivity and bicarbonate conductivity showed close values for each sample at the same temperature. Studies on conductivity with different counter ions showed similar behavior in previously reported research.[70,153] In addition, the ionic conductivity of different counter ions showed strong dependence on IEC values and water uptake. The samples with higher IEC values and higher water uptake exhibited higher conductivity at any temperature or with any counter ion.

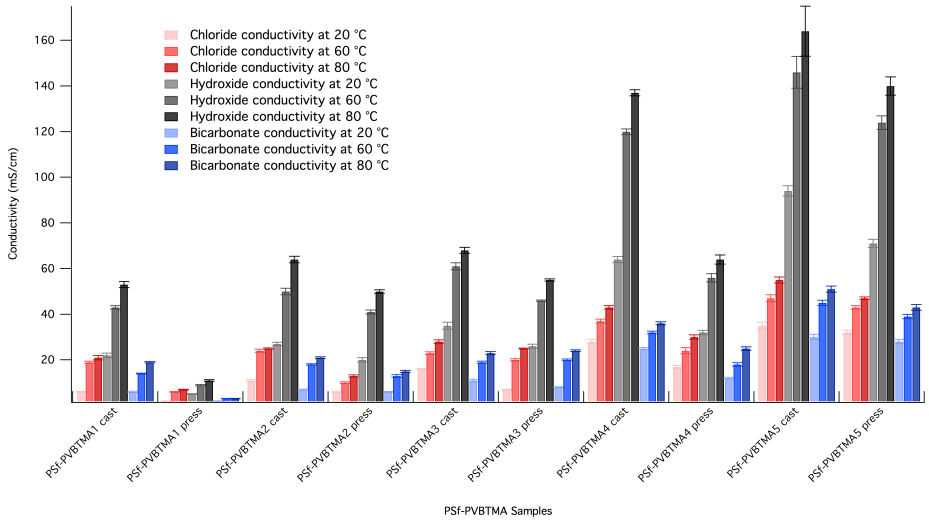

Figure 4.15. Conductivity of PSf-PVBTMA membranes in their chloride forms (red series), hydroxide forms (black series) and bicarbonate forms (blue series) in water at 20 °C, 60 °C and 80 °C.

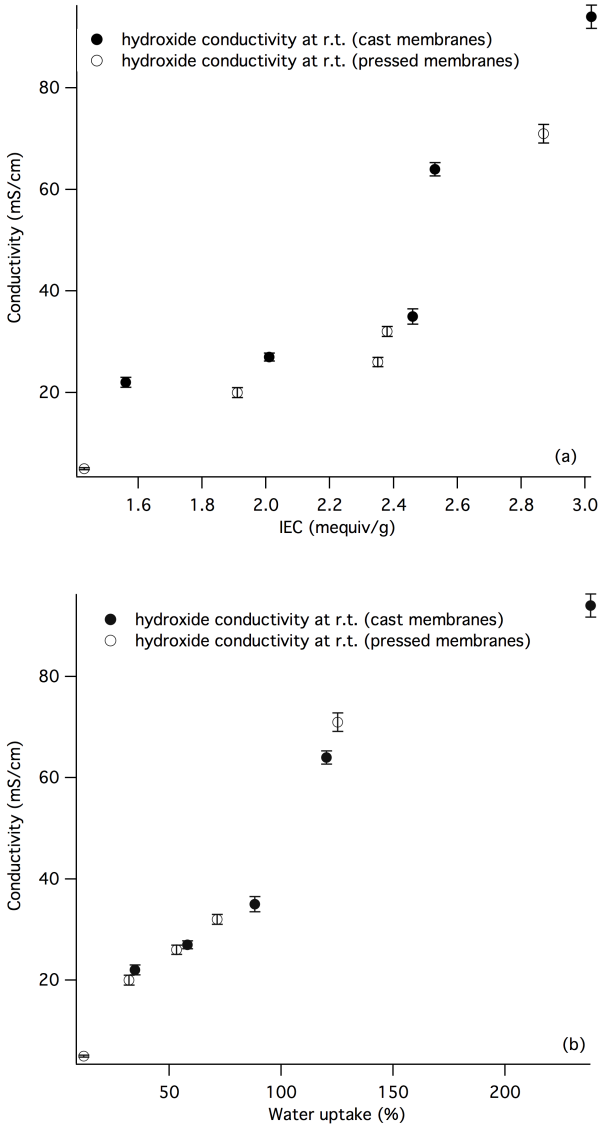

Figure 4.16. Conductivity of PSf-PVBC samples prepared from solvent casting (solid markers) and melt pressing (open markers) in chloride form (round markers) and hydroxide form (triangle markers) at room temperature as a function of IEC (a) and water uptake (b).

The relationship between conductivity and IEC and water uptake was studied to examine the dependence of conductivity on the number of cationic groupds and water absorption. Figure 4.16 (a) displays chloride and hydroxide conductivity at room temperature under fully hydrated conditions for PSf-PVBTMA films prepared from both solvent casting and melt pressing.

Elevated ionic conductivity along with increasing IEC was observed in the relationship between conductivity and IEC. The relationship between conductivity and IEC in Figure 4.16 (a) for cast membranes displays a significant increase from PSf-PVBTMA3 to PSf-PVBTMA4, corresponding to the same IEC with 2.5 mequiv/g, while the hydroxide conductivity substantially increased from 35 ± 1.5 mS/cm to 64 ± 1.3 mS/cm, indicating the formation of better connected ion conducting networks in PSf-PVBTMA4.

In contrast, the conductivity change for the pressed membranes was observed from PSf-PVBTMA4 to PSf-PVBTMA5, correlating to IEC increase from 2.6 to 3.1 mequiv/g, and hydroxide conductivity increase from 32 ± 1.0 mS/cm to 71 ± 1.8 mS/cm, suggesting the higher IEC requirement for the crosslinking system to gain continuous ion conducting networks and achieve higher conductivity. Figure 4.16 (b) has a similar tendency in the relationship between ionic conductivity and water uptake. The increased conductivity accompanied by increased IEC and water uptake can be explained by the factors affecting conductivity: higher concentration of benzyltrimethylammonium groups for hydroxide transport and higher water content to assist the transport. Figure 4.16 (b) also showed a linear increase of conductivity as a function of water uptake, indicating the high dependence of conductivity on membrane water sorption.

The temperature dependence feature is depicted in Figure 4.17 for both the cast and pressed PSf-PVBTMA membranes based on their chloride conductivity under 95 % relatively humidity. Assuming Arrhenius behavior, the activation energy to each membrane was calculated through the slope, giving the result in the range of 7 to 14 kJ/mol independent of IEC or water uptake. The activation energy values for PSf-PVBTMA membranes were found similar to other reported anionic exchange membranes.[137]

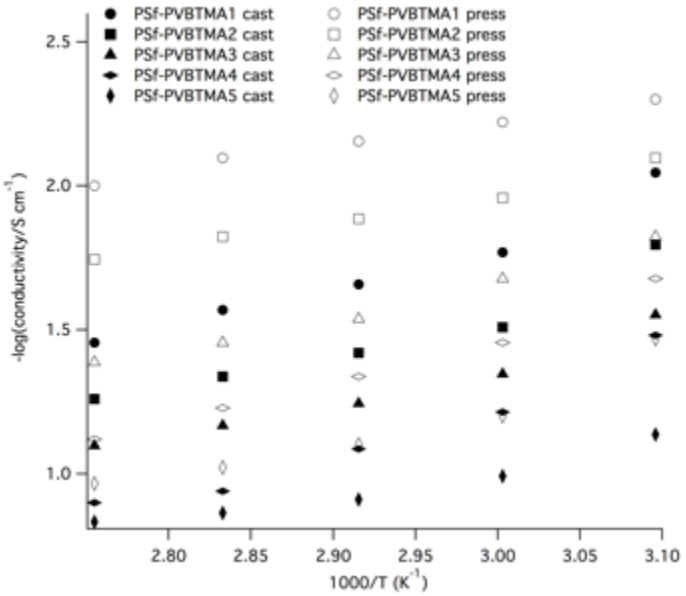

Figure 4.17. Arrhenius plot of chloride conductivity of PSf-PVBTMA membranes under 95 % relative humidity at different temperatures.

4.6 Conclusion

We developed a simple synthetic route to synthesize anion exchange membranes through combining polycondensation and nitroxide mediated polymerization. A series of triblock copolymers were synthesized with polysulfone as the center block and PVBC as the outer blocks. The triblock copolymers were processed through both solvent casting and melt pressing before quaternization. Tough, quaternized films at both dry and hydrated conditions were obtained for all the membranes prepared from both processing methods, except that the cast membrane of PSf-PVBTMA5 became fragile because of the excessive swelling. Melt pressed membranes were found effectively suppressed water uptake compared to the solvent cast membranes. The crosslinking reactions during melt pressing are likely the reasons that melt pressed membranes have reduced water uptake, and decreased IEC values. Phase separation was found for both solvent cast and melt pressed membranes from their SAXS profiles. The solvent

cast films have more distinct phase separation than melt pressed ones. This is due to the weakened ionic domains correlation induced by crosslinking reaction during melt pressing. The conductivity measurement exhibited high conductivities compared to the reported values. The membranes in this research can tolerate IEC values up to 3.0 meq/cm, which is possibly due to the long hydrophobic blocks in the membranes. The high ionic conductivity is attributed to the pronounced phase separation between polysulfone block and PVBTMA blocks, and the long hydrophilic blocks induced better-connected ion conducting pathways. We anticipate that the combined polycondensation with NMP could contribute to the simplified synthesis of anion exchange membranes with new structures that benefit ionic conductivity and mechanical properties. The block copolymer with distinct phase separation and long hydrophobic/hydrophilic blocks could benefit both ionic conductivity and mechanical properties.

Acknowledgement

Funding was provided by the Army Research Office MURI grant (W911NF-10-1-0520). The NMR spectroscopy was possible with a grant from the NSF-MRI CHE-0923537.

CHAPTER 5 SUMMARY AND CONCLUSIONS

Anion exchange membranes have drawn scientists' attention because the solid polymer electrolyte can solve the precipitation problem coming from using KOH as the electrolyte and also can be easier handled. Compared to proton exchange membranes, anion exchange membranes suffer from lower ionic conductivity resulting from lower ion mobility. Furthermore the cationic groups in AEMs are susceptible to hydroxide attack, therefore the alkaline stability assessment to the cationic groups is important to determine the lifetime of the anion exchange membranes. In this dissertation, guanidinium cations were evaluated for the application in anion exchange membranes. Phase separated block copolymers were designed to achieve high ionic conductivity and suppressed water uptake.

^{1}H NMR spectroscopy was employed to measure the alkaline stability of guanidinium through model compounds BPMGdmCl and TPTMGdmCl. The ^{1}H NMR spectra of BPMGdmCl before adding base and after based showed that the characteristic peaks of BPMGdmCl disappeared, along with the appearance of new peaks, indicating the instability of BPMGdmCl under alkaline environment. The ^{1}H NMR spectra taken from different time showed BPMGdmCl decomposed into one molecule of dimethylamine and one molecule of benzyltrimethylurea. Different measuring conditions were applied to the BPMGdmCl to study the degradation features under three temperatures and two concentrations. The results showed that degradation was accelerated by increased temperature and increased concentration of sodium hydroxide. TPTMGdmCl was also found instable under alkaline environment, which decomposed into one molecule of benzylmethylamine and one molecule of dibenzyldimethylurea. The degradation of

TPTMGdmCl was even faster than that of BPMGdmCl with the same temperature and base concentration, which was possibly due to the increased strain in TPTMGdmCl because of the bigger size of benzene groups. The stability results showed negative tendency of guanidinium group to be applied in alkaline fuel cells.

Phase separation was considered beneficial to the formation of connected ion-conducting pathways, therefore increasing the ionic conductivity of anion exchange membranes. PPO-*b*-PVBTMA block copolymers were synthesized through nitroxide mediated polymerization. The hydroxyl end groups of PPO were combined with TEMPO moieties to initiate polymerization with VBC to produce PPO-*b*-PVBC block copolymers. These copolymers were proved to be phase separated based on the observed double glass transition temperatures from the DSC measurements. The PPO-*b*-PVBCx films were prepared through hot pressing to obtain crosslinking within the membranes, while was expected to provide extra mechanical support. The quaternized PPO-*b*-PVBTMA films were obtained through Menshutkin reaction between the PPO-*b*-PVBCx block copolymer and trimethylamine. The crosslinking was proved by the solubility difference between the PPO-*b*-PVBCx powders and the PPO-*b*-PVBCx films. A series of PPO-*b*-PVBTMA block copolymers was synthesized with different weight percentages of the PVBTMA blocks in this research. A flexible film was obtained with IEC value as high as 3.2 meq/g instead of a hydrogel under hydrated conditions. The PPO-*b*-PVBTMA membranes exhibited suppressed water uptake and dimentional swelling compared to the reported membranes with the same IEC values. Film PPO-*b*-PVBTMA11 was found to be the optimized membrane because its high hydroxide conductivity at 60 °C (132 ± 3.8 mS/cm), at the same time maintain as a flexible film under both dry and wet conditions.

Triblock copolymers were also investigated with hydrophlilic blocks in the ends and hydrophobic block as the center block. PSf-PVBTMA triblock copolymers were synthesized by combining polycondensation produced polysulfone as the center block and NMP produced PVBC as the outer blocks. Two processing methods were tried for the triblock copolymers PSf-PVBC: solvent casting and melt pressing. The copolymers were then quaternized with aqueous trimethylamine solution. The obtained membranes from both solvent casting and melt pressing were all mechanically robust under either dry or wet conditions, except the wet solvent cast membrane of PSf-PVBTMA5, which was possibly due to excessive swelling accompanying with high weight percentage of PVBTMA. Compared to the solvent cast membranes, melt pressed membranes showed reduced titrated IEC values, suppressed water uptake due to the crosslinking within the membranes. Compared the swelling in different directions, melt pressed membranes showed more higher swelling ratio in the in-plane direction than the through-plane direction. In contrast, solvent cast membranes showed more swelling in the through-plane direction. SAXS profiles revealed both solvent cast and melt pressed membranes had phase separation from the scattering peaks. Melt pressed membranes showed broad scattering peak due to the weakened ionic domains correlation because of the crosslinking within the membranes. Crosslinking helped the melt pressed membrane achieved IEC of 3.0 meq/g while still appeared as flexible film. Because of the higher IEC and water uptake, solvent cast membranes exhibited higher conductivities compared to the melt pressed membranes. The solvent cast membrane reached hydroxide conductivity as high as 146 ± 7.1 mS/cm at 60 °C with IEC as 3.0 meq/g, while pressed membrane reached 124 ± 3.0 mS/cm with IEC as 2.9 meq/g. The hydrophilic/ hydrophobic phase separation and long connected ionic groups were expected beneficial to achieve high ionic conductivity.

Other projects have been conducted but were not included in this thesis due to their disqualification as anion exchange membranes. Benzimidazolium group was studied as cationic group for AEM. Qaternized 2-phenylbenzimidazolium iodide was synthesized to determine the alkaline stability and the result showed that this cation was unstable under alkaline environment. Benzyltrimethylammonium cation was found stable at room temperature with equal molar for the cation and the base. Degradation was present for benzyltrimethylammonium cation at higher temperature. Random copolymers with polysulfone as backbone and aminobenzyltrimethylammonium were synthesized and evaluated as anion exchange membranes. The random copolymers showed absence of phase separation and low ionic conductivity. In addition, the random copolymers were investigated on ionic conductivity of cast membranes prepared from different solvent. The membranes cast from DMSO showed the highest conductivity, the ones cast from DMAc and DMF showed lower and the lowest conductivity, respectively.

For future AEM designing, alkaline stability of cationic groups are necessary to be evaluated. Guanidinium groups and benzimidazolium groups should be avoided for applications in AEMs due to their degradation under alkaline environment. Benzyltrimethylammonium cations were widely chosen for AEM studies because the solubility for the quaternized polymer electrolytes tends to be problematic and quaternization by trimethylamine can be completed as solid films. However, the alkaline stability of benzyltrimethylammonium is not sufficient to be used at elevated temperature so new cations need to be developed to fulfill both the requirements of alkaline stability and synthetic process. Efficient phase separation was demonstrated to be beneficial to enhance the ionic conductivity. Block copolymers show phase separation due to the connected cationic groups therefore should be considered in AEMs. Phase separated blocks

before quaternization need to be employed in designing of AEMs if the preparation of films is before quaternization. Crosslinking could suppress the water uptake. In order to achieve high ionic conductivity and reduced water uptake, crosslinking need to be controlled within one phase.

CHAPTER 6 FUTURE WORKS

The results from the current research proved the potential of phase separated block copolymer between the hydrophilic and hydrophobic phase for anion exchange membranes. The membranes in this dissertation exhibited high ionic conductivity comparable to the highest conductivity reported to date.

However, efforts are still needed to increase the mechanical properties and decrease the water uptake of anion exchange membranes, in order to increase the membranes' durability and commercialize them in fuel cells. Holdcroft and coworkers found that graft copolymers could reach higher ion exchange capacity without excessive water uptake and swelling compared to diblock copolymers.[154] The reason was attributed to the higher ordered configuration of diblock copolymer than that of graft copolymer. The higher degree of long-range order therefore lead to excessive water uptake at low ion exchange capacity and restricted the attainable ion exchange capacity.

Polyethylene is a crystalline polymer with excellent mechanical properties. The crystalline feature could potentially reduce the water uptake of the quaternized polymer electrolytes. Coates and coworkers developed multiple anion exchange membranes with polyethylene as the backbone.[46,70,73] The resulted anion exchange membranes exhibited outstanding mechanical properties and high hydroxide conductivities. Beyer and coworkers synthesized bicontinuous anion exchange membranes based on crosslinked polyethylene and PVBTMA.[110] Phase separation was found for these membranes as well as high hydroxide conductivity.

The PVBTMA grafted polyethylene was expected to have similar features as the crosslinked copolymers developed by the two groups above. Phase separation behavior should also present in the PVBTMA grafted polyethylene as well as the excellent mechanical properties of the membrane. This research has been initiated in our group with the synthetic route like Scheme 6.1. We already synthesized TEMPO substituted unsaturated polyethylene. Followed work include the synthesis of PVBC grafted copolymer, hydrogenation, and quaternization.

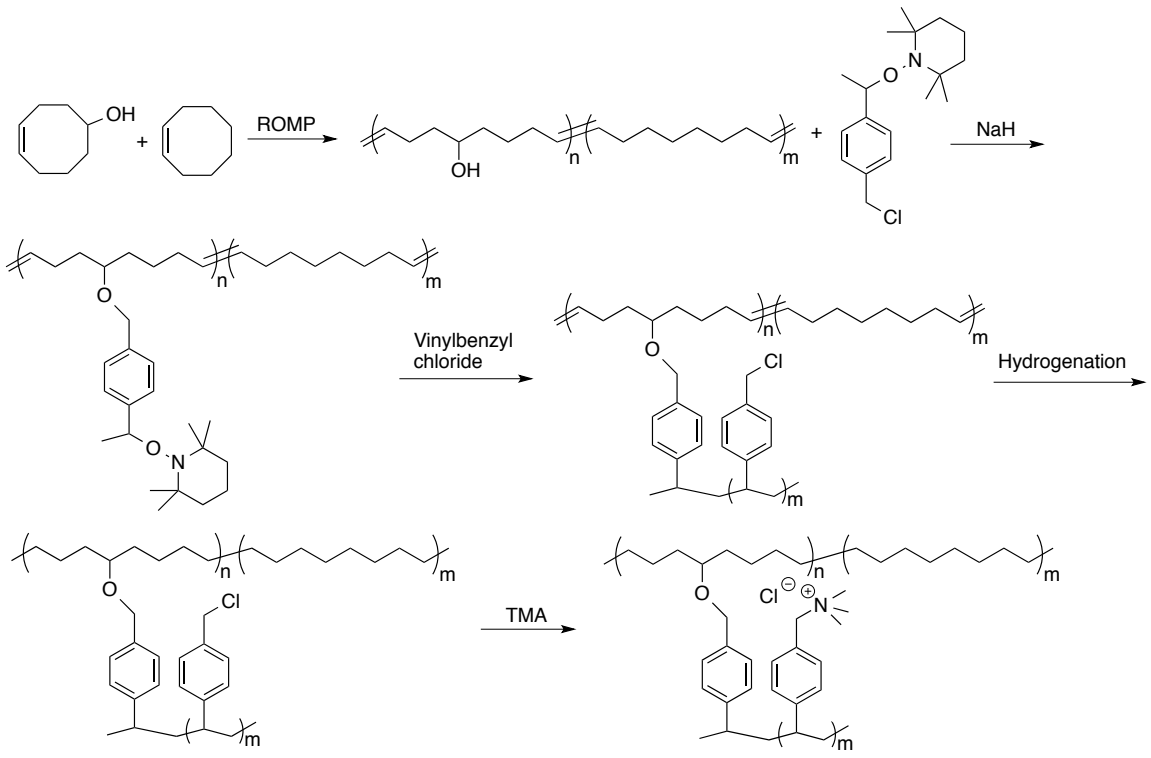

Scheme 6.1 Synthetic route of PVBTMA grafted polyethylene.

Copyright Clearance Center RightsLink®

Home | Account Info | Help | Live Cl

Title: Novel silica/poly(2,6-dimethyl-1,4-phenylene oxide) hybrid anion-exchange membranes for alkaline fuel cells: Effect of silica content and the single cell performance

Author: Yonghui Wu,Cuiming Wu,John R. Varcoe,Simon D. Poynton,Tongwen Xu,Yanxun Fu

Publication: Journal of Power Sources

Publisher: Elsevier

Date: 15 May 2010

Copyright © 2009 Elsevier B.V. All rights reserved.

Logged in as:
Yating Yang
LOGOUT

Order Completed

Thank you very much for your order.

This is a License Agreement between Yating Yang ("You") and Elsevier ("Elsevier"). The license consists of your order details, the terms and conditions provided by Elsevier, and the payment terms and conditions.

Get the printable license.

License Number	3466590083164
License date	Sep 12, 2014
Licensed content publisher	Elsevier
Licensed content publication	Journal of Power Sources
Licensed content title	Novel silica/poly(2,6-dimethyl-1,4-phenylene oxide) hybrid anion-exchange membranes for alkaline fuel cells: Effect of silica content and the single cell performance
Licensed content author	Yonghui Wu,Cuiming Wu,John R. Varcoe,Simon D. Poynton,Tongwen Xu,Yanxun Fu
Licensed content date	15 May 2010
Licensed content volume number	195
Licensed content issue number	10
Number of pages	8
Type of Use	reuse in a thesis/dissertation
Portion	figures/tables/illustrations
Number of figures/tables/illustrations	1
Format	both print and electronic
Are you the author of this Elsevier article?	No
Will you be translating?	No
Title of your thesis/dissertation	Cationic Polymers for Alkaline Fuel Cells Applications
Expected completion date	Nov 2014
Estimated size (number of pages)	150
Elsevier VAT number	GB 494 6272 12
Permissions price	0.00 USD
VAT/Local Sales Tax	0.00 USD / 0.00 GBP
Total	0.00 USD

Copyright Clearance Center RightsLink®

Home | Account Info | Help

Title: Anion exchange membranes: Current status and moving forward

Author: Michael A. Hickner,Andrew M. Herring,E. Bryan Coughlin

Publication: Journal of Polymer Science Part B: Polymer Physics

Publisher: John Wiley and Sons

Date: Oct 29, 2013

Copyright © 2013 Wiley Periodicals, Inc.

Logged in as:
Yating Yang

LOGOUT

Order Completed

Thank you very much for your order.

This is a License Agreement between Yating Yang ("You") and John Wiley and Sons ("John Wiley and Sons"). The license consists of your order details, the terms and conditions provided by John Wiley and Sons, and the payment terms and conditions.

Get the printable license.

License Number	3466591029872
License date	Sep 12, 2014
Licensed content publisher	John Wiley and Sons
Licensed content publication	Journal of Polymer Science Part B: Polymer Physics
Licensed content title	Anion exchange membranes: Current status and moving forward
Licensed copyright line	Copyright © 2013 Wiley Periodicals, Inc.
Licensed content author	Michael A. Hickner,Andrew M. Herring,E. Bryan Coughlin
Licensed content date	Oct 29, 2013
Start page	1727
End page	1735
Type of use	Dissertation/Thesis
Requestor type	University/Academic
Format	Print and electronic
Portion	Figure/table
Number of figures/tables	1
Original Wiley figure/table number(s)	Figure 1
Will you be translating?	No
Title of your thesis / dissertation	Cationic Polymers for Alkaline Fuel Cells Applications
Expected completion date	Nov 2014
Expected size (number of pages)	150
Total	0.00 USD

Copyright Clearance Center RightsLink®

Home | Account Info | Help

Title: Directing the self-assembly of block copolymers
Author: S.B. Darling
Publication: Progress in Polymer Science
Publisher: Elsevier
Date: October 2007

Copyright © 2007 Elsevier Ltd. All rights reserved.

Logged in as:
Yating Yang
Account #:
3000832845

LOGOUT

Order Completed

Thank you very much for your order.

This is a License Agreement between Yating Yang ("You") and Elsevier ("Elsevier"). The license consists of your order details, the terms and conditions provided by Elsevier, and the payment terms and conditions.

Get the printable license.

License Number	3470430706184
License date	Sep 15, 2014
Licensed content publisher	Elsevier
Licensed content publication	Progress in Polymer Science
Licensed content title	Directing the self-assembly of block copolymers
Licensed content author	S.B. Darling
Licensed content date	October 2007
Licensed content volume number	32
Licensed content issue number	10
Number of pages	53
Type of Use	reuse in a thesis/dissertation
Portion	figures/tables/illustrations
Number of figures/tables/illustrations	1
Format	both print and electronic
Are you the author of this Elsevier article?	No
Will you be translating?	No
Title of your thesis/dissertation	Cationic Polymers for Alkaline Fuel Cells Applications
Expected completion date	Nov 2014
Estimated size (number of pages)	150
Elsevier VAT number	GB 494 6272 12
Permissions price	0.00 USD
VAT/Local Sales Tax	0.00 USD / 0.00 GBP
Total	0.00 USD

Copyright Clearance Center RightsLink®

Home | Account Info | Help

Logged in as:
Yating Yang
Account #:
3000832845
LOGOUT

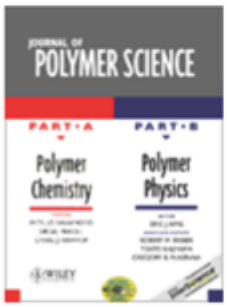

Title: Synthesis and structure–conductivity relationship of polystyrene-block-poly(vinyl benzyl trimethylammonium) for alkaline anion exchange membrane fuel cells

Author: Tsung-Han Tsai,Ashley M. Maes,Melissa A. Vandiver,Craig Versek,Sönke Seifert,Mark Tuominen,Matthew W. Liberatore,Andrew M. Herring,E. Bryan Coughlin

Publication: Journal of Polymer Science Part B: Polymer Physics

Publisher: John Wiley and Sons

Date: Sep 21, 2012

Copyright © 2012 Wiley Periodicals, Inc.

Order Completed

Thank you very much for your order.

This is a License Agreement between Yating Yang ("You") and John Wiley and Sons ("John Wiley and Sons"). The license consists of your order details, the terms and conditions provided by John Wiley and Sons, and the payment terms and conditions.

Get the printable license.

License Number	3470880492206
License date	Sep 16, 2014
Licensed content publisher	John Wiley and Sons
Licensed content publication	Journal of Polymer Science Part B: Polymer Physics
Licensed content title	Synthesis and structure–conductivity relationship of polystyrene-block-poly(vinyl benzyl trimethylammonium) for alkaline anion exchange membrane fuel cells
Licensed copyright line	Copyright © 2012 Wiley Periodicals, Inc.
Licensed content author	Tsung-Han Tsai,Ashley M. Maes,Melissa A. Vandiver,Craig Versek,Sönke Seifert,Mark Tuominen,Matthew W. Liberatore,Andrew M. Herring,E. Bryan Coughlin
Licensed content date	Sep 21, 2012
Start page	1751
End page	1760
Type of use	Dissertation/Thesis
Requestor type	University/Academic
Format	Print and electronic
Portion	Figure/table
Number of figures/tables	6
Original Wiley figure/table number(s)	Figure 6
Will you be translating?	No
Title of your thesis / dissertation	Cationic Polymers for Alkaline Fuel Cells Applications
Expected completion date	Nov 2014

Copyright Clearance Center RightsLink®

Home | Create Account | Hel

ACS Publications Most Trusted. Most Cited. Most Read.

Title: Phosphonium-Functionalized Polyethylene: A New Class of Base-Stable Alkaline Anion Exchange Membranes

Author: Kevin J. T. Noonan, Kristina M. Hugar, Henry A. Kostalik, et al

Publication: Journal of the American Chemical Society

Publisher: American Chemical Society

Date: Nov 1, 2012

Copyright © 2012, American Chemical Society

User ID

Password

Enable Auto Login

LOGIN

Forgot Password/User ID

If you're a copyright.com user, you can login to RightsLink using your copyright.com credentials. Already **a RightsLink user** want to learn more?

PERMISSION/LICENSE IS GRANTED FOR YOUR ORDER AT NO CHARGE

This type of permission/license, instead of the standard Terms & Conditions, is sent to you because n fee is being charged for your order. Please note the following:

- Permission is granted for your request in both print and electronic formats, and translations.
- If figures and/or tables were requested, they may be adapted or used in part.
- Please print this page for your records and send a copy of it to your publisher/graduate school.
- Appropriate credit for the requested material should be given as follows: "Reprinted (adapted) with permission from (COMPLETE REFERENCE CITATION). Copyright (YEAR) American Chemical Society." Insert appropriate information in place of the capitalized words.
- One-time permission is granted only for the use specified in your request. No additional uses are granted (such as derivative works or other editions). For any other uses, please submit a new request.

If credit is given to another source for the material you requested, permission must be obtained from that source.

REFERENCE

(1) Arges, C. G.; Ramani, V.; Pintauro, P. N.: Fuel Cells. *Electrochemical Society Interface*, 31-35.

(2) Winter, M.; Brodd, R. J.: What are batteries, fuel cells, and supercapacitors? *Chemical reviews* **2004**, *104*, 4245-69.

(3) Demirdöven, N.; Deutch, J.: Hybrid cars now, fuel cell cars later. *Science (New York, N.Y.)* **2004**, *305*, 974-6.

(4) Powertrains, E.; Report, L.-d. V. F.: Ref: Kromer & Heywood, "Electric Powertrains: Opportunities & Challenges in the U.S. Light-Duty Vehicle Fleet Report # LFEE 2007-03RP, MIT, May, 2007, Table 53. *Fuel Cell* **2009**.

(5) Acres, G.: Recent advances in fuel cell technology and its applications. *Journal of Power Sources* **2001**, *100*, 60-66.

(6) Andújar, J. M.; Segura, F.: Fuel cells: History and updating. A walk along two centuries. *Renewable and Sustainable Energy Reviews* **2009**, *13*, 2309-2322.

(7) Steele, B. C.; Heinzel, a.: Materials for fuel-cell technologies. *Nature* **2001**, *414*, 345-52.

(8) Andújar, J. M.; Segura, F.: Fuel cells: History and updating. A walk along two centuries. *Renewable and Sustainable Energy Reviews* **2009**, *13*, 2309-2322.

(9) Guan, Y.; Pu, H.; Pan, H.; Chang, Z.; Jin, M.: Proton conducting membranes based on semi-interpenetrating polymer network of Nafion® and polybenzimidazole. *Polymer* **2010**.

(10) Kim, H.; Kang, M.; Lee, D.; Won, J.; Kim, J.; Kang, Y.: Proton exchange membranes with high cell performance based on Nafion/poly(p-phenylene vinylene) composite polymer electrolyte. *Journal of Membrane Science* **2007**, *304*, 60-64.

(11) Mauritz, K. a.; Moore, R. B.: State of understanding of nafion. *Chemical reviews* **2004**, *104*, 4535-85.

(12) Borup, R.; Meyers, J.; Pivovar, B.; Kim, Y. S.; Mukundan, R.; Garland, N.; Myers, D.; Wilson, M.; Garzon, F.; Wood, D.; Zelenay, P.; More, K.; Stroh, K.; Zawodzinski, T.; Boncella, J.; McGrath, J. E.; Inaba, M.; Miyatake, K.; Hori, M.; Ota, K.; Ogumi, Z.; Miyata, S.; Nishikata, A.; Siroma, Z.; Uchimoto, Y.; Yasuda, K.; Kimijima, K.-I.; Iwashita, N.: Scientific aspects of polymer electrolyte fuel cell durability and degradation. *Chemical reviews* **2007**, *107*, 3904-51.

(13) Smitha, B.; Sridhar, S.; Khan, a.: Solid polymer electrolyte membranes for fuel cell applications—a review. *Journal of Membrane Science* **2005**, *259*, 10-26.

(14) Varcoe, J. R.; Slade, R. C. T.; Lam How Yee, E.: An alkaline polymer electrochemical interface: a breakthrough in application of alkaline anion-exchange membranes in fuel cells. *Chemical communications (Cambridge, England)* **2006**, 1428-9.

(15) Varcoe, J. R.; Slade, R. C. T.: Prospects for Alkaline Anion-Exchange Membranes in Low Temperature Fuel Cells. *Fuel Cells* **2005**, *5*, 187-200.

(16) Coutanceau, C.; Demarconnay, L.; Lamy, C.; Léger, J. M.: Development of electrocatalysts for solid alkaline fuel cell (SAFC). *Journal of Power Sources* **2006**, *156*, 14-19.

(17) Varcoe, J. R.; Slade, R. C. T.; Yee, E. L. H.; Poynton, S. D.; Driscoll, D. J.: Investigations into the ex situ methanol, ethanol and ethylene glycol permeabilities of alkaline polymer electrolyte membranes. *Journal of Power Sources* **2007**, *173*, 194-199.

(18) Varcoe, J. R.; Slade, R. C. T.; Wright, G. L.; Chen, Y.: Steady-state dc and impedance investigations of H2/O2 alkaline membrane fuel cells with commercial Pt/C, Ag/C, and Au/C cathodes. *The journal of physical chemistry. B* **2006**, *110*, 21041-9.

(19) Varcoe, J. R.; Slade, R. C. T.: Prospects for Alkaline Anion-Exchange Membranes in Low Temperature Fuel Cells. *Fuel Cells* **2005**, *5*, 187-200.

(20) Merle, G.; Wessling, M.; Nijmeijer, K.: Anion exchange membranes for alkaline fuel cells: A review. *Journal of Membrane Science* **2011**, *377*, 1-35.

(21) Zhang, H.; Ohashi, H.; Tamaki, T.; Yamaguchi, T.: Direction and Management of Water Movement in Solid-State Alkaline Fuel Cells. *The Journal of Physical Chemistry C* **2012**, *116*, 7650-7657.

(22) Huo, S.; Deng, H.; Chang, Y.; Jiao, K.: Water management in alkaline anion exchange membrane fuel cell anode. *International Journal of Hydrogen Energy* **2012**, *37*, 18389-18402.

(23) Brandon, N. P.; Skinner, S.; Steele, B. C. H.: RECENT ADVANCES IN MATERIALS FOR FUEL CELLS. *Annual Review of Materials Research* **2003**, *33*, 183-213.

(24) Litster, S.; McLean, G.: PEM fuel cell electrodes. *Journal of Power Sources* **2004**, *130*, 61-76.

(25) Li, N.; Leng, Y.; Hickner, M. a.; Wang, C.-Y.: Highly Stable, Anion Conductive, Comb-Shaped Copolymers for Alkaline Fuel Cells. *Journal of the American Chemical Society* **2013**.

(26) Hibbs, M. R.; Fujimoto, C. H.; Cornelius, C. J.: Synthesis and Characterization of Poly(phenylene)-Based Anion Exchange Membranes for Alkaline Fuel Cells. *Macromolecules* **2009**, *42*, 8316-8321.

(27) Ong, A. L.; Saad, S.; Lan, R.; Goodfellow, R. J.; Tao, S.: Anionic membrane and ionomer based on poly(2,6-dimethyl-1,4-phenylene oxide) for alkaline membrane fuel cells. *Journal of Power Sources* **2011**, *196*, 8272-8279.

(28) Abuin, G. C.; Nonjola, P.; Franceschini, E. a.; Izraelevitch, F. H.; Mathe, M. K.; Corti, H. R.: Characterization of an anionic-exchange membranes for direct methanol alkaline fuel cells. *International Journal of Hydrogen Energy* **2010**, *35*, 5849-5854.

(29) Danks, T. N.; Slade, R. C. T.; Varcoe, J. R.: Alkaline anion-exchange radiation-grafted membranes for possible electrochemical application in fuel cells. *Journal of Materials Chemistry* **2003**, *13*, 712-721.

(30) Li, W.; Fang, J.; Lv, M.; Chen, C.; Chi, X.; Yang, Y.; Zhang, Y.: Novel anion exchange membranes based on polymerizable imidazolium salt for alkaline fuel cell applications. *Journal of Materials Chemistry* **2011**, *21*, 11340-11346.

(31) Tanaka, M.; Fukasawa, K.; Nishino, E.; Yamaguchi, S.; Yamada, K.; Tanaka, H.; Bae, B.; Miyatake, K.; Watanabe, M.: Anion Conductive Block Poly(arylene ether)s: Synthesis, Properties, and Application in Alkaline Fuel Cells. *Journal of the American Chemical Society* **2011**, *133*, 10646-54.

(32) Zeng, Q. H.; Liu, Q. L.; Broadwell, I.; Zhu, A. M.; Xiong, Y.; Tu, X. P.: Anion exchange membranes based on quaternized polystyrene-block-poly(ethylene-ran-butylene)-block-polystyrene for direct methanol alkaline fuel cells. *Journal of Membrane Science* **2010**, *349*, 237-243.

(33) Tsai, T.-H.; Maes, A. M.; Vandiver, M. a.; Versek, C.; Seifert, S.; Tuominen, M.; Liberatore, M. W.; Herring, A. M.; Coughlin, E. B.: Synthesis and structure-conductivity relationship of polystyrene- block -poly(vinyl benzyl trimethylammonium) for alkaline anion exchange membrane fuel cells. *Journal of Polymer Science Part B: Polymer Physics* **2013**, *51*, 1751-1760.

(34) Hay, A. S.: In *High performance polymers: their origin and development, in: Proceedings of the Symposium on the History of High Performance Polymers at the American Chemical Society Meeting*; Elsevier: New York, 1986; pp 209-214.

(35) Xu, T.; Wu, D.; Wu, L.: Poly(2,6-dimethyl-1,4-phenylene oxide) (PPO)—A versatile starting polymer for proton conductive membranes (PCMs). *Progress in Polymer Science* **2008**, *33*, 894-915.

(36) Percec, S.; Li, G.: Chemical Modification of Poly(2,6-dimethyl-1,4-phenylene oxide) and Properties of the Resulting Polymers. In *Chemical Reactions on Polymers*; American Chemical Society, 1988; Vol. 364; pp 46-59.

(37) Líška, J.; Borsig, E.: Polymer-Analogous Reactions on Poly(2, 6-dimethyl-1, 4-phenylene Oxide). *Journal of Macromolecular Science, Part C* **1995**, *35*, 517-529.

(38) Zhang, S.; Xu, T.; Wu, C.: Synthesis and characterizations of novel, positively charged hybrid membranes from poly(2,6-dimethyl-1,4-phenylene oxide). *Journal of Membrane Science* **2006**, *269*, 142-151.

(39) Wu, Y.; Wu, C.; Xu, T.; Lin, X.; Fu, Y.: Novel silica/poly(2,6-dimethyl-1,4-phenylene oxide) hybrid anion-exchange membranes for alkaline fuel cells: Effect of heat treatment. *Journal of Membrane Science* **2009**, *338*, 51-60.

(40) Wu, Y.; Wu, C.; Varcoe, J. R.; Poynton, S. D.; Xu, T.; Fu, Y.: Novel silica/poly(2,6-dimethyl-1,4-phenylene oxide) hybrid anion-exchange membranes for alkaline fuel cells: Effect of silica content and the single cell performance. *Journal of Power Sources* **2010**, *195*, 3069-3076.

(41) Wu, L.; Xu, T.; Wu, D.; Zheng, X.: Preparation and characterization of CPPO/BPPO blend membranes for potential application in alkaline direct methanol fuel cell. *Journal of Membrane Science* **2008**, *310*, 577-585.

(42) Ter Meulen, B. P.: Basic Principles of Membrane Technology. M. Mulder. Kluwer, Dordrecht, 1991. 372 pp., Hardbound Dfl. 200.00/£69.00. Paperback Dfl. 70.00/£24.00. ISBN 0-7923-0978-2 Hardbound. ISBN 0-7923-0979-2 Paperback. *Recueil des Travaux Chimiques des Pays-Bas* **1992**, *111*, 458-458.

(43) Wang, G.; Weng, Y.; Chu, D.; Chen, R.; Xie, D.: Developing a polysulfone-based alkaline anion exchange membrane for improved ionic conductivity. *Journal of Membrane Science* **2009**, *332*, 63-68.

(44) Pan, J.; Lu, S.; Li, Y.; Huang, A.; Zhuang, L.; Lu, J.: High-Performance Alkaline Polymer Electrolyte for Fuel Cell Applications. *Advanced Functional Materials* **2010**, *20*, 312-319.

(45) Tanaka, M.; Koike, M.; Miyatake, K.; Watanabe, M.: Synthesis and properties of anion conductive ionomers containing fluorenyl groups for alkaline fuel cell applications. *Polymer Chemistry* **2011**, *2*, 99.

(46) Kostalik, H. a.; Clark, T. J.; Robertson, N. J.; Mutolo, P. F.; Longo, J. M.; Abruña, H. c. D.; Coates, G. W.: Solvent Processable Tetraalkylammonium-Functionalized Polyethylene for Use as an Alkaline Anion Exchange Membrane. *Macromolecules* **2010**, *43*, 7147-7150.

(47) Hibbs, M. R.; Hickner, M. a.; Alam, T. M.; McIntyre, S. K.; Fujimoto, C. H.; Cornelius, C. J.: Transport Properties of Hydroxide and Proton Conducting Membranes. *Chemistry of Materials* **2008**, *20*, 2566-2573.

(48) Beers, K. M.; Balsara, N. P.: Design of Cluster-free Polymer Electrolyte Membranes and Implications on Proton Conductivity. *ACS Macro Letters* **2012**, *1*, 1155-1160.

(49) Albert, J. N. L.; Epps Iii, T. H.: Self-assembly of block copolymer thin films. *Materials Today* **2010**, *13*, 24-33.

(50) Darling, S. B.: Directing the self-assembly of block copolymers. *Progress in Polymer Science* **2007**, *32*, 1152-1204.

(51) Leibler, L.: Theory of Microphase Separation in Block Copolymers. *Macromolecules* **1980**, *13*, 1602-1617.

(52) Cooke, D. M.; Shi, A.-C.: Effects of Polydispersity on Phase Behavior of Diblock Copolymers. *Macromolecules* **2006**, *39*, 6661-6671.

(53) Coessens, V.; Pintauer, T.; Matyjaszewski, K.: Functional polymers by atom transfer radical polymerization. *Progress in Polymer Science* **2001**, *26*, 337-377.

(54) Smart, T.; Lomas, H.; Massignani, M.; Flores-Merino, M. V.; Perez, L. R.; Battaglia, G.: Block copolymer nanostructures. *Nano Today* **2008**, *3*, 38-46.

(55) Wang, W.; Yan, D.; Bratton, D.; Howdle, S. M.; Wang, Q.; Lecomte, P.: Charge Transfer Complex Inimer: A Facile Route to Dendritic Materials. *Advanced Materials* **2003**, *15*, 1348-1352.

(56) Gaynor, S. G.; Edelman, S.; Matyjaszewski, K.: Synthesis of Branched and Hyperbranched Polystyrenes. *Macromolecules* **1996**, *29*, 1079-1081.

(57) Sudre, G.; Inceoglu, S.; Cotanda, P.; Balsara, N. P.: Influence of Bound Ion on the Morphology and Conductivity of Anion-Conducting Block Copolymers. *Macromolecules* **2013**, *46*, 1519-1527.

(58) Weber, R. L.; Ye, Y.; Schmitt, A. L.; Banik, S. M.; Elabd, Y. a.; Mahanthappa, M. K.: Effect of Nanoscale Morphology on the Conductivity of Polymerized Ionic Liquid Block Copolymers. *Macromolecules* **2011**, *44*, 5727-5735.

(59) Wang, L.; Hickner, M. A.: Low-temperature crosslinking of anion exchange membranes. *Polymer Chemistry* **2014**, *5*, 2928-2935.

(60) Hossain, M. A.; Lim, Y.; Lee, S.; Jang, H.; Choi, S.; Jeon, Y.; Lim, J.; Kim, W. G.: Comparison of alkaline fuel cell membranes of random & block poly(arylene ether sulfone) copolymers containing tetra quaternary ammonium hydroxides. *International Journal of Hydrogen Energy* **2014**, *39*, 2731-2739.

(61) Li, N.; Zhang, Q.; Wang, C.; Lee, Y. M.; Guiver, M. D.: Phenyltrimethylammonium Functionalized Polysulfone Anion Exchange Membranes †. *Macromolecules* **2012**.

(62) Lafitte, B.; Jannasch, P.: Proton-Conducting Aromatic Polymers Carrying Hypersulfonated Side Chains for Fuel Cell Applications. *Advanced Functional Materials* **2007**, *17*, 2823-2834.

(63) Kim, D. S.; Robertson, G. P.; Kim, Y. S.; Guiver, M. D.: Copoly(arylene ether)s Containing Pendant Sulfonic Acid Groups as Proton Exchange Membranes † † NRCC Publication No. 50899. *Macromolecules* **2009**, *42*, 957-963.

(64) Li, N.; Shin, D. W.; Hwang, D. S.; Lee, Y. M.; Guiver, M. D.: Polymer Electrolyte Membranes Derived from New Sulfone Monomers with Pendent Sulfonic Acid Groups†. *Macromolecules* **2010**, *43*, 9810-9820.

(65) Li, Q.; Liu, L.; Miao, Q.; Jin, B.; Bai, R.: Hydroxide-conducting polymer electrolyte membranes from aromatic ABA triblock copolymers. *Polymer Chemistry* **2014**, *5*, 2208-2213.

(66) Xie, D.; Wang, G.; Weng, Y.; Chu, D.; Chen, R.: Polysulfone-composed Alkaline Anion Exchange Membrane for Improved Ionic Conductivity. *ECS Transactions* **2010**, *25*, 3-14.

(67) B.R. Einsla L.R. Pratt, J. M. B., J. Rau, C. Macomber, S Chempath; Pivovar, a. B. S. S.; Pivovar, B. S.; B.R. Einsla, S. C., L.R. Pratt, J.M. Boncella, J. Rau, C. Macomber: Stability of Cations for Anion Exchange Membrane Fuel Cells. *Society* **2007**, *11*, 1173-1180.

(68) Sarode, H. N.; Lindberg, G. E.; Yang, Y.; Felberg, L. E.; Voth, G. A.; Herring, A. M.: Insights into the Transport of Aqueous Quaternary Ammonium Cations: A Combined Experimental and Computational Study. *The Journal of Physical Chemistry B* **2014**, *118*, 1363-1372.

(69) Slade, R.; Varcoe, J.: Investigations of conductivity in FEP-based radiation-grafted alkaline anion-exchange membranes. *Solid State Ionics* **2005**, *176*, 585-597.

(70) Robertson, N. J.; Kostalik, H. a.; Clark, T. J.; Mutolo, P. F.; Abruña, H. D.; Coates, G. W.: Tunable high performance cross-linked alkaline anion exchange membranes for fuel cell applications. *Journal of the American Chemical Society* **2010**, *132*, 3400-4.

(71) Tomoi, M.; Yamaguchi, K.; Ando, R.; Kantake, Y.; Aosaki, Y.; Kubota, H.: Synthesis and thermal stability of novel anion exchange resins with spacer chains. *Journal of Applied Polymer Science* **1997**, *64*, 1161-1167.

(72) Gu, S.; Cai, R.; Luo, T.; Chen, Z.; Sun, M.; Liu, Y.; He, G.; Yan, Y.: A soluble and highly conductive ionomer for high-performance hydroxide exchange membrane fuel cells. *Angewandte Chemie (International ed. in English)* **2009**, *48*, 6499-502.

(73) Noonan, K. J. T.; Hugar, K. M.; Kostalik, H. a.; Lobkovsky, E. B.; Abruña, H. D.; Coates, G. W.: Phosphonium-functionalized polyethylene: a new class of base-stable

alkaline anion exchange membranes. *Journal of the American Chemical Society* **2012**, *134*, 18161-4.

(74) Wang, J.; Li, S.; Zhang, S.: Novel Hydroxide-Conducting Polyelectrolyte Composed of an Poly(arylene ether sulfone) Containing Pendant Quaternary Guanidinium Groups for Alkaline Fuel Cell Applications. *Macromolecules* **2010**, *43*, 3890-3896.

(75) Kim, D. S.; Fujimoto, C. H.; Hibbs, M. R.; Labouriau, A.; Choe, Y.-k.; Kim, Y. S.: Resonance Stabilized Per fl uorinated Ionomers for Alkaline Membrane Fuel Cells. **2013**.

(76) Ran, J.; Wu, L.; Varcoe, J. R.; Ong, A. L.; Poynton, S. D.; Xu, T.: Development of imidazolium-type alkaline anion exchange membranes for fuel cell application. *Journal of Membrane Science* **2012**, *415–416*, 242-249.

(77) Lin, B.; Qiu, L.; Qiu, B.; Peng, Y.; Yan, F.: A Soluble and Conductive Polyfluorene Ionomer with Pendant Imidazolium Groups for Alkaline Fuel Cell Applications. *Macromolecules* **2011**, *44*, 9642-9649.

(78) Qiu, B.; Lin, B.; Qiu, L.; Yan, F.: Alkaline imidazolium- and quaternary ammonium-functionalized anion exchange membranes for alkaline fuel cell applications. *Journal of Materials Chemistry* **2012**, *22*, 1040-1045.

(79) Price, S. C.; Williams, K. S.; Beyer, F. L.: Relationships between Structure and Alkaline Stability of Imidazolium Cations for Fuel Cell Membrane Applications. **2014**, 7-12.

(80) Si, Z.; Qiu, L.; Dong, H.; Gu, F.; Li, Y.; Yan, F.: Effects of Substituents and Substitution Positions on Alkaline Stability of Imidazolium Cations and Their Corresponding Anion-Exchange Membranes. *ACS Applied Materials & Interfaces* **2014**, *6*, 4346-4355.

(81) Zha, Y.; Disabb-Miller, M. L.; Johnson, Z. D.; Hickner, M. A.; Tew, G. N.: Metal-Cation-Based Anion Exchange Membranes. *Journal of the American Chemical Society* **2012**, *134*, 4493-4496.

(82) Chempath, S.; Einsla, B. R.; Pratt, L. R.; Macomber, C. S.; Boncella, J. M.; Rau, J. a.; Pivovar, B. S.: Mechanism of Tetraalkylammonium Headgroup Degradation in Alkaline Fuel Cell Membranes. *Journal of Physical Chemistry C* **2008**, *112*, 3179-3182.

(83) Macomber, C. S.; Boncella, J. M.; Pivovar, B. S.; Rau, J. a.: Decomposition pathways of an alkaline fuel cell membrane material component via evolved gas analysis. *Journal of Thermal Analysis and Calorimetry* **2008**, *93*, 225-229.

(84) Simonyan, S. S.; Kletskii, M. E.; Chernov, M. S.; Gol, V. E.: Structure and Stability of Quaternary Ammonium Interhalides : Experimental and Quantum-Chemical Study. *Russian Journal of General Chemistry* **2003**, *73*, 575-582.

(85) Clark, T. J.; Robertson, N. J.; Kostalik, H. a.; Lobkovsky, E. B.; Mutolo, P. F.; Abruña, H. D.; Coates, G. W.: A ring-opening metathesis polymerization route to alkaline anion exchange membranes: development of hydroxide-conducting thin films from an ammonium-functionalized monomer. *Journal of the American Chemical Society* **2009**, *131*, 12888-9.

(86) Robertson, N. J.; Kostalik, H. a.; Clark, T. J.; Mutolo, P. F.; Abruña, H. D.; Coates, G. W.: Tunable high performance cross-linked alkaline anion exchange membranes for fuel cell applications. *Journal of the American Chemical Society* **2010**, *132*, 3400-4.

(87) You, N.-H.; Higashihara, T.; Oishi, Y.; Ando, S.; Ueda, M.: Highly Refractive Poly(phenylene thioether) Containing Triazine Unit. *Macromolecules* **2010**, *43*, 4613-4615.

(88) Zhao, Z.; Ueno, K.; Angell, C. A.: High Conductivity, and "Dry" Proton Motion, in Guanidinium Salt Melts and Binary Solutions. *The Journal of Physical Chemistry B* **2011**, *115*, 13467-13472.

(89) Rozas, I.; Kruger, P. E.: Theoretical Study of the Interaction between the Guanidinium Cation and Chloride and Sulfate Anions. *Journal of Chemical Theory and Computation* **2005**, *1*, 1055-1062.

(90) Wang, J.; Li, S.; Zhang, S.: Novel Hydroxide-Conducting Polyelectrolyte Composed of an Poly(arylene ether sulfone) Containing Pendant Quaternary Guanidinium Groups for Alkaline Fuel Cell Applications. *Macromolecules* **2010**, *43*, 3890-3896.

(91) Lin, X.; Wu, L.; Liu, Y.; Ong, A. L.; Poynton, S. D.; Varcoe, J. R.; Xu, T.: Alkali resistant and conductive guanidinium-based anion-exchange membranes for alkaline polymer electrolyte fuel cells. *Journal of Power Sources* **2012**, *217*, 373-380.

(92) Hibbs, M. R.: Alkaline stability of poly(phenylene)-based anion exchange membranes with various cations. *Journal of Polymer Science Part B: Polymer Physics* **2013**, *51*, 1736-1742.

(93) Xie, H.; Zhang, S.; Duan, H.: An ionic liquid based on a cyclic guanidinium cation is an efficient medium for the selective oxidation of benzyl alcohols. *Tetrahedron Letters* **2004**, *45*, 2013-2015.

(94) Santoro, A. V.; Mickevicius, G.: Hindered rotation in hexasubstituted guanidine salts. *The Journal of Organic Chemistry* **1979**, *44*, 117-120.

(95) Azumaya, I.; Yamaguchi, K.; Kagechika, H.: Total Asymmetric Transformation of an N-Methylbenzamide. *J. Am. Chem. SOC.* **1995**, *117*, 9083-9084.

(96) Butschies, M.; Sauer, S.; Kessler, E.; Siehl, H.-U.; Claasen, B.; Fischer, P.; Frey, W.; Laschat, S.: Influence of N-alkyl substituents and counterions on the structural and mesomorphic properties of guanidinium salts: experiment and quantum chemical

calculations. *Chemphyschem : a European journal of chemical physics and physical chemistry* **2010**, *11*, 3752-65.

(97) Oelkers, B.; Sundermeyer, J.: Pentaalkylmethylguanidinium methylcarbonates – versatile precursors for the preparation of halide-free and metal-free guanidinium-based ILs. *Green Chemistry* **2011**, *13*, 608.

(98) Zhang, X.; Bau, R.; A. Sheehy, J.; Christe, K. O.: Crystal structure of hexamethylguanidinium hexafluorosilicate hexahydrate. *Journal of Fluorine Chemistry* **1999**, *98*, 121-126.

(99) Tanatani, A.; Yamaguchi, K.; Azumaya, I.; Fukutomi, R.; Shudo, K.; Kagechika, H.: N -Methylated Diphenylguanidines: Conformations, Propeller-Type Molecular Chirality, and Construction of Water-Soluble Oligomers with Multilayered Aromatic Structures. *Journal of the American Chemical Society* **1998**, *120*, 6433-6442.

(100) Schmidt, C. C.: The Dielectric Constants of four Electrolytes as given by the Carman Electrometer Method. *Physical Review* **1927**, *30*, 925.

(101) Wyman, J.: Measurements of the Dielectric Constants of Conducting Media. *Physical Review* **1930**, *35*, 623.

(102) Chempath, S.; Einsla, B. R.; Pratt, L. R.; Macomber, C. S.; Boncella, J. M.; Rau, J. a.; Pivovar, B. S.: Mechanism of Tetraalkylammonium Headgroup Degradation in Alkaline Fuel Cell Membranes. *Journal of Physical Chemistry C* **2008**, *112*, 3179-3182.

(103) Yu, Y.; Li, H.; Wang, H.; Yuan, X.-Z.; Wang, G.; Pan, M.: A review on performance degradation of proton exchange membrane fuel cells during startup and shutdown processes: Causes, consequences, and mitigation strategies. *Journal of Power Sources* **2012**, *205*, 10-23.

(104) Kusoglu, A.; Karlsson, A. M.; Santare, M. H.; Cleghorn, S.; Johnson, W. B.: Mechanical behavior of fuel cell membranes under humidity cycles and effect of swelling anisotropy on the fatigue stresses. *Journal of Power Sources* **2007**, *170*, 345-358.

(105) Mohanty, A. D.; Lee, Y.-B.; Zhu, L.; Hickner, M. a.; Bae, C.: Anion Exchange Fuel Cell Membranes Prepared from C–H Borylation and Suzuki Coupling Reactions. *Macromolecules* **2014**, *47*, 1973-1980.

(106) Yan, J.; Hickner, M. a.: Anion Exchange Membranes by Bromination of Benzylmethyl-Containing Poly(sulfone)s. *Macromolecules* **2010**, *43*, 2349-2356.

(107) Li, L.; Wang, Y.: Quaternized polyethersulfone Cardo anion exchange membranes for direct methanol alkaline fuel cells. *Journal of Membrane Science* **2005**, *262*, 1-4.

(108) Sherazi, T. a.; Yong Sohn, J.; Moo Lee, Y.; Guiver, M. D.: Polyethylene-based radiation grafted anion-exchange membranes for alkaline fuel cells. *Journal of Membrane Science* **2013**, *441*, 148-157.

(109) Lin, B.; Qiu, L.; Lu, J.; Yan, F.: Cross-Linked Alkaline Ionic Liquid-Based Polymer Electrolytes for Alkaline Fuel Cell Applications. *Chemistry of Materials* **2010**, *22*, 6718-6725.

(110) Price, S. C.; Ren, X.; Jackson, A. C.; Ye, Y.; Elabd, Y. a.; Beyer, F. L.: Bicontinuous Alkaline Fuel Cell Membranes from Strongly Self-Segregating Block Copolymers. *Macromolecules* **2013**, *46*, 7332-7340.

(111) Cao, Y.-C.; Wang, X.; Mamlouk, M.; Scott, K.: Preparation of alkaline anion exchange polymer membrane from methylated melamine grafted poly(vinylbenzyl chloride) and its fuel cell performance. *Journal of Materials Chemistry* **2011**, *21*, 12910.

(112) Hay, A. S.: Polymerization by oxidative coupling: Discovery and commercialization of PPO® and Noryl® resins. *Journal of Polymer Science Part A: Polymer Chemistry* **1998**, *36*, 505-517.

(113) Hay, A. S.; Blanchard, H. S.; Endres, G. F.; Eustance, J. W.: POLYMERIZATION BY OXIDATIVE COUPLING. *Journal of the American Chemical Society* **1959**, *81*, 6335-6336.

(114) Li, N.; Wang, L.; Hickner, M.: Cross-linked comb-shaped anion exchange membranes with high base stability. *Chemical Communications* **2014**, *50*, 4092-4095.

(115) Lin, X.; Varcoe, J. R.; Poynton, S. D.; Liang, X.; Ong, A. L.; Ran, J.; Li, Y.; Xu, T.: Alkaline polymer electrolytes containing pendant dimethylimidazolium groups for alkaline membrane fuel cells. *Journal of Materials Chemistry A* **2013**, *1*, 7262-7269.

(116) Li, Q.; Liu, L.; Miao, Q.; Jin, B.; Bai, R.: A novel poly(2,6-dimethyl-1,4-phenylene oxide) with trifunctional ammonium moieties for alkaline anion exchange membranes. *Chemical Communications* **2014**, *50*, 2791-2793.

(117) Li, N.; Yan, T.; Li, Z.; Thurn-Albrecht, T.; Binder, W. H.: Comb-shaped polymers to enhance hydroxide transport in anion exchange membranes. *Energy & Environmental Science* **2012**, *5*, 7888-7892.

(118) Deavin, O. I.; Murphy, S.; Ong, A. L.; Poynton, S. D.; Zeng, R.; Herman, H.; Varcoe, J. R.: Anion-exchange membranes for alkaline polymer electrolyte fuel cells: comparison of pendent benzyltrimethylammonium- and benzylmethylimidazolium-head-groups. *Energy & Environmental Science* **2012**, *5*, 8584-8597.

(119) Lin, X.; Liang, X.; Poynton, S. D.; Varcoe, J. R.; Ong, A. L.; Ran, J.; Li, Y.; Li, Q.; Xu, T.: Novel alkaline anion exchange membranes containing pendant benzimidazolium groups for alkaline fuel cells. *Journal of Membrane Science* **2013**, *443*, 193-200.

(120) Wu, L.; Xu, T.: Improving anion exchange membranes for DMAFCs by inter-crosslinking CPPO/BPPO blends. *Journal of Membrane Science* **2008**, *322*, 286-292.

(121) Ye, Y.; Sharick, S.; Davis, E. M.; Winey, K. I.; Elabd, Y. A.: High Hydroxide Conductivity in Polymerized Ionic Liquid Block Copolymers. *ACS Macro Letters* **2013**, *2*, 575-580.

(122) Elabd, Y. a.; Hickner, M. a.: Block Copolymers for Fuel Cells. *Macromolecules* **2011**, *44*, 1-11.

(123) Rebeck, N. T.; Li, Y.; Knauss, D. M.: Poly(phenylene oxide) copolymer anion exchange membranes. *Journal of Polymer Science Part B: Polymer Physics* **2013**, *51*, 1770-1778.

(124) Bothe, M.; Schmidt-Naake, G.: An Improved Catalytic Method for Alkoxyamine Synthesis – Functionalized and Biradical Initiators for Nitroxide-Mediated Radical Polymerization. *Macromolecular Rapid Communications* **2003**, *24*, 609-613.

(125) J. S. Riffle, E. S., A. K. Banthia, R. G. Freelin, T. C. Ward, J. E. Mcgrath: Hydroxy terminated polysulfone end group analysis. *Journal of Polymer Science: Polymer Chemistry Edition* **1982**, *20*, 12.

(126) Park, A. M.; Turley, F. E.; Wycisk, R. J.; Pintauro, P. N.: Electrospun and Cross-Linked Nanofiber Composite Anion Exchange Membranes. *Macromolecules* **2013**, *47*, 227-235.

(127) Kumar, A.; Pisula, W.; Markova, D.; Klapper, M.; Müllen, K.: Proton-Conducting Poly(phenylene oxide)–Poly(vinyl benzyl phosphonic acid) Block Copolymers via Atom Transfer Radical Polymerization. *Macromolecular Chemistry and Physics* **2012**, *213*, 489-499.

(128) Ran, J.; Wu, L.; Wei, B.; Chen, Y.; Xu, T.: Simultaneous Enhancements of Conductivity and Stability for Anion Exchange Membranes (AEMs) through Precise Structure Design. *Sci. Rep.* **2014**, *4*.

(129) Li, Y.; Jackson, A. C.; Beyer, F. L.; Knauss, D. M.: Poly(2,6-dimethyl-1,4-phenylene oxide) Blended with Poly(vinylbenzyl chloride)-b-polystyrene for the Formation of Anion Exchange Membranes. *Macromolecules* **2014**, *47*, 6757-6767.

(130) Messé, L.; Prud'homme, R. E.: Orientation and relaxation study of polystyrene: Polystyrene/poly(phenylene oxide) blends. *Journal of Polymer Science Part B: Polymer Physics* **2000**, *38*, 1405-1415.

(131) Sharma, K. R.: *Polymer Thermodynamics: Blends, Copolymers and Reversible Polymerization*; Taylor & Francis, 2011.

(132) Song, J.-M.; Lee, S.-Y.; Woo, H.-S.; Sohn, J.-Y.; Shin, J.: Thermal behavior of poly(vinylbenzyl chloride)-grafted poly(ethylene-co-tetrafluoroethylene) films. *Journal of Polymer Science Part B: Polymer Physics* **2014**, *52*, 517-525.

(133) Zhang; Painter, P. C.; Runt, J.: Coupling of Component Segmental Relaxations in a Polymer Blend Containing Intermolecular Hydrogen Bonds. *Macromolecules* **2002**, *35*, 9403-9413.

(134) Xu, H.; Fang, J.; Guo, M.; Lu, X.; Wei, X.; Tu, S.: Novel anion exchange membrane based on copolymer of methyl methacrylate, vinylbenzyl chloride and ethyl acrylate for alkaline fuel cells. *Journal of Membrane Science* **2010**, *354*, 206-211.

(135) Marino, M. G.; Melchior, J. P.; Wohlfarth, A.; Kreuer, K. D.: Hydroxide, halide and water transport in a model anion exchange membrane. *Journal of Membrane Science* **2014**, *464*, 61-71.

(136) Hickner, M. a.; Herring, A. M.; Coughlin, E. B.: Anion exchange membranes: Current status and moving forward. *Journal of Polymer Science Part B: Polymer Physics* **2013**, *51*, 1727-1735.

(137) Tanaka, M.; Koike, M.; Miyatake, K.; Watanabe, M.: Anion Conductive Aromatic Ionomers Containing Fluorenyl Groups. *Macromolecules* **2010**, *43*, 2657-2659.

(138) Couture, G.; Alaaeddine, A.; Boschet, F.; Ameduri, B.: Polymeric materials as anion-exchange membranes for alkaline fuel cells. *Progress in Polymer Science* **2011**, *36*, 1521-1557.

(139) Lee, H.-C.; Liu, K.-L.; Tsai, L.-D.; Lai, J.-Y.; Chao, C.-Y.: Anion exchange membranes based on novel quaternized block copolymers for alkaline direct methanol fuel cells. *RSC Advances* **2014**, *4*, 10944-10954.

(140) Zhang, M.; Kim, H. K.; Chalkova, E.; Mark, F.; Lvov, S. N.; Chung, T. C. M.: New Polyethylene Based Anion Exchange Membranes (PE–AEMs) with High Ionic Conductivity. *Macromolecules* **2011**, *44*, 5937-5946.

(141) Disabb-Miller, M. L.; Zha, Y.; DeCarlo, A. J.; Pawar, M.; Tew, G. N.; Hickner, M. A.: Water Uptake and Ion Mobility in Cross-Linked Bis(terpyridine)ruthenium-Based Anion Exchange Membranes. *Macromolecules* **2013**, *46*, 9279-9287.

(142) Thomas, O. D.; Soo, K. J. W. Y.; Peckham, T. J.; Kulkarni, M. P.; Holdcroft, S.: A stable hydroxide-conducting polymer. *Journal of the American Chemical Society* **2012**, *134*, 10753-6.

(143) Kulkarni, M. P.; Peckham, T. J.; Thomas, O. D.; Holdcroft, S.: Polybenzimidazoles with Pendant Quaternary Ammonium Groups as Anion Exchange Membranes: Synthesis, Characterization and Alkaline Stability. *MRS Online Proceedings Library* **2014**, *1677*, null-null.

(144) Dizman, C.; Tasdelen, M. A.; Yagci, Y.: Recent advances in the preparation of functionalized polysulfones. *Polymer International* **2013**, n/a-n/a.

(145) Hossain, M. A.; Lim, Y.; Lee, S.; Jang, H.; Choi, S.; Jeon, Y.; Lee, S.; Ju, H.; Kim, W. G.: Anion conductive aromatic membrane of poly(tetra phenyl ether sulfone) containing hexa-imidazolium hydroxides for alkaline fuel cell application. *Solid State Ionics* **2014**, *262*, 754-760.

(146) Di Vona, M. L.; Narducci, R.; Pasquini, L.; Pelzer, K.; Knauth, P.: Anion-conducting ionomers: Study of type of functionalizing amine and macromolecular cross-linking. *International Journal of Hydrogen Energy* **2014**, *39*, 14039-14049.

(147) Mei, W.; lv, C.; Yan, J.; Wang, Z.: Anion Exchange Membranes by Bromination of Benzylmethyl-containing Poly (fluorene ether sulfone)s. *RSC Advances* **2014**.

(148) Bothe, M.; Schmidt-Naake, G.: An Improved Catalytic Method for Alkoxyamine Synthesis – Functionalized and Biradical Initiators for Nitroxide-Mediated Radical Polymerization. *Macromolecular Rapid Communications* **2003**, *24*, 609-613.

(149) Liu, Z.; Li, X.; Shen, K.; Feng, P.; Zhang, Y.; Xu, X.; Hu, W.; Jiang, Z.; Liu, B.; Guiver, M. D.: Naphthalene-based poly(arylene ether ketone) anion exchange membranes. *Journal of Materials Chemistry A* **2013**, *1*, 6481-6488.

(150) Nuñez, S. A.; Hickner, M. A.: Quantitative 1H NMR Analysis of Chemical Stabilities in Anion-Exchange Membranes. *ACS Macro Letters* **2012**, *2*, 49-52.

(151) Kim, W. N.; Burns, C. M.: Phase behavior of blends of polycarbonate with partially miscible polymers. *Journal of Applied Polymer Science* **1990**, *41*, 1575-1593.

(152) Beckman, E. J.; Karasz, F. E.; Porter, R. S.; MacKnight, W. J.; Van Hunsel, J.; Koningsveld, R.: Estimation of the interfacial fraction in partially miscible polymer blends from DSC measurements. *Macromolecules* **1988**, *21*, 1193-1194.

(153) Koshikawa, H.; Yoshimura, K.; Sinnananchi, W.; Yamaki, T.; Asano, M.; Yamamoto, K.; Yamaguchi, S.; Tanaka, H.; Maekawa, Y.: Counter-Anion Effect on the Properties of Anion-Conducting Polymer Electrolyte Membranes Prepared by Radiation-Induced Graft Polymerization. *Macromolecular Chemistry and Physics* **2013**, *214*, 1756-1762.

(154) Tsang, E. M. W.; Zhang, Z.; Shi, Z.; Soboleva, T.; Holdcroft, S.: Considerations of Macromolecular Structure in the Design of Proton Conducting Polymer Membranes: Graft versus Diblock Polyelectrolytes. *Journal of the American Chemical Society* **2007**, *129*, 15106-15107.